UNIVERSITY OF OKLAHOMA

GRADUATE COLLEGE

NATURAL PRODUCTS AS A SOURCE OF NEW THERAPIES FOR NEURODEGENERATIVE DISEASE AND EFFORTS TOWARD THE DEVELOPMENT OF A METABOLOMICS-BASED DRUG DISCOVERY PLATFORM

A DISSERTATION

SUBMITTED TO THE GRADUATE FACULTY

in partial fulfillment of the requirements for the

Degree of

DOCTOR OF PHILOSOPHY

By

PHILLIP M. JOYNER
Norman, Oklahoma
2010

NATURAL PRODUCTS AS A SOURCE OF NEW THERAPIES FOR NEURODEGENERATIVE DISEASE AND EFFORTS TOWARD THE DEVELOPMENT OF A METABOLOMICS-BASED DRUG DISCOVERY PLATFORM

A DISSERTATION APPROVED FOR THE
DEPARTMENT OF CHEMISTRY AND BIOCHEMISTRY

BY

Dr. Robert Cichewicz, Chair

Dr. Michael Ashby

Dr. Ken Nicholas

Dr. Ralph Tanner

Dr. Ann West

Acknowledgements

I would like to thank Dr. Cichewicz for showing me how to be a good scientist and for all of his help and support during my time as a graduate student. I greatly appreciate all of the training and assistance I have received from Dr. Susan Nimmo in the use of NMR spectroscopy. I am grateful to Dr. West for teaching me how to do yeast transformations and for her help and guidance during my doctoral research. I also appreciate all of the feedback I have received from the other members of my advisory committee: Drs. Ashby, Nicholas and Tanner.

I would like to thank the University of Oklahoma Department of Chemistry and Biochemistry, the Department of Education Graduate Assistance in Areas of National Need (GAANN) program, the University of Oklahoma Graduate College and the National Institutes of Health for financial support during my graduate studies.

Finally, I would like to thank my wife, Brittany, for providing endless love, encouragement and support. I would not be where I am today without her help.

Table of Contents

List of Tables

List of Figures

Abstract

Natural products have traditionally played an important role in drug discovery research. They have been particularly important in the search for therapies for neurodegenerative diseases. Although there are numerous forms of neurodegenerative diseases, the disorders associated with protein misfolding (e.g. Alzheimer's, Parkinson's, Huntington's and prion diseases) represent a unique area for natural products drug discovery as these diseases share many pathological features, suggesting that therapies developed for any one of these diseases may have applications for the others. There have been many reports of secondary metabolites with biological activities related to neurodegeneration associated with protein misfolding, and emerging drug targets for these diseases are fueling interest in finding natural products which can serve as leads for therapeutic development. The literature surrounding the topic of natural products and neurodegenerative disease has been summarized in the first chapter of this dissertation.

Although there have already been many natural products identified as potential therapeutic leads for neurodegenerative diseases, there is still a significant need for the enhancement of methodologies used for bioassay screening of secondary metabolites. Metabolomic approaches to drug discovery have the potential to combine the advantages of phenotypic disease models and molecular target assays. The metabolomic examination of a phenotypic disease model can provide detailed information concerning the molecular target and/or the mechanism of action of a compound while simultaneously revealing its phenotypic effects. The third chapter of this dissertation describes the metabolomic examination of a phenotypic model of Huntington's disease. This detailed exploration of the metabolic changes associated with mutant huntingtin toxicity has

revealed many intriguing new insights into the specific processes which are involved in the cellular response to protein aggregation. The results in this chapter show that the metabolic response of cells to mutant huntingtin can be detected using a metabolomic approach and that these metabolic changes can be used to identify potential therapeutic targets for Huntington's disease. These results also show the importance of the metabolites alanine, glutamine, glycerol and valine in the metabolic response to mutant huntingtin in multiple species. This work provides the foundation for the future development of a metabolomic-based drug discovery platform for natural products.

In the fourth chapter of this dissertation, the use of metabolic profiling to examine the protective role of the metabolite trehalose is described. Trehalose is a disaccharide that has been previously identified as having therapeutic implications for neurodegenerative diseases. In order to explore the role that trehalose plays in the yeast model of Huntington's disease, a series of yeast strains with gene deletions for each step in the metabolic cycle of trehalose were engineered to express normal and mutant huntingtin protein fragments. One of these gene deletion strains, deficient in the production of the acid trehalase protein, exhibited a prounouced reduction in the toxicity associated with mutant huntingtin, the aggregation of mutant huntingtin and the elimination of the metabolic aberrations associated with mutant huntingtin expression. This investigation of the role of trehalose in the yeast model of Huntington's disease provides evidence for the therapeutic potential of the manipulation of chemical chaperone systems in mammalian cells.

The final chapter of this dissertation diverges from the topic of neurodegeneration and instead describes the isolation and characterization of a series of briarane diterpenes

from a *Briareum* sp. of octocoral. The ichthyotoxic properties of these compounds are described as well as their metabolic transformation by fish. The scientific merits of this study make it an important and significant part of my doctoral research and demonstrate the multidisciplinary nature of my research.

Chapter 1 The emerging role of natural products for the treatment of neurodegenerative diseases associated with protein misfolding

1.1 Introduction

Neurodegenerative diseases caused by misfolded proteins have become a significant problem in developing countries as life expectancies continue to rise. Today millions of people suffer from neurodegenerative diseases such as Alzheimer's, Parkinson's, Huntington's and prion diseases (Farooqui and Farooqui 2009; Stefani 2007). These disorders share many common pathological features, including the formation of protein aggregates in the brain, dysregulation of cell signaling, oxidative stress, inflammation, and apoptosis (Amor, et al. 2010; Davies, et al. 2006; Skovronsky, et al. 2006). The search for new therapies for these conditions is urgent since there are currently no effective treatments available to halt or reverse their progress (Scatena, et al. 2007).

The United States National Institute of Neurological Disorders and Stroke (NINDS) estimates that over 4.5 million people suffer from these diseases in the U.S. alone (NINDS 2010), and there are many millions more suffering in other countries around the world (Figure 1.1). Alzheimer's disease is the most common of these neurodegenerative conditions, with an estimated 4 million diagnosed cases in the U.S. Parkinson's disease is the second most common with around half a million diagnosed cases. Huntington's disease and prion diseases are much rarer, but the crippling and fatal effects of these diseases are no less severe for those suffering from them. Because of the millions of people affected by these diseases, there is considerable work underway to

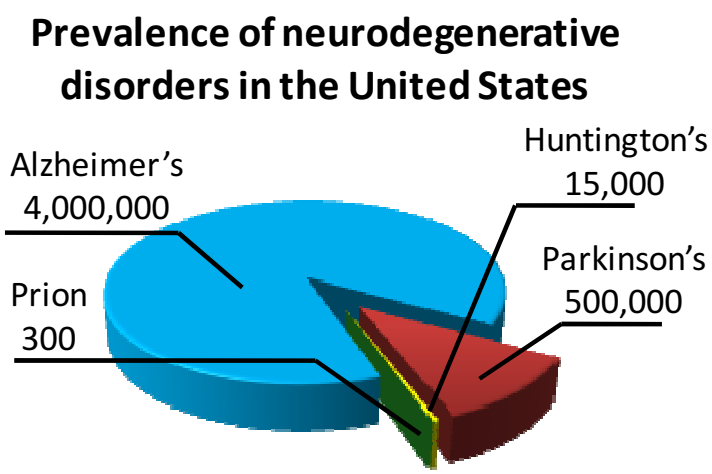

Figure 1.1 Estimated prevalence of neurodegenerative diseases associated with protein misfolding in the United States. Data from the United Stated National Institutes of Health, National Institute of Neurological Disorders and Stroke.

search for new therapies for patients with these disorders (Cornelis, et al. 2007; Gilgun-Sherki, et al. 2006; Gold and Villafranca 2003; Lleo 2007; Planells-Cases, et al. 2006; Scatena, et al. 2007; Van der Schyf, et al. 2006; Van der Schyf, et al. 2007).

Natural products are expected to play a significant role in the search for neurodegenerative disease therapeutics since historically secondary metabolites have been an excellent source for the development of small molecule therapeutics (Butler 2004; Newman 2008; Newman and Cragg 2007). The unique combination of novel chemical space occupied by natural products coupled with their potent bioactivities has made them an attractive resource for drug discovery. Neurodegenerative diseases pose a particularly difficult problem for drug discovery efforts since the mechanisms of many of these diseases are still not clearly understood. The exceptional properties of natural products make them excellent tools for answering the difficult problems posed by drug discovery efforts for neurodegenerative disorders. Two molecules have already demonstrated the potential of natural products for treating neurodegenerative disease: galanthamine (**1**) and huperzine A (**2**). Both of these compounds inhibit the enzyme acetylcholinesterase and are in clinical use for the treatment of Alzheimer's disease (Dong, et al. 2009; Heinrich and Lee Teoh 2004).

A small number of review articles have appeared previously summarizing discoveries in natural products limited to Alzheimer's and Parkinson's disease (Houghton and Howes 2005) or the very broad topic of biological activity in the central nervous system with little space given to neurodegenerative diseases (Clement, et al. 2004; Gomes, et al. 2009). Somewhat more common have been reviews of natural products discoveries related to a single biological target for neurodegenerative disease, such as acetylcholinesterase (Barbosa Filho, et al. 2006; Jung and Park 2007; Loizzo, et al. 2008; Orhan, et al. 2009; Viegas Jr, et al. 2005) or neurotrophins (Ohizumi, et al. 2004; Tohda, et al. 2005). There have also been reviews of specific classes of compounds such as the flavonoids and polyphenols and their biological activities pertaining to neurodegeneration (Bastianetto, et al. 2007; Patel, et al. 2008; Vafeiadou, et al. 2007). However, there has never been a comprehensive review of the natural products literature that summarizes the data concerning protein aggregation related neurodegenerative diseases. This review summarizes the literature pertaining to bioactive natural products and their primary application to neurodegenerative diseases associated with protein misfolding. Compounds with very broad or non-specific bioactivities, such as antioxidants, have been excluded since their therapeutic applications are limited. Instead this review is focused on summarizing the role of natural products in drug discovery efforts for established as

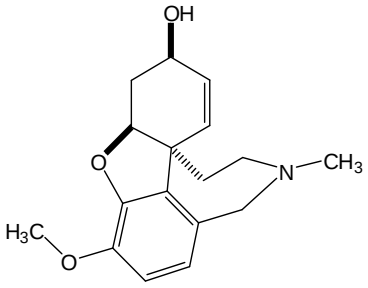

1

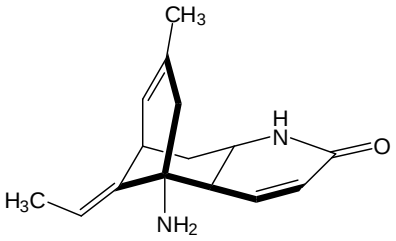

2

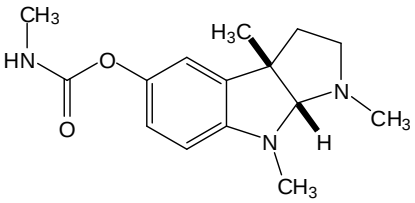

3

well as emerging targets for neurodegenerative diseases. The following sections will provide a brief introduction to each disease followed by a summary of natural products discoveries related to therapeutic targets specific for each disease.

1.2 Alzheimer's disease

Alzheimer's disease (AD) is characterized by the presence of insoluble amyloid plaques in the extracellular region between neurons; these plaques consist primarily of the β-amyloid (Aβ) peptide, the aggregation-prone agent that is central to AD neuropathology (Pallas and Camins 2006). The misfolding and aggregation of Aβ is believed to lead to disruption of normal neuronal functions, including decreased production and altered regulation of neurotransmitters and neurotrophins, mitochondrial dysfunction, oxidative stress, inflammation, and tau hyperphosphorylation (Pallas and Camins 2006; Querfurth and LaFerla). The combined effects of these problems lead to the degeneration of cholinergic neurons, especially in the hippocampus, which results in the primary symptom of AD (i.e. memory loss) (Pallas and Camins 2006; Querfurth and LaFerla).

Because AD is caused by such a multi-faceted collection of disrupted cellular processes, there are many potential therapeutic targets for this disease. It has even been proposed that drug discovery efforts would benefit from a polypharmacological approach that modulates multiple targets (Van der Schyf, et al. 2006; Van der Schyf, et al. 2007). In the following sections, the reported activities of natural products against a variety of AD targets have been summarized. In some cases these targets are specific enzymes, in others the target is simply the general alleviation of toxic agents associated with AD. The relevant biological activity and structural features are discussed in each case.

1.2.1 Acetylcholinesterase inhibitors. Natural products with inhibitory activity against cholinesterases, such as physostigmine (**3**), have been known since the 1920's (Triggle, et al. 1998), although it wasn't until later in the 20th century that these compounds began to receive attention as potential therapeutics for AD (Orhan, et al. 2009). The therapeutic effect of these compounds for AD is due to the increase in concentration of the neurotransmitter acetylcholine at the synapse, which is normally deactivated by the enzyme acetylcholinesterase (Lleo 2007). Acetylcholinesterase inhibitors are commonly used to treat AD; the natural product galanthamine (**1**), originally isolated from *Galanths* spp. of plants, is an approved therapy for AD in the United States and Europe as well as many other countries (Heinrich and Lee Teoh 2004). Huperzine A (**2**) is another well known acetylcholinesterase inhibitor which was originally isolated from *Huperzia serrata*, a plant with traditional use in Chinese folk medicine (Yuan, et al. 2008). It has entered clinical use in China and is being developed for use in other countries (Dong, et al. 2009). The activity of **2** and other naturally occurring inhibitors of acetylcholinesterase have been thoroughly reviewed elsewhere (Barbosa Filho, et al. 2006; Jung and Park 2007; Loizzo, et al. 2008; Orhan, et al. 2009; Viegas Jr, et al. 2005; Yuan, et al. 2008; Zangara 2003).

1.2.2 Kinase inhibitors (Cdk5 and Gsk3). Two protein kinases have been implicated in AD, cyclin dependent kinase 5 (Cdk5) and glycogen synthase kinase 3 (Gsk3), both of which are promising targets for the development of new therapies against AD. Although Gsk3 has multiple functions, it is known to play an important role in the phosphorylation of tau and in the production of Aβ; inhibition of Gsk3 has also been shown to decrease the production of Aβ in a mouse model of AD (Giese 2009;

Hernandez and Avila 2008). Cdk5 is essential for neuronal development, but its function in adults is not as clear (Liu, et al. 2007). It has been shown that Cdk5 phosphorylates both tau and the amyloid precursor protein (APP), leading to the formation of neurofibrillary tangles (NFT's) and increased production of the toxic Aβ peptide (Liu, et al. 2007). Inhibitors of Gsk3 and Cdk5 have exciting potential as targets for the treatment of AD and several promising natural products leads have been identified.

Hymenialdisine (**4**), marine sponge metabolite, was identified as an extremely potent inhibitor of both Gsk3 (IC_{50} = 10 nM) and Cdk5 (IC_{50} = 28 nM) (Meijer, et al. 2000). A variety of structurally related compounds were also tested against a series of kinases in the same study, but **4** was significantly more potent than all of the other compounds.

The manzamines are a series of marine sponge alkaloids with impressive activity as inhibitors of Gsk3 and Cdk5 (Hamann, et al. 2007). Manzamine A (**5**), 8-hydroxymanzamine A (**6**), manzamine E (**7**), manzamine F (**8**), manzamine Y (**9**), and the unique manzamine dimer, *neo*-kauluamine (**10**) all inhibit Gsk3 *in vitro* at a concentration of 25 μM (Cheng, et al. 2006; El Sayed, et al. 2001). Manzamine A also inhibits Cdk5 (IC_{50} = 1.5 μM) and decreases tau phosphorylation in human neuroblastoma SH-S5Y5 cells (Hamann, et al. 2007). Compounds **5-10** all inhibited Gsk3 *in vitro*, but in a cell-based assay only **5** and **6** inhibited Gsk3 (Cheng, et al. 2006). None of the manzamines are active against acetylcholinesterase or β-secretase (BACE1), nor do they protect SH-SY5Y cells against oxidative-stress induced death (Cheng, et al. 2006). Manzamine A (**5**), B (**11**), C (**12**) and D (**13**) exhibit low micromolar anti-inflammatory activity, but **7** and **8** do not (Mayer, et al. 2005). A recent molecular

docking study also suggests that **6** binds to the ATP-noncompetitive pocket of Gsk3 (Peng, et al. 2010).

1.2.3 β-amyloid toxicity. Because of its central role in AD pathogenesis, several models of AD based upon Aβ induced toxicity have been developed. These include rodent and insect models as well as cell culture models (Bateman and Chakrabartty 2004; Bloom, et al. 2005; Iijima and Iijima-Ando 2008). Some of these models transgenically express the amyloid precursor protein (APP), which is then cleaved by a series of secretases to form toxic Aβ, while other models utilize Aβ peptide infused into cultured

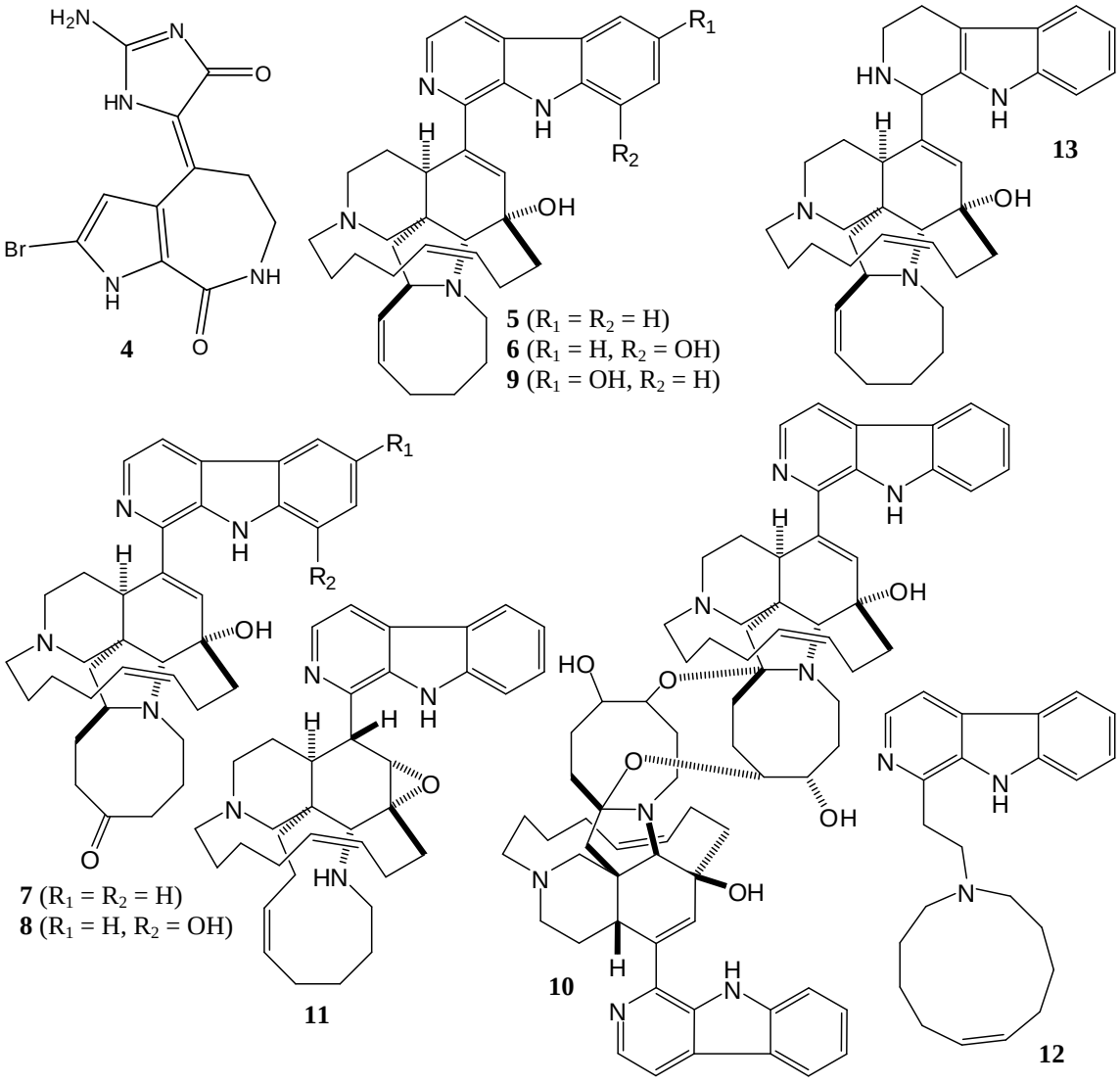

cells or rodent brains. These models accurately recapitulate many of the pathological features of AD, such as neurotoxicity, apoptosis, formation of amyloid plaques, tau hyperphosphorylation, and memory loss (Bateman and Chakrabartty 2004; Bloom, et al. 2005; Iijima and Iijima-Ando 2008).

Akebia saponin D (**14**), isolated from the plant *Dipsacus asperoides*, protects PC12 cells from toxicity associated with Aβ treatment at concentrations as low as 0.1 μg/mL (Ouyang, et al. 2009). Treatment with **14** also decreases the influx of Ca^{2+} into the Aβ treated cells, decreases the amount of lactate dehydrogenase released by the cells and reduces the morphological defects caused by Aβ treatment of PC12 cells (Ouyang, et al. 2009).

Two compounds, withanamide A (**15**) and C (**16**), isolated from the fruit of the Ayurvedic plant *Withania somnifera*, protect PC12 cells against toxicity induced by Aβ treatment (Jayaprakasam, et al. 2009). Compound **15** significantly protects cells against

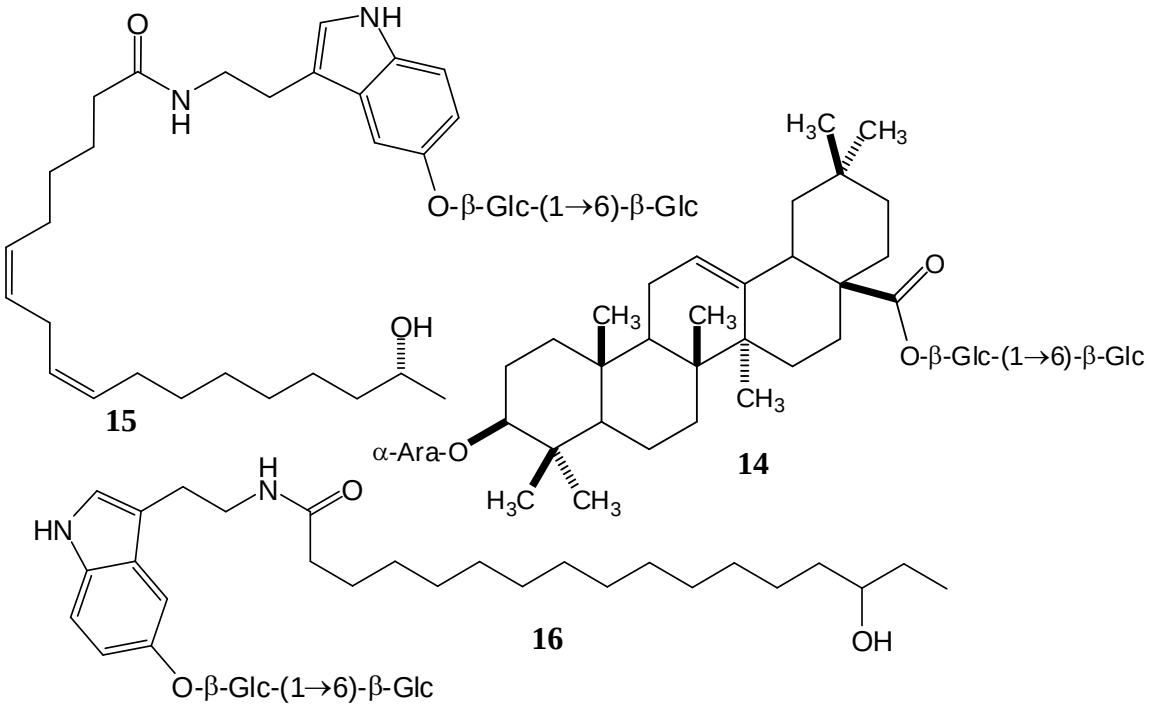

Aβ toxicity at a concentration of 50 μg/mL, but **16** has no significant effect on cell viability. The authors suggest that the difference in activity is due to the unique way in which the unsaturated hydrophobic side chain of **15** binds to the active motif of the Aβ peptide (Jayaprakasam, et al. 2009).

Eight iridoid glycosides, isolated from *Gardenia jasminoides*, enhance the short-term memory in a transgenic Aβ *Drosophila* model of AD (Hong, et al. 2009). Compounds including 6′-*O*-*trans*-*p*-coumaroylgeniposide (**17**), 10-*O*-succinoylgeniposide (**18**), 6′-*O*-acetylgeniposide (**19**), 6′-*O*-*trans*-sinapoylgeniposide (**20**), geniposide (**21**), 10-*O*-acetylgeniposide (**22**), 11-(6-*O*-*trans*-sinapoylglucopyranosyl)gardendiol (**23**), and 10-(6-*O*-*trans*-sinapoylglucopyranosyl)gardendiol (**24**) all significantly enhance the performance index of flies expressing human Aβ42 in an assay testing the short-term memory of the flies (Hong, et al. 2009). The compounds were administered to the flies in a 4% sucrose solution at a concentration of 0.00076 % (w/v) for 7 days prior to testing the short-term memory of the flies.

A stilbene monomer, 2,3,5,4′-tetrahydroxystilbene-2-*O*-β-D-glucoside (**25**), was isolated from the roots of *Polygonum multiflorum*(Yan 1981). When administered to a transgenic mouse model of AD at a dosage of 240 μmol/kg/day, **25** effectively reduces learning-memory deficits in the mice (Zhang, et al. 2006).

The quinazoline alkaloid dehydroevodiamine (**26**), first isolated from *Evodia rutaecarpa* (Nakasato, et al. 1962), significantly reduces Aβ induced amnesia in mice with a minimum effective dose of 0.75 mg/kg (Wang, et al. 2001). Compound **26** also

reduces tau hyperphosphorylation in an activated Gsk3 rat model of AD (Hamann, et al. 2007), and in calyculin A treated rat brain slices (Fang, et al. 2007).

1.2.4 β-secretase inhibitors. The toxic Aβ peptide is formed from the enzymatic cleavage of APP. There are three enzymes or enzyme complexes that cleave APP: α-secretase, β-secretase (BACE1) and the γ-secretase complex (Giese). BACE1 and the γ-secretase complex have both been implicated as therapeutic targets for AD since their inhibition may be able to reduce the amount of Aβ in the brain (Panza, et al. 2009). There have also been some attempts to increase the activity of α-secretase since it is responsible for the production of non-toxic Aβ, but these have met with only limited success (Giese). Most of the work in the development of secretase inhibitors for AD drug discovery has focused on BACE1 because it is a single enzyme and thus allows for more focused targeting by drugs. BACE1 activity is elevated in the brains of AD patients and it has been shown that a reduction in this activity is beneficial in AD models (Vassar, et al. 2009).

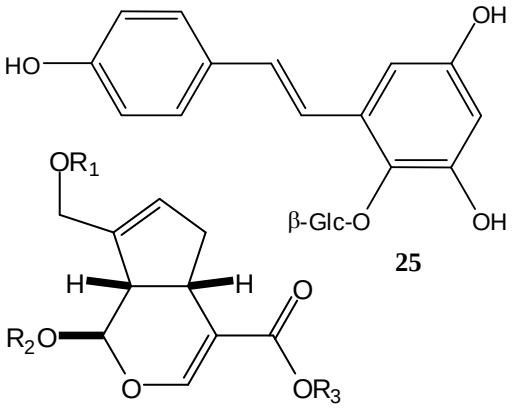

25

17 (R_1 = H, R_2 = β-Glc-6-*O*-*trans*-*p*-coumaroyl, R_3 = CH_3)
18 (R_1 = succinoyl, R_2 = β-Glc, R_3 = CH_3)
19 (R_1 = H, R_2 = β-Glc-6-*O*-Ac, R_3 = CH_3)
20 (R_1 = H, R_2 = β-Glc-6-*O*-*trans*-sinapoyl, R_3 = CH_3)
21 (R_1 = R_2 = H, R_3 = CH_3)
22 (R_1 = Ac, R_2 = H, R_3 = CH_3)

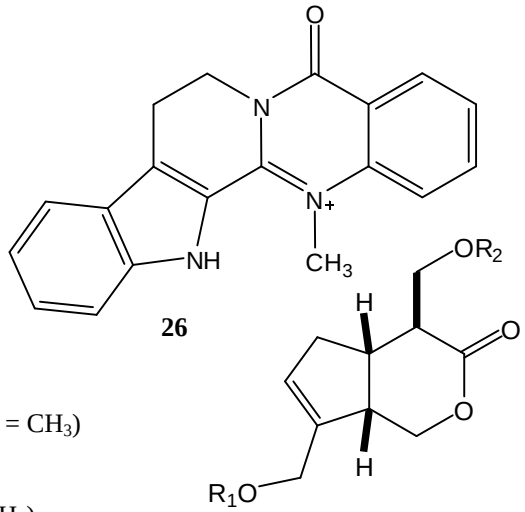

26

23 (R_1 = H, R_2 = 6-*O*-*trans*-sinapoyl-β-Glc)
24 (R_1 = 6-*O*-*trans*-sinapoyl-β-Glc, R_2 = H)

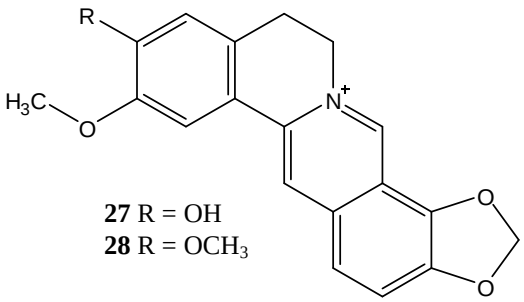

27 R = OH
28 R = OCH_3

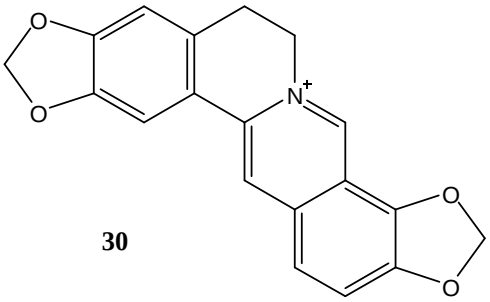

30

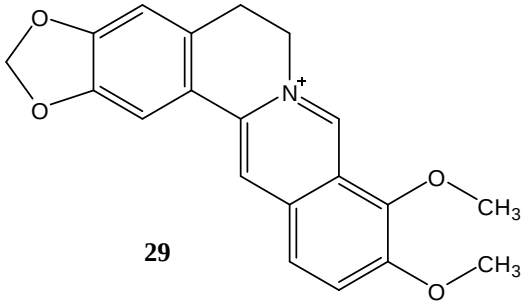

29

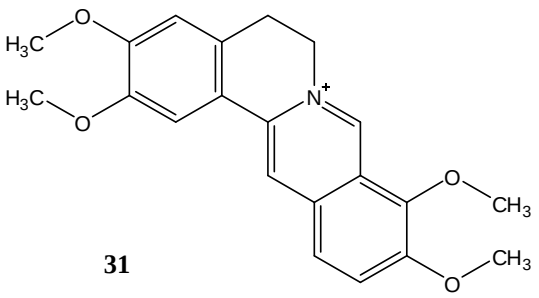

31

A series of alkaloids isolated from the rhizome of *Coptis chinensis* yielded several compounds with inhibitory activity against BACE1 (Jung, et al. 2009). Groenlandicine (**27**) and epiberberine (**28**) both inhibit BACE1 *in vitro* with IC_{50} values of 19.7 µM and 8.6 µM, respectively. Berberine (**29**) was not reported to show significant *in vitro* BACE1 inhibition in this study, but another study from 2007 reported a decrease in the production of Aβ in cells transgenically expressing APP upon treatment with **29** (Asai, et al. 2007). This decrease indicates that although **29** does not inhibit BACE1, it may be active against another part of the APP processing machinery such as the γ-secretase complex. Two other isoquinoline alkaloids, coptisine (**30**) and palmatine (**31**), along with **29** significantly enhance neurite outgrowth in PC12 cells at a concentration of 5 µg/mL, 25 µg/mL and 5 µg/mL, respectively (Shigeta, et al. 2002).

1.3 Parkinson's disease

The primary symptoms of Parkinson's disease (PD) are a loss of motor function and coordination, which is largely due to the specific degeneration of dopaminergic neurons in the brain (Lees, et al. 2009). The affected regions of the brain in PD

accumulate protein aggregates, called Lewy bodies, which consist largely of the misfolded protein α-synuclein (Brundin, et al. 2008). The native function of α-synuclein is still not clear. The investigation of α-synuclein function is difficult, in part because it changes its conformation in an environment-dependent fashion (Uversky 2007). While the role of α-synuclein in the neuropathology is still not completely understood, it is known that the protein can act as a neurotoxin and it is believed to participate in the pathogenesis of the disease (Brundin, et al. 2008; Uversky 2007). Other cellular features of PD include mitochondrial dysfunction, inflammation, oxidative damage and apoptosis (Allain, et al. 2008).

Unfortunately, nearly all of the current therapies approved for PD exclusively enhance the dopaminergic activity in the brain, which is only effective for treating the symptoms of PD rather than its cause (Lees, et al. 2009). The lack of a clear understanding of the underlying biochemical causes of PD has made the development of effective neuroprotective treatments for PD very difficult (Schapira, et al. 2006). The following section will describe the small number of natural products that have been identified as having promise for development as therapies for PD.

1.3.1 6-hydroxydopamine toxicity. There are not as many good models of PD as there are for AD, but there are some models which recapitulate enough of the features of PD to be useful in the development of new therapies (Jenner 2008). Perhaps the most commonly used model is 6-hydroxydopamine (6-OHDA) induced toxicity. 6-OHDA is a neurotoxin which specifically targets catecholaminergic (dopaminergic and noradrenalinergic) neurons and induces a handful of cellular features that are also observed in PD, primarily oxidative stress but also mitochondrial dysfunction as well

(Simola, et al. 2007). A disadvantage to the 6-OHDA model of PD is its lack of usefulness in identifying compounds which reduce the non-dopaminergic defects of PD; however, efforts to develop non-dopaminergic therapies utilize targets which not specific for PD (Colosimo, et al. 2006; Simola, et al. 2007).

Three compounds isolated from the roots of *Stemona tuberosa* were found to protect SH-SY5Y cells against toxicity from 6-OHDA treatment (Lee, et al. 2006). Stilbostemin B 3′-*β*-D-glucopyranoside (**32**), stilbostemin H 3′-*β*-D-glucopyranoside (**33**), and stilbostemin I 2″-*β*-D-glucopyranoside (**34**) all protected cells from 6-OHDA induced toxicity at concentrations of 1 μM (Lee, et al. 2006).

Paeoniflorin (**35**), a compound with a very unique cage-like pinane moiety, has shown the ability to decrease the behavioral abnormalities induced by 6-OHDA in rats at doses as low as 5 mg/kg (Durairajan, et al.). Interestingly, this report also showed that **35** does not directly antagonize dopamine receptors, which may indicate the potential for this compound as non-dopaminergic therapy for PD.

The quinolizidine alkaloid cytisine (**36**) and its derivative 5-bromocytisine (**37**) significantly reduce the decrease in striatal dopamine induced by 6-OHDA administration to rats, but the 3-bromocytisine (**38**) derivative had no effect on striatal dopamine concentrations (Abin-Carriquiry, et al. 2008). A decrease in striatal dopamine levels is a key pathological feature of the 6-OHDA model of PD (Simola, et al. 2007).

1.4 Huntington's disease

Huntington's disease (HD) is a progressive neurodegenerative disorder arising from a CAG trinucleotide repeat expansion mutation in the *huntingtin* (*Htt*) gene (Imarisio, et al. 2008; Walker 2007). Individuals carrying mutant forms of *huntingtin* (m*Htt*) encoding for ≥35 glutamine repeats are at risk of developing HD. The number of polyglutamine-encoding CAG repeats in m*Htt* strongly influences the age of disease onset, symptom severity, and rate of HD progression (Langbehn, et al. 2010). Although all of the mechanisms associated with m*Htt* toxicity are not clear, it is known that they involve both gain-of-function and loss-of-function processes (Imarisio, et al. 2008). Many of the same neuropathological features observed in other neurodegenerative diseases are present in HD, including protein aggregates, oxidative stress, mitochondrial dysfunction and apoptosis (Imarisio, et al. 2008). The majority of drug discovery efforts for HD are focused on either reducing aggregation of the m*Htt* protein, enhancing clearance of the m*Htt* protein from the cell or promoting survival in m*Htt* expressing cells (Fecke, et al. 2009).

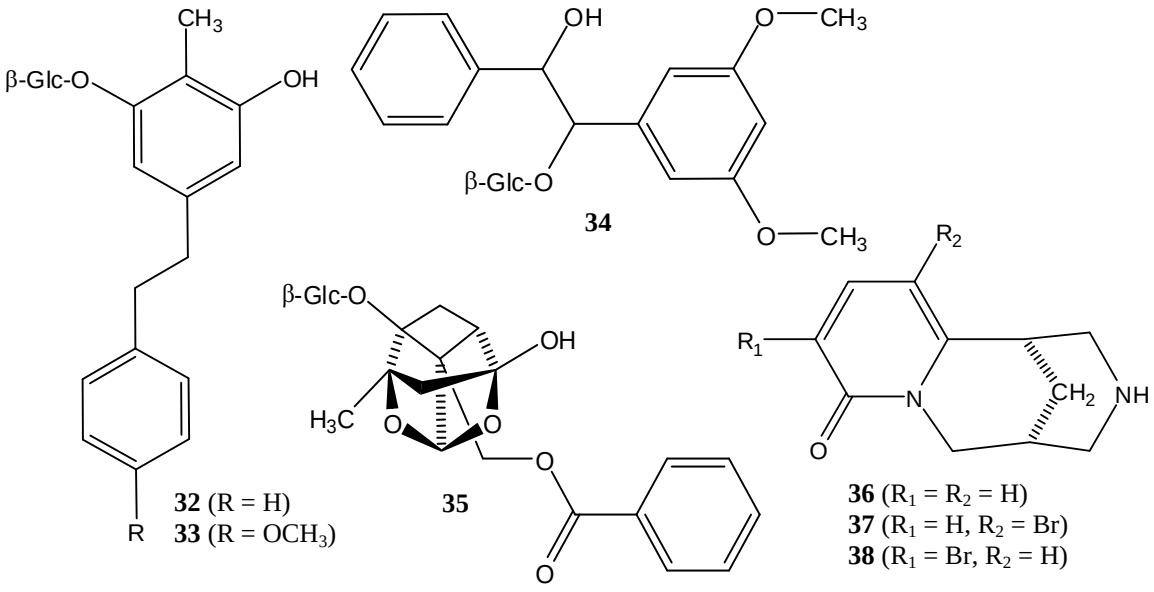

1.4.1 Gsk3 as a target for HD. Although Gsk3 has been identified as a therapeutic target for AD (Giese 2009), there is evidence that it may be useful for HD as well. It has been shown that inhibition of Gsk3 protected cells against m*Htt* toxicity (Carmichael, et al. 2002), and it is possible that the Gsk3 inhibitors described previously (i.e. the manzamines and **4**) as potential AD therapies may also have applications for HD.

1.4.2 Caspase inhibitors. Apoptosis has been implicated as playing an important role in HD, and the blocking of the apoptotic signals through the inhibition of caspases has been proposed to be another potential therapeutic target for this disease (Pattison, et al. 2006). Caspases 1 and 3 are upregulated in HD patients and in HD mouse models and they also are able to enzymatically cleave the huntingtin protein, resulting in an increase in the amount of toxic mutant huntingtin fragments in diseased cells (Cornelis, et al. 2007; Pattison, et al. 2006). Caspase inhibitors have the potential to directly block this causative enzymatic step in the pathogenesis of HD, and as such they make attractive targets for drug discovery efforts.

Discorhabdin P (**39**), isolated from a *Batzella* sp. of deep-water marine sponge, inhibits the caspase CPP32 with an IC_{50} value of 0.78 µM (Gunasekera, et al. 1999). The related compound discorhabdin C (**40**) shows no inhibitory activity against CPP32, which is intriguing since the only structural differences between the two compounds is the presence of a methylamine group on the iminoquinone moiety of **39** as opposed to a secondary amine at the same position in **40**.

1.4.3 Autophagy enhancement. Autophagy refers to the combined processes whereby a cell is able to degrade and recycle large masses, including protein bodies and

even organelles (Davies, et al. 2007). It has been shown that increasing autophagy in cells containing toxic misfolded protein fragments can enhance survival of the cells and increase the clearance of the misfolded proteins from the cells (Davies, et al. 2007). It has been proposed that the enhancement of autophagy may be a good therapeutic target for HD and possibly for other neurodegenerative diseases as well (Davies, et al. 2007; Ravikumar, et al. 2006; Roze, et al. 2008).

Rapamycin (**41**) is a well known secondary metabolite which was first isolated from the bacterium *Streptomyces hygroscopicus* (Sehgal, et al. 1975). Through interactions with its biological target, FKB12, **41** inhibits the mTOR complex, resulting in an upregulation of autophagy, as well as other downstream effects (Graziani 2009; Kang, et al. 2008). It was recently suggested that this ability to increase autophagy may be a useful therapeutic approach to treating HD, especially in combination with lithium treatment, which enhances autophagy through an mTOR independent pathway (Sarkar, et al. 2008). The potential of this combination approach was demonstrated by the protection of flies against m*Htt* induced neurodegeneration in an HD *Drosophila* model (Sarkar, et al. 2008).

1.5 Prion diseases

Prion diseases, also known as transmissible spongiform encephalopathies, are a rare but fatal group of neurodegenerative diseases observed in humans and other mammals (Fontaine and Brown 2009; Geissen, et al. 2007). Although it is estimated that there are only 200 cases diagnosed in the U.S. each year, these diseases require a focused effort for therapeutic development since they are usually fatal within one year of diagnosis and because they are transmissible diseases (NINDS 2010). The most common

prion disease in humans is Creutzfeldt-Jakob disease, but other forms of the disease include kuru, fatal familial insomnia (FFI), and Gerstmann-Straussler-Scheinker disease (NINDS 2010). These diseases are believed to be caused by an infectious agent called a prion, which is a misfolded protein that forms amyloid plaques and is able to transfer its misfolded confirmation to other proteins (Krammer, et al. 2009).

Several cellular models of prion diseases have been developed which have been useful in the development of drug discovery efforts for prion diseases (Krammer, et al. 2009). Almost all of the strategies under investigation as therapies for prion diseases target the prion protein itself and aim to either inhibit the prion misfolding process, reduce the total amount of prion protein in cells or to stabilize the natively folded prion protein (Nicoll and Collinge 2009). Some efforts have been made to identify small molecules that can inhibit the amyloidogenic properties of prions, but these have been almost exclusively from synthetic sources (Schatzl 2009). The investigations of natural products with inhibitory activity against prions have been summarized in the following

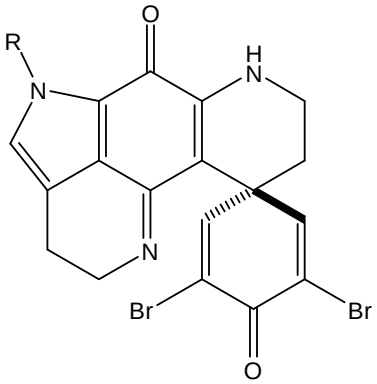

39 (R = CH_3)
40 (R = H)

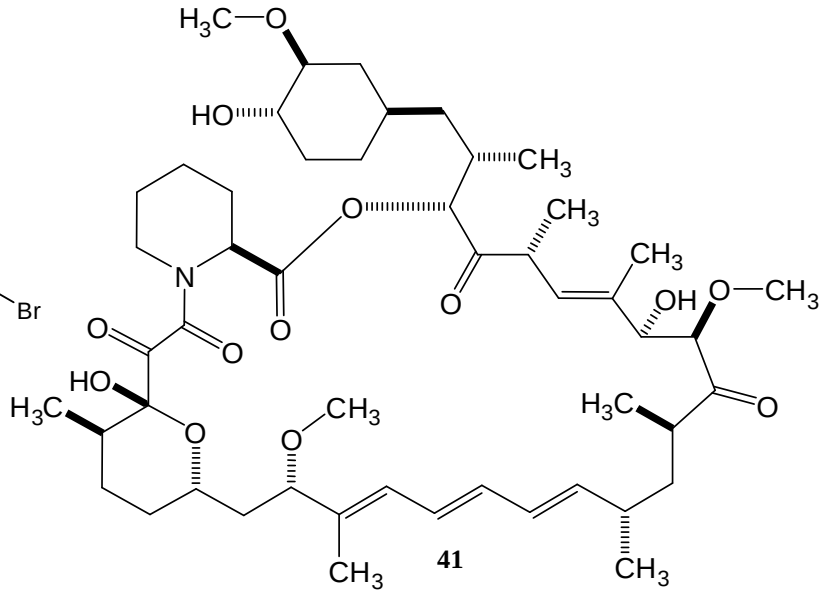

41

sections.

1.5.1 Prion amyloidogenesis inhibition. The polyene macrocycle amphotericin B (**42**) was originally isolated from the *Streptomyces nodosus* in 1955 and has been widely used as an antifungal drug over the past 50 years (Abu-Salah 1996; Lemke, et al. 2005; Mechlinski, et al. 1970; Oura, et al. 1955; Stiller, et al. 1955). Compound **42** reduces the generation of the misfolded form of the prion protein in prion-infected GT1-7 and S12 cells when applied to the cells at a concentration of 4.5 μg/mL (Mange, et al. 2000). No toxicity due to **42** was observed in these cell lines.

The plant metabolite curcumin (**43**) was originally isolated from *Curcuma longa* and a wide variety of biological activities have been reported for it, including several related to other neurodegenerative diseases (Anand, et al. 2008; Lin, et al. 2006). The accumulation of the misfolded form of the prion protein in prion-infected neuroblastoma cells are reduced by treatment with **43** ($IC_{50} \approx 10$ nM) (Caughey, et al. 2003).

The screening of a library of 2000 natural products and drugs was completed in order to identify compounds that inhibit the accumulation of misfolded form of the prion protein in prion-infected cells (Kocisko, et al. 2003). This screening effort identified 17 active compounds with IC_{50} values of ≤ 1 μM. A series of naturally occurring polyphenols, including epicatechin monogallate (**44**), epigallocatechin 3-monogallate (**45**) and 2,3,5,7,3′,4′-pentahydroxyflavin (**46**), were identified which were active both *in vitro* and *in vivo* (Kocisko, et al. 2003).

A series of tetracycline derivatives was recently shown to have anti-prion activity (Forloni, et al. 2009). The analogues doxycycline (**47**) and minocycline (**48**) were particularly effective, both *in vivo* and *in vitro*. These are attractive compounds for therapeutic development since they are already FDA approved antibiotics and are currently undergoing early stage clinical trials (Forloni, et al. 2009).

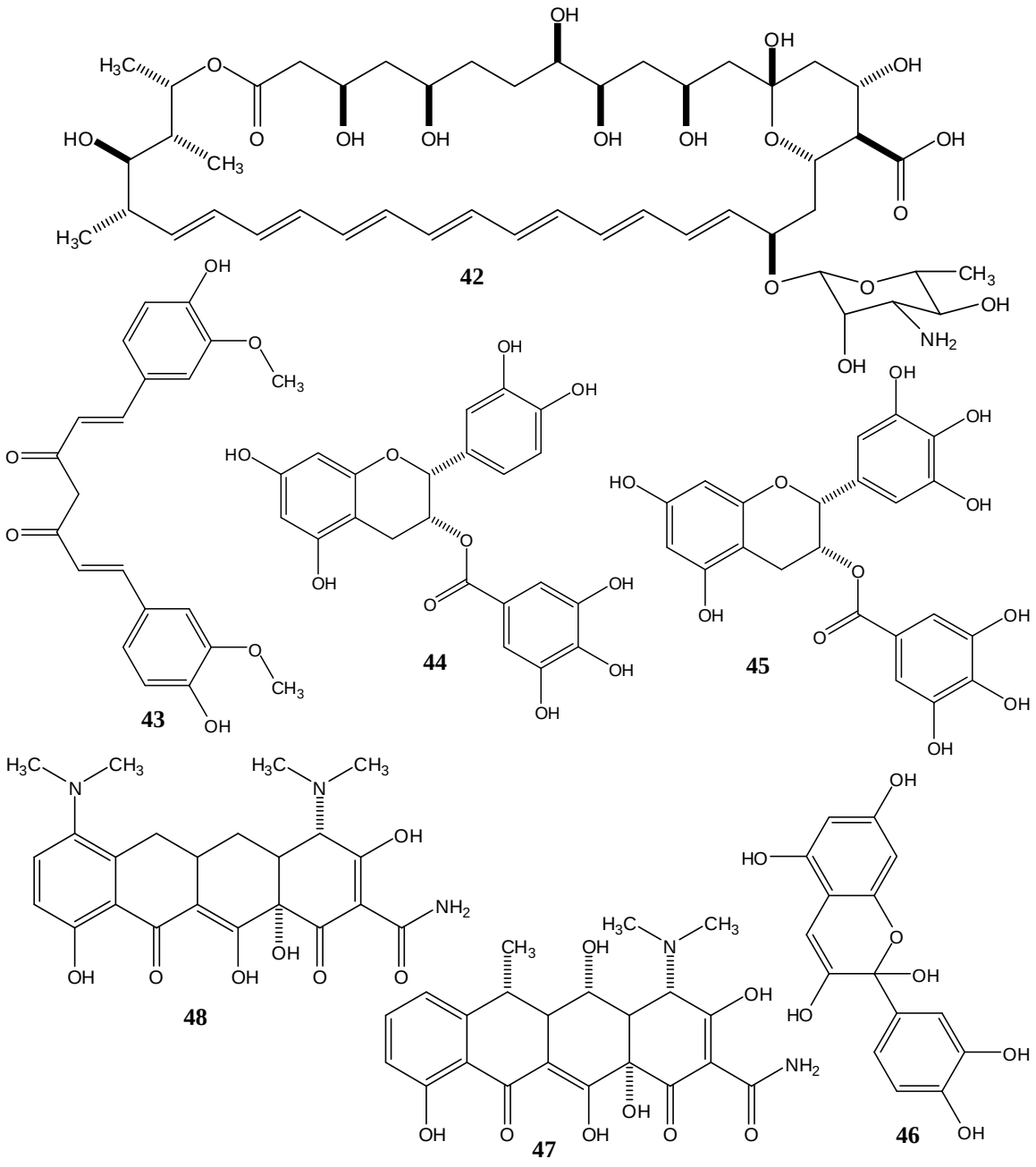

1.6 General neurodegeneration

The similarity of cellular dysfunctions among the neurodegenerative diseases which have been described in the previous sections suggests that therapies may be developed which can effectively ameliorate these diseases through a mechanism which is not specific to any single disorder. There are a variety of bioassays available to identify natural products with therapeutic potential for general neurodegeneration. The most commonly used assays measure protection against glutamate induced neurotoxicity (Dong, et al. 2009; Planells-Cases, et al. 2006; Sheldon and Robinson 2007), neurotrophic activity (Gold and Villafranca 2003; Ohizumi, et al. 2004; Price, et al. 2007; Tohda, et al. 2005), anti-inflammatory activity (Dheen, et al. 2007; Gilgun-Sherki, et al. 2006), and monoamine oxidase inhibition (Van der Schyf, et al. 2006). The various secondary metabolites that have been tested in these assays are summarized here, grouped according to the assays in which they exhibited activity.

1.6.1 Glutamate induced neurotoxicity. Glutamate is a major neurotransmitter in the brain, but excessive exposure to glutamate can lead to the death of neurons due to a process called excitotoxicity (Dong, et al. 2009). Cell death related to glutamate induced excitotoxicity has been implicated in AD, PD, and HD (Planells-Cases, et al. 2006). Many of the damaging effects of excitoxicity are attributed to excessive Ca^{2+} efflux in neurons, which can in turn trigger a signal cascade leading to apoptosis and oxidative stress (Dong, et al. 2009; Sheldon and Robinson 2007). These shared features among a variety of neurodegenerative disorders makes glutamate induced toxicity an attractive target in the search for therapies for neurodegeneration.

Seven iridoid glycosides, 8-*O*-*E*-*p*-methoxycinnamoylharpagide (**49**), 8-*O*-*Z*-*p*-methoxycinnamoylharpagide (**50**), 6′-*O*-*E*-*p*-methoxycinnamoylharpagide (**51**), 6′-*O*-*Z*-*p*-methoxycinnamoylharpagide (**52**), *E*-harpagoside (**53**), *Z*-harpagoside (**54**), and harpagide (**55**), isolated from the roots of *Scrophularia buergeriana* have shown the ability to increase the viability of rat cortical cells upon treatment at concentrations ranging from approximately 0.1-10.0 μM (Kim, et al. 2002). Neural toxicity was determined by the measurement of the release of lactate dehydrogenase into the medium from the cells.

Six dihydropyranocoumarin analogues, 4″-hydroxytigloyldecursinol (**56**), 4″-hydroxydecursin (**57**), (2″*S*,3″*S*)-epoxyangeloyldecursinol (**58**), (2″*R*,3″*R*)-epoxyangeloyldecursinol (**59**), decursinol (**60**), and decursin (**61**), showed the ability to enhance the viability of rat cortical cells treated with a toxic concentration of glutamate (100 μM) (Kang, et al. 2005). All six compounds (**56**-**61**) significantly increased cell viability of the glutamate treated cells at concentrations of 0.1-1.0 μM (Kang, et al. 2005).

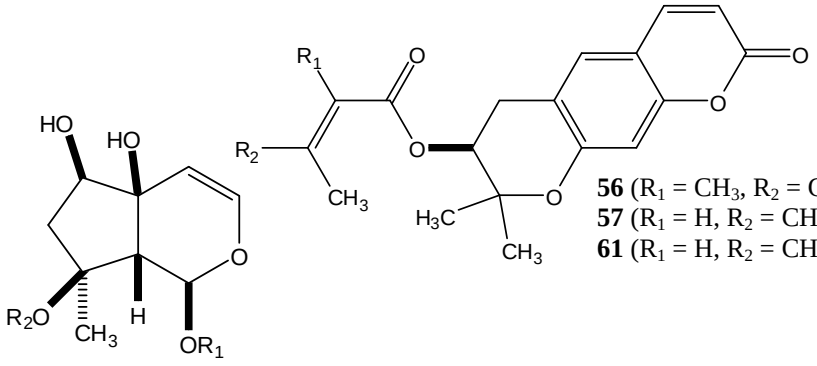

49 (R_1 = β-Glc, R_2 = *E*-*p*-methoxycinnamoyl)
50 (R_1 = β-Glc, R_2 = *Z*-*p*-methoxycinnamoyl)
51 (R_1 = β-Glc-6-*O*-*E*-*p*-methoxycinnamoyl, R_2 = H)
52 (R_1 = β-Glc-6-*O*-*Z*-*p*-methoxycinnamoyl, R_2 = H)
53 (R_1 = β-Glc, R_2 = *E*-cinnamoyl)
54 (R_1 = β-Glc, R_2 = *Z*-cinnamoyl)
55 (R_1 = β-Glc, R_2 = H)

56 (R_1 = CH_3, R_2 = CH_2OH)
57 (R_1 = H, R_2 = CH_2OH)
61 (R_1 = H, R_2 = CH_3

60

58 (2″*S*, 3″*S*)
59 (2″*R*, 3″*R*)

Six liminoid analogues isolated from the root bark of *Dictamnus dasycarpus*, dictamnusine (**62**), dictamdiol A (**63**), fraxinellone (**64**), calodendrolide (**65**), obacunone (**66**), and limonin (**67**), showed significant neuroprotective activity against glutamate-induced neurotoxicity in primary cultures of rat cortical cells at a concentration of 0.1 μM (Kang, et al. 2008). The neuroprotective activity of **62**-**67** was greater than the positive control used in the assay, dizocilpine maleate, a noncompetitive agonist of the NMDA receptor (Kang, et al. 2008).

1.6.2 Neurotrophic activity. Healthy neuronal activity is promoted and maintained by neurotrophins, small proteins which participate in the regulation of a variety of neuronal processes including survival, neurite outgrowth and differentiation of neural stem cells (Connor and Dragunow 1998; Price, et al. 2007). Due to the neuroprotective and neurodegenerative effects of neurotrophins, they have potential for use as therapeutics for neurodegenerative diseases (Connor and Dragunow 1998; Yuen

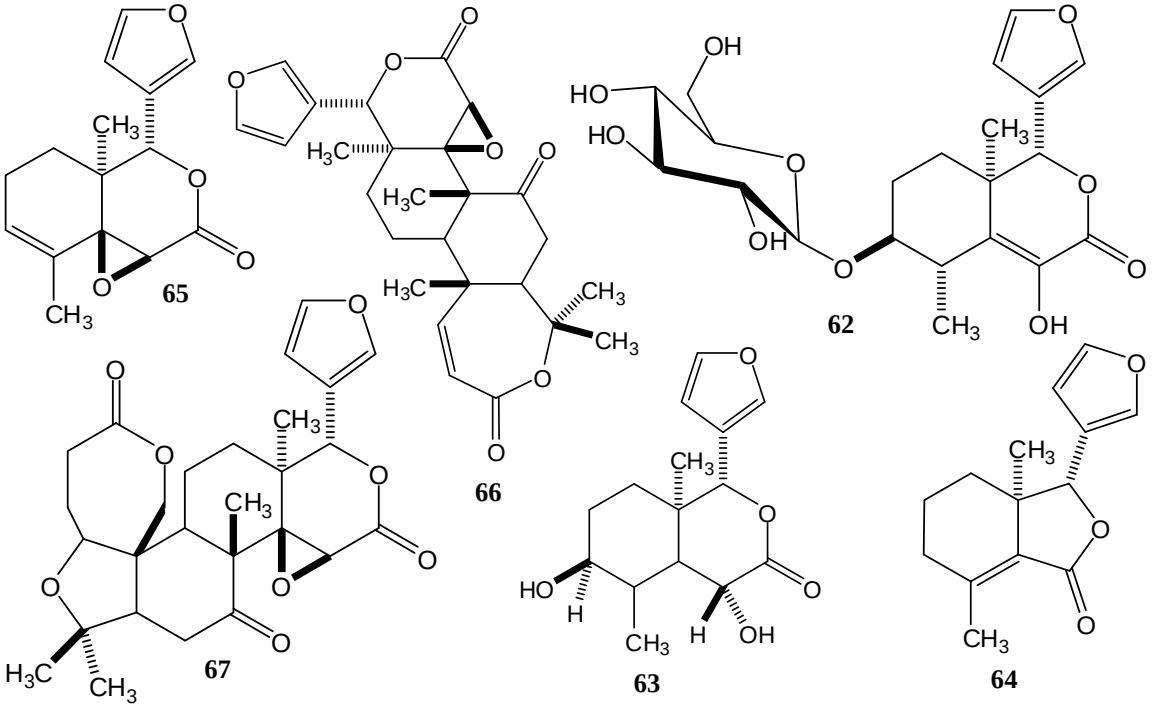

and Mobley 1996), but their poor pharmacological properties make them inferior candidates for therapeutic development (Price, et al. 2007). Therefore, small molecules with good pharmacological properties which are able to potentiate the effects of endogenous neurotrophins such as nerve growth factor (NGF) or modulate neurotrophic targets such as TrkA (the cellular receptor for NGF), hold great promise as therapies for neurodegeneration (Webster and Pirrung 2008). Related to the neurotrophin-focused approach is the attempt to develop stem cell-based therapies for neurodegenerative diseases (Kim and de Vellis 2009). Stem-cell approaches to treating neurodegeneration could be greatly enhanced by the availability of small molecules that can effectively control the differentiation of neural stem cells (NSCs). Although there have been a small number of reviews concerning natural products with neurotrophic activity (Gold and Villafranca 2003; Ohizumi, et al. 2004; Tohda, et al. 2005), the most promising results in this area of research as well as highlights of more recent discoveries are presented here.

Farnisone A (**68**) and C (**69**), isolated from the fungus *Paecylomyces farinosus* RCEF 0101, enhance neurite outgrowth in PC12 cells at a concentrations of 20 and 50 μM, respectively (Cheng, et al. 2004). A third compound, farnisone B, did not enhance neurite growth, even though it differs from **68** only by the presence of a hydroxylamine in the pyridone ring (Cheng, et al. 2004). Although both **68** and **69** induced neurite growth independent of NGF, neither compound was as effective as NGF by itself (Cheng, et al. 2004).

Three diterpenes, kansuinins A (**70**), D (**71**) and E (**72**), isolated from the roots of *Euphorbia kansui* L., were tested for their stimulatory effects on TrkA, the cellular binding target of NGF (Colby, et al. 2004). The survival of TrkA expressing fibroblasts

were specifically promoted by **72** (ED_{50} = 0.2 µg/mL), while **70** and **71** promoted the survival of fibroblasts expressing both TrkA and TrkB (ED_{50} = 7.9 and 0.6 µg/mL, respectively, for TrkA expressing fibroblasts). TrkB is the receptor for brain-derived neurotrophic factor (BDNF), a neurotrophin that has a variety of functions and supports the healthy function of neurons, including cholinergic and dopaminergic neurons (Connor and Dragunow 1998).

The militarinones are a series of alkaloids isolated from the fungus *Paecilomyces militaris* RCEF 0095 (Cheng, et al. 2006; Schmidt, et al. 2002; Schmidt, et al. 2003). Militarinone A (**73**) is the most active in this series, showing a significant enhancement of neurite outgrowth in PC12 cells at a concentration of 33 µM with no associated toxicity. The dehydroxy analog of **73**, (+)-*N*-deoxymilitarinone (**74**), also enhances neurite outgrowth in PC12 cells, but at a concentration of 100 µM. Treatment of human

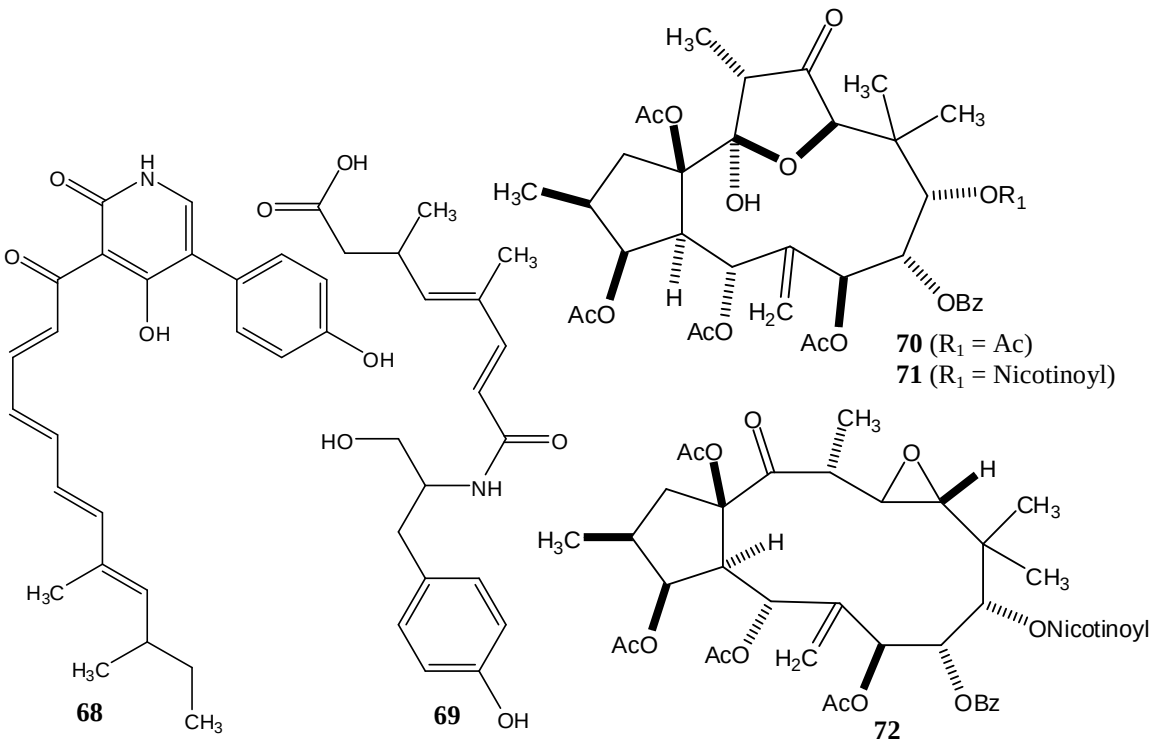

neurons (IMR-32) with **74** at the same concentration (100 µM) is toxic to the cells (Cheng, et al. 2006; Schmidt, et al. 2002). Treatment of PC12 cells with militarinone B (**75**) and C (**76**) at concentrations of 100 µM results in only "marginal" enhancement of neurite outgrowth with very low levels toxicity (Schmidt, et al. 2003).

Ginsenosides Rg3 (**77**), Rk1 (**78**) and Rg5 (**79**), isolated from the roots of *Panax Sanchi-ginseng*, enhance neuronal differentiation of neural stem cells (NSCs) (Durairajan, et al.). The most active of the three compounds is **79**, and its activity is dependent on Ca^{2+} influx through Ca^{2+} channels. The optimal procedure for the induction of differentiation to neurons in NSCs required transient exposure of the NSCs to 8 μM **79** for 24 h followed by 72 h incubation with the same compound at 1 μM (Durairajan, et al.). This treatment causes a general enhancement of cell growth in NSC cultures as well as an increase in the number of neurons and a decrease in the number of astrocytes present in the culture.

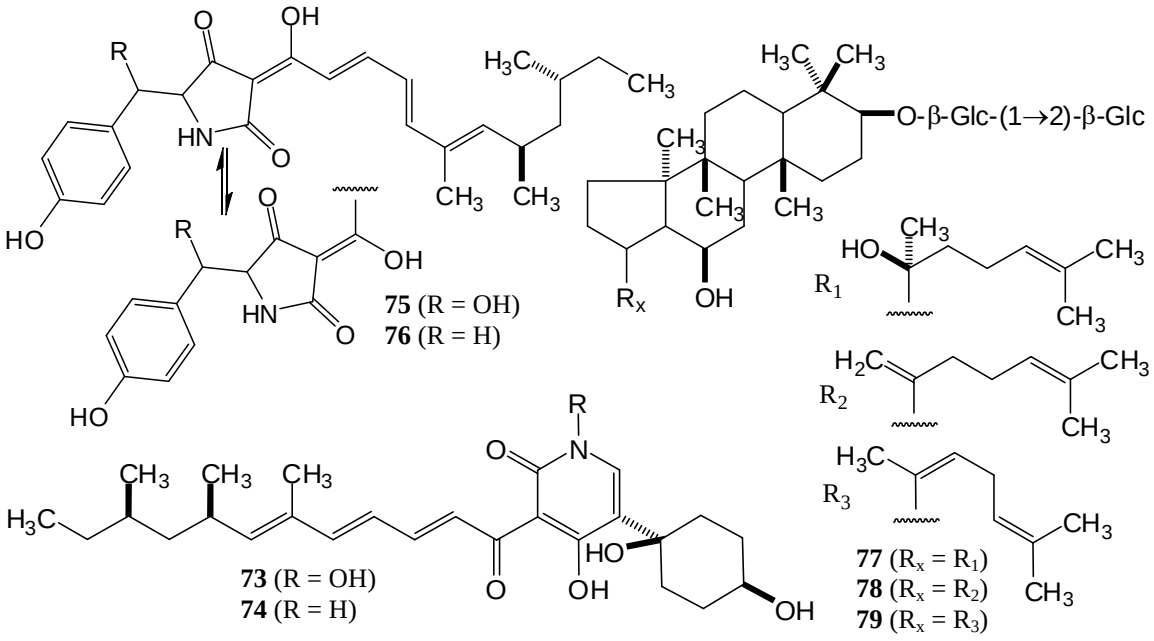

Four sphingolipids, (4*E*,6*E*,2*S*,3*R*)-2-*N*-eicosanoyl-4,6-tetradecasphingadienine (**80**), (4*E*,2*S*,3*R*)-2-*N*-eicosanoyl-4-tetradecasphingenine (**81**), and (4*E*,6*E*,2*S*,3*R*)-2-*N*-docosanoyl-4,6-tetradecasphingadienine (**82**) and (4*E*,2*S*,3*R*)-2-*N*-octadecanoyl-4-tetradecasphingenine (**83**), potentiate the ability of nerve growth factor (NGF) to enhance the outgrowth of neurites in PC12 cells at concentrations of 10 μM (Kwon, et al. 2003). The four compounds (**80**-**83**) were isolated from Bombycis Corpus 101A, a traditional Korean medicinal resource used for the treatment of movement disorders; Bombycis Corpus 101A is made by killing *Bombyx mori* (silk moth) larvae with the fungus *Beauveria bassiana* 101A (Kwon, et al. 2003). Compounds **80** and **82** had greater activity than **81** and **83**, with the primary difference between these compounds being the presence of the C-6 double bond in the more active compounds (Kwon, et al. 2003).

1.6.3 Anti-inflammatory. The inflammatory response in the brain can play a beneficial role in combating neurodegeneration, but chronic inflammation is associated with a variety of neurodegenerative diseases and it has been shown to be a contributing factor to neuronal death (Amor, et al. 2010). Microglia are the resident macrophages in the brain and when activated they are able to combat pathogens, but they can also cause damage to neuronal cells (Dheen, et al. 2007). Activated microglia are the prime participants in neuroinflammation, and they can contribute to neuronal death through a variety of mechanisms, such as the production of reactive nitrogen species (e.g. nitric oxide) and reactive oxygen species (e.g. hydrogen peroxide) (Brown 2007). Consequently, anti-

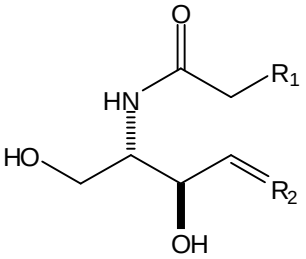

80 ($R_1 = (CH_2)_{17}CH_3$, $R_2 = (CH)_3(CH_2)_6CH_3$)
81 ($R_1 = (CH_2)_{17}CH_3$, $R_2 = CH(CH_2)_8CH_3$)
82 ($R_1 = (CH_2)_{19}CH_3$, $R_2 = (CH)_3(CH_2)_6CH_3$)
83 ($R_1 = (CH_2)_{15}CH_3$, $R_2 = CH(CH_2)_8CH_3$)

inflammatory drugs have been proposed as good candidates for neurodegenerative disease therapies, and some compounds have already entered clinical trials (Gilgun-Sherki, et al. 2006).

The diarylheptanoid (3*R*)-1,7-diphenyl-(4*E*,6*E*)-4,6-heptadien-3-ol (**84**), isolated from the plant *Curcuma comosa*, significantly reduces the expression of inducible nitric oxide synthase (iNOS) and cyclooxygenase 2 (COX-2) in lipopolysaccharide (LPS) treated HAPI microglial cells when applied at a concentration of 1 μM (Thampithak, et al. 2009). In addition, the concentration of the products of iNOS and COX-2, nitric oxide (NO) and prostaglandin E_2 (PGE_2), respectively, were observed to decrease in the treated microglial cells.

Four oxindole alkaloids and one indole alkaloid glycoside exhibited the ability to reduce the amount of NO released by LPS treated rat microglial cells (Durairajan, et al.). Corynoxeine (**85**), rhynchophylline (**86**), isocorynoxeine (**87**), isorhynchophylline (**88**) and vincoside lactam (**89**), isolated from the leaves of *Uncaria rhynchophylla*, were active with IC_{50} values of 15.7, 18.5, 13.7, 19.0 and 16.4 μM, respectively. These values compare favorably with the activity of resveratrol (IC_{50} = 11.5 μM) in the same assay. Interestingly, two other oxindole alkaloids, 18,19-dehydrocorynoxinic acid B (**90**) and 18,19-dehydrocorynoxinic acid (**91**), were not active in the assay, even though the only structural differences between them and compounds **85** and **87** was the stereochemistry of the ethylene groups and the presence of a carboxylic acid rather than a methyl ester (Durairajan, et al.).

Plakortide P (**92**), isolated from the marine sponge *Plakortis angulospiculatus*, reduces the amount of thromboxane B_2 (TXB_2) released by LPS treated rat microglia (IC_{50} = 0.93 µM) (Kossuga, et al. 2008). No cytotoxicity was observed upon treatment with **92** in a variety of mammalian cell lines and it induced the release of only low concentrations of lactate dehydrogenase.

Lobetyolin (**93**) and tetradeca-4*E*,8*E*,12*E*-triene-l0-yne-l,6,7-triol (**94**), isolated from the roots of *Platycodon grandiflorum*, were examined for their ability to activate nuclear factor-κ B (NF-κB) (Dong, et al. 2009). NF-κB is a transcription factor which participates in the activation of microglia and other pro-inflammatory responses (Dheen, et al. 2007). These two compounds (**93** and **94)** increase the transcriptional activity of NF-κB in HEK293 human embryonic kidney cells at a concentration of 20 µM.

1.6.4 Monoamine oxidase inhibitors. Monoamine oxidase (MAO) is an enzyme which deaminates monoamine neurotransmitters, generating hydrogen peroxide as a byproduct (Van der Schyf, et al. 2006). Both the MAO A and B isoforms have been

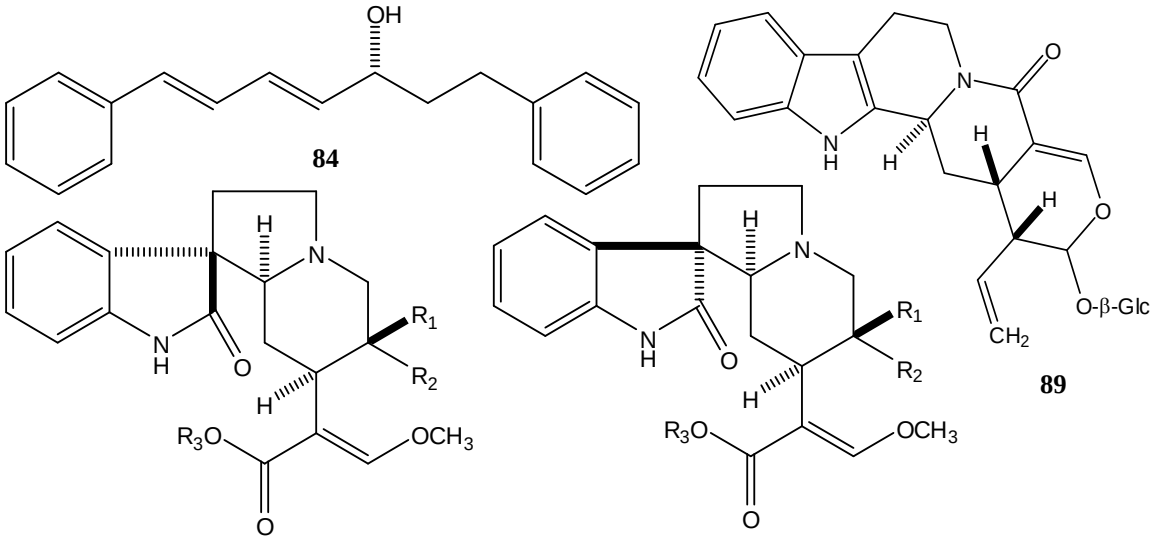

85 (R_1 = H, R_2 = CH=CH_2, R_3 = H)
86 (R_1 = H, R_2 = CH_2CH_3, R_3 = CH_3)
87 (R_1 = H, R_2 = CH=CH_2, R_3 = CH_3)
88 (R_1 = H, R_2 = CH_2CH_3, R_3 = CH_3)
90 (R_1 = CH=CH_2, R_2 = H, R_3 = H)
91 (R_1 = CH=CH_2, R_2 = H, R_3 = H)

implicated as potential targets for neurodegenerative disease (Van der Schyf, et al. 2006). Recent evidence suggests that inhibition of both forms of this enzyme confers neuroprotection through antiapoptotic mechanisms, the reduction of ROS production and stabilization of the mitochondrial membrane (Naoi, et al. 2009). MAO inhibitors have a long history of use in the treatment of PD, but they have more recently shown to have potential as therapeutics for other neurodegenerative diseases (i.e. AD and HD) as well (Van der Schyf, et al. 2006).

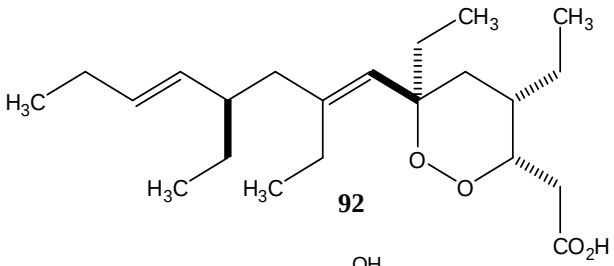

92

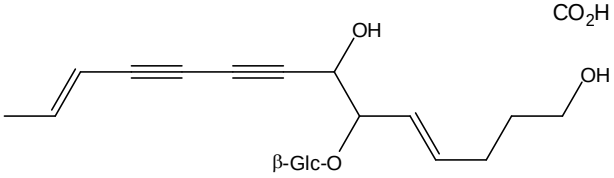

93

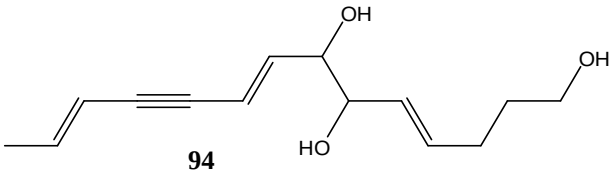

94

Seven xanthone glycosides, corymbiferin 3-*O*-β-D-glucopyranoside (**95**), corymbiferin 1-*O*-β-D-glucopyranoside (**96**), triptexanthone C (**97**), veratriloside (**98**), swertianolin (**99**), norswertianolin (**100**), and swertiabisxanthone-I 8′-*O*-β-D-glucopyranoside (**101**), and three xanthone aglycones, bellidin (**102**), bellidifolin (**103**) and swertiabisxanthone-I (**104**), were isolated from *Gentianella amarella* ssp. *acuta* and examined for their inhibitory activity against MAO A and B (Urbain, et al. 2008). Compounds **102** and **103** show the greatest inhibition of MAO A (91% and 99%, respectively), and these values are greater than that of the positive control pargyline (60%). Paragyline is a known inhibitor of MAO A and B. All 10 compounds inhibit

MAO B, but **96** and **99** show the greatest activity (94% and 71%, respectively), although this activity is less than that of the positive control pargyline (98%) (Urbain, et al. 2008).

1.7 Summary and conclusions

Natural products have been an excellent source of new therapies for neurodegenerative diseases for many decades. Because of their naturally refined biological activities and novel structural features, natural products are well positioned to lead the way in future drug discovery efforts for these disorders. Although there are currently no effective therapies for AD, HD, PD and prion diseases, the increasing number of natural products which can modulate potential drug targets for these diseases points to the development of new therapies in the near future.

Historically, natural products have been heavily utilized in therapies for neurodegenerative disorders, as demonstrated by the clinical use of the acetylcholinesterase inhibitors **1** and **2** in the treatment of AD. Biological targets such as

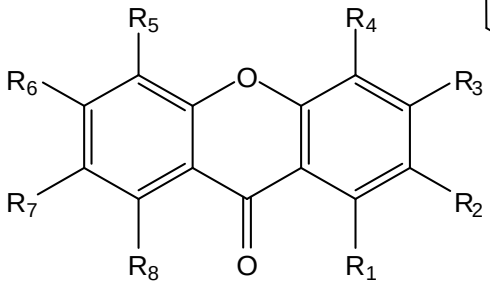

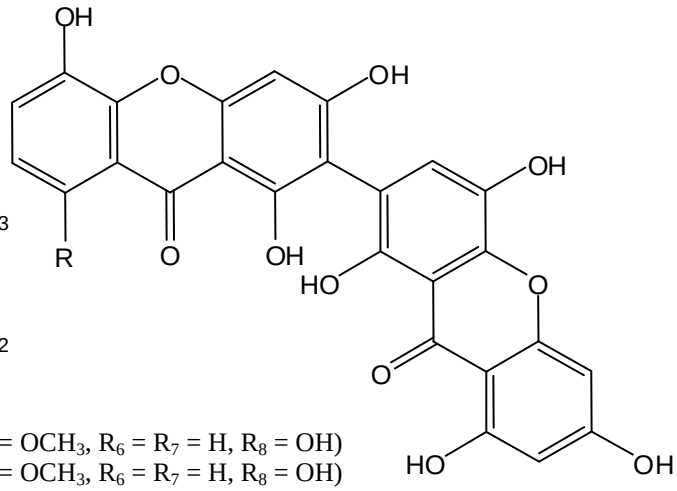

95 (R_1 = OH, R_2 = H, R_3 = β-Glc, R_4 = R_5 = OCH_3, R_6 = R_7 = H, R_8 = OH)
96 (R_1 = β-Glc, R_2 = H, R_3 = OH, R_4 = R_5 = OCH_3, R_6 = R_7 = H, R_8 = OH)
97 (R_1 = OH, R_2 = β-Glc, R_3 = R_4 = H, R_5 = R_6 = OCH_3, R_7 = H, R_8 = OH)
98 (R_1 = OH, R_2 = H, R_3= R_4 = OCH_3, R_5 = R_6 = H, R_7 = β-Glc, R_8 = H)
99 (R_1 = OH, R_2 = H, R_3 = OCH_3, R_4 = H, R_5 = OH, R_6 = R_7 =H, R_8 = β-Glc)
100 (R_1 = OH, R_2 = H, R_3 = OH, R_4 = H, R_5 = OH, R_6 = R_7 =H, R_8 = β-Glc)
102 (R_1 = OH, R_2 = H, R_3 = OH, R_4 = H, R_5 = OH, R_6 = R_7 = H, R_8 = OH)
103 (R_1 = OH, R_2 = H, R_3 = OCH_3, R_4 = H, R_5 = OH, R_6 = R_7 =H, R_8 = OH)

101 (R = β-Glc)
104 (R = OH)

acetylcholinesterase inhibitors for AD and dopamine receptor agonists for PD have traditionally been the focus of investigations of natural products for neurodegeneration. There are many emerging targets for neurodegenerative diseases, however, that are beginning to receive more focus in natural products drug discovery efforts.

Enzymes such as Gsk3 and Cdk5 have generated interest as targets for AD and HD. Compounds such as the manzamines (**5-13**) have demonstrated potent activity against these targets. Secondary metabolites such as **14** and **29**, which can alleviate the toxic effects of Aβ or inhibit its production through inhibition of BACE1, are also receiving attention as potential therapies for AD. Enhancement of autophagy using compounds such as **41** has also been proposed as a therapy for HD and other protein misfolding associated diseases. There are many targets which can be used to ameliorate neurodegeneration in general. A number of natural products have been identified which are able to reduce the harmful effects of glutamate toxicity or chronic inflammation associated with neurodegeneration (i.e. **63** and **84**). Other compounds have neurotrophic activity and hold the potential to reverse the degeneration caused by AD, HD, PD and prion diseases (i.e. **72** and **79**).

More than 100 secondary metabolites have been described in this comprehensive review of the literature pertaining to natural products drug discovery efforts for neurodegenerative diseases associated with protein misfolding. Considering that millions of people suffer from these diseases, the work summarized here provides hope that new, effective therapies for curing these diseases will be available in the future.

The information in Chapter 1 has been adapted from a review paper that is in preparation for the journal Natural Products Reports.

Chapter 2 Hypothesis and Specific Aims

2.1 Hypothesis

Natural products have served a critical role in the development of modern Western medicine (Newman 2008). As shown in the preceding chapter, there are many exciting developments emerging from natural products that may lead to effective therapies for neurodegenerative diseases. The potential drug targets for neurodegenerative diseases which can be modulated by natural products are varied and numerous. Therefore, tools are needed to simultaneously evaluate the activity of many targets at once. Metabolomics, which is the concurrent examination of a pool of metabolites, has demonstrated the capacity to meet this demand for multifaceted drug discovery approaches (Kaddurah-Daouk and Krishnan 2008; Kaddurah-Daouk, et al. 2008).

Given the contributions of natural products towards the development of new therapies for neurodegeneration and the utility of metabolomics for investigating these diseases, it is expected that the metabolomic investigation of a yeast model of neurodegeneration will lead to the identification of metabolic pathways which are perturbed due to the toxicity associated with protein aggregation. Therefore, the following hypothesis has been proposed for this dissertation: **modulation of the metabolic processes which are perturbed due to the toxicity associated with protein aggregation will alter the cellular response to protein aggregation.** In order to explore the validity of this hypothesis, Specific Aims 1 and 2 have been investigated. Specific Aim 3 diverges from the topic of neurodegeneration and instead describes the characterization of a series of diterpenes isolated from a soft coral specimen. Although

the focus of this final project is substantially different from the other work described in this dissertation, its scientific merits make it an important and significant part of my doctoral research.

2.2 Specific Aim 1: Identify the metabolic aberrations underlying mutant huntingtin toxicity in yeast and assess their degree of preservation in humans and mice

Natural products-based drug discovery investigations are reliant upon assays which can identify compounds with biological activities that are relevant to the disease of interest. Although a variety of molecular targets have begun to emerge for developing therapeutics to treat neurodegenerative disease, phenotypic disease models offer several advantages for drug discovery. Phenotypic models have the great advantage of being mechanism blind, allowing for the identification of compounds which are able to modulate disease processes without requiring any prior knowledge of the mechanism. Therefore, phenotypic models can help facilitate the discovery of previously unidentified targets for the disease. However, phenotypic models are often difficult to incorporate into target-specific drug discovery efforts that are common in modern high-throughput pipelines.

Metabolomics is a powerful multi-parameter tool for evaluating phenotypic traits associated with disease processes and provides the means to combine the advantages of phenotypic disease models with the mechanistic information afforded by molecular target approaches. ^{1}H NMR metabolome profiling has been employed in this project to characterize the metabolic aberrations in a yeast model of HD that are attributable to the mutant huntingtin protein's gain-of-toxic-function effects. Multivariate statistical

analysis has been used to compare the results from the yeast HD model to metabolomic data reported from transgenic mice expressing a m*Htt* gene fragment and HD patients.

2.3 Specific Aim 2: Alter the cellular response to toxicity associated with protein aggregation through the modulation of trehalose metabolism

The results of the investigation of Specific Aim 1 revealed that the intracellular concentration of the metabolite trehalose is dramatically altered in response to the presence of m*Htt*. Trehalose is a disaccharide which is found in a variety of microbes, plants and insects (Elbein, et al. 2003). The trehalose cycle in yeast is primarily maintained by seven proteins, encoded for by the genes *TPS1*, *TPS2*, *TPS3*, *TSL1*, *NTH1*, *NTH2* and *ATH1* (Francois and Parrou 2001; Voit 2003). Trehalose is highly effective as a protectant of biomolecules from various types of stress, including desiccation and heat (Crowe 2007; Jain and Roy 2009; Kaushik and Bhat 2003). It has been shown that trehalose can also prevent the aggregation of misfolded proteins both *in vitro* and *in vivo* (Singer and Lindquist 1998).

The effects of m*Htt* expression have been evaluated in a series of yeast strains with gene knockouts for the seven enzymes which participate in trehalose cycle in order to elucidate the role that trehalose plays in the response of yeast to m*Htt*. Each of these knockout strains has been engineered to express either a normal *Htt* protein fragment or a m*Htt* protein fragment. Metabolic profiling has been used in combination with molecular techniques to investigate the altered cellular responses of these engineered strains to m*Htt* protein.

2.4 Specific Aim 3: Ichthyotoxicity and Metabolic Transformation of Select Briarane Diterpenes

Briaranes represent a structurally diverse group of marine-derived diterpenes that are found among several coral species and other invertebrates. The briaranes have demonstrated remarkable biosynthetic adaptability to structural variation, as shown by the fact that changes in structural features have been observed at all 20 positions of the briarane carbon skeleton. More than 500 different briaranes have been reported and many of these have been tested in a wide variety of assays to investigate their biological activities (Sung, et al. 2005; Sung, et al. 2008; Sung, et al. 2002). Many of these assays have examined the potential application of briaranes to human health, but some have also endeavored to ascertain the ecological role of these compounds. Although the ecological function of the briaranes still remains uncertain, an ichthyotoxic role as chemical defensive agents against foraging reef fish is highly probable.

The exploration of a *Briarium* sp. of soft coral collected from Vanuatu has led to the isolation of the three new briaranes designated RAMs A–C. The structures and absolute configurations of these compounds have been determined using a combination of NMR, MS, X-ray diffraction and other techniques. The ecological role of these compounds has been investigated using an ichthyotoxicity assay.

Chapter 3: Identification of the metabolic aberrations underlying mutant huntingtin toxicity in yeast and assessment of their degree of preservation in humans and mice

3.1 Introduction

Huntington's disease (HD) is a progressive neurodegenerative disorder arising from a CAG trinucleotide repeat expansion mutation in the *huntingtin* (*Htt*) gene (Imarisio, et al. 2008; Walker 2007). Individuals carrying mutant forms of *huntingtin* (m*Htt*) encoding for ≥35 glutamine repeats are at risk of developing HD. The number of polyglutamine-encoding CAG repeats in m*Htt* strongly influences the age of disease onset, symptom severity, and rate of HD progression (Langbehn, et al. 2010). Unfortunately, the mechanisms by which m*Htt* and its aggregation-prone protein product causes HD have not yet been determined (Fang, et al. 2007). This lack of information has hampered the establishment of disease-specific biochemical markers for gauging the toxic effects of mutant huntingtin, which has impeded efforts to develop chemical methods for monitoring HD progression.

Several cellular and animal HD models have been constructed to help elucidate the mechanisms responsible for the toxicity of the mutant huntingtin protein including monkeys (Kang, et al. 2008), mice (Masuda, et al. 2008; Menalled, et al. ; Van Raamsdonk, et al. 2007), zebrafish (Diekmann, et al. 2009; Lumsden, et al. 2007; Schiffer, et al. 2007), fruit flies (Branco, et al. 2008; Jackson, et al. 1998; Ravikumar, et al. 2006; Wolfgang, et al. 2005), nematodes (Faber, et al. 1999; Faber, et al. 2002; Jeong, et al. 2009; Satyal, et al. 2000), mammalian cells (Desai, et al. 2006; Igarashi, et al. 2003;

Subramaniam, et al. 2009), and yeast (Giorgini and Muchowski 2009; Krobitsch and Lindquist 2000; Meriin, et al. 2002). Each of these systems has provided important new insights regarding the cellular dysfunctions arising from m*Htt* expression and several of these models have served as screening platforms for HD drug discovery (Barsby and Kubanek 2005; Desai, et al. 2006; Krammer, et al. 2009; Sarkar, et al. 2007b; Wang, et al. 2005; Zhang, et al. 2005). Among these models, the yeast *Saccharomyces cerevisiae* has proven to be exceptionally informative with respect to HD processes due to its ability to recapitulate many of the cellular and molecular features of the disease (Giorgini and Muchowski 2009). Expression of the *N*-terminal portion of m*Htt* in yeast is sufficient to cause the rapid onset of characteristic huntingtin aggregation (Krobitsch and Lindquist 2000) and cell death (Meriin, et al. 2002). The ability of this organism to recapitulate many of the defining phenotypic features of mutant huntingtin is quite remarkable given the fact that yeast lack *Htt* orthologs (Outeiro and Giorgini 2006). Consequently, the yeast model is a valuable tool for understanding the unique gain-of-toxic function properties attributable to m*Htt* and for probing the cellular mechanisms of HD.

S. cerevisiae expressing m*Htt* were used for the purpose of characterizing metabolic biomarkers associated with mutant huntingtin's toxicity. This is the first report in which a non-mammalian transgenic model has been used to critically evaluate perturbations in primary metabolites that stem from mutant huntingtin's toxicity. In addition, a systematic review of published metabolomics studies performed on transgenic mice expressing m*Htt* and humans with HD was conducted in order to identify conserved metabolic features that are disrupted by mutant huntingtin. The data obtained from human and mouse studies were qualitatively compared to results generated from the yeast

model, and this has provided new insight regarding the metabolic disturbances that are attributable to mutant huntingtin's gain-of-toxic-function effects. This information is anticipated to enhance our understanding of mutant huntingtin's impact on biochemical processes in cells and improve strategies for selecting HD biomarkers.

3.2 Experimental Procedures

3.2.1 Yeast strains and media. Construction and maintenance of the HD yeast model has been previously described (Williams, et al. 2007). Briefly, *S. cerevisiae* strains designated "103Q" and "25Q" were prepared that expressed the *N*-terminal fragment of human *Htt* followed by CAG codon repeats encoding for 103 and 25 glutamine (Q) repeats, respectively. The *Htt* fragments were fused to enhanced green fluorescent protein (EGFP) reporters (*C*-terminus) and the constructs were placed under the control of GAL1 promoters. The 103Q and 25Q strains were maintained on uracil-free (plasmid selective marker) synthetic complex media (SC) supplemented with yeast nitrogen base (without amino acids, Sigma-Aldrich), yeast drop-out supplement (with histidine and methionine, Sigma-Aldrich), 0.5% (w/v) ammonium sulfate, and 2% (w/v) glucose. Compared to the 25Q yeast, the 103Q yeast exhibited distinctive phenotypic traits attributable to expression of the human m*Htt* fragment. These features included the characteristic aggregation of the EGFP-labeled mutant huntingtin in 103Q yeast, as well as their significantly reduced viability when cultured under conditions that were permissive for m*Htt*-expression (Appendix, Figure A1).

3.2.2 Metabolomic analysis of 103Q and 25Q yeast. Yeast were grown using a two-stage (I and II) culture process. Stage I cultures were grown in 250 mL wide-mouth Erlenmeyer flasks containing 50 mL SC media supplemented with 2% glucose and

placed on a rotary shaker/incubator (140 rpm, 30 °C) for 24 h. Stage II cultures were prepared by centrifuging stage I cultures (3,000×*g*, 5 min), decanting the supernatant, and suspending the cell pellet in 50 mL SC media supplemented with 2% galactose to induce *Htt* gene fragment expression. Stage II cultures were then incubated with shaking for 16.5 h (140 rpm, 30 °C). Next, stage II cultures were centrifuged (3,000×*g*, 5 min), the supernatant decanted, and the cell pellet immediately suspended in 50 mL methanol (25 °C) and vortexed vigorously. This entire process was carefully monitored to ensure that precisely 20 ± 5 min reproducibly elapsed from the time cultures were removed from the incubator to the moment cells were placed in methanol.

Following 3 h of extraction at 25 °C, cell suspensions were centrifuged (3,000×*g*, 5 min) and the methanol was immediately decanted. The resulting extracts were evaporated *in vacuo* and the remaining organic residues were weighed and stored in 5 dram vials at -20 °C until NMR analysis. Samples were prepared for NMR by adding to each vial a 666 µL aliquot of a solution containing deuterium oxide (D_2O, 99.9% D) with 0.2% w/v sodium azide (bacterial growth inhibitor), 10 mM imidazole (pH indicator), and 0.5 mM 2,2-dimethyl-2-silapentane-5-sulfonate (DSS). The DSS standard is used by the data analysis software (Chenomx NMR Suite v 5.0, described below) as a chemical shift reference, an internal standard for quantification, and chemical shape indicator to assess the shim quality and predict line widths for each analyte. No additional sample clean-up was performed prior to NMR analysis. ^{1}H NMR spectra were collected on a 500 MHz Varian VNMRS-500 spectrometer with a triple resonance probe at 20 °C. Data collection parameters were as follows: number of scans = 64, relaxation delay = 1 s, pulse width = 2.9 µs, acquisition time = 4 s, spectral width = 6200 Hz, temperature = 20.0 °C,

spinning = 20 Hz, data points = 24,876; no steady-state scans were collected and no solvent suppression was used.

3.2.3 Metabolomics data analysis. All ^{1}H NMR FIDs were imported into Chenomx NMR Suite v 5.0 (Chenomx, Inc.) for processing and binning. Each spectrum (0–6 ppm region) was divided into 0.005 ppm bins and the regions containing the residual water (4.750–4.900 ppm) and methanol (3.335–3.350 ppm) signals were removed from further analysis. For the purpose of this investigation, focus has been placed on the 0–6 ppm portions of the ^{1}H NMR spectra because preliminary analyses showed that no significant changes occurred in the downfield portions of the full spectra (up to 12 ppm).

Prior to statistical analyses, all Fourier-transformed ^{1}H NMR data sets were normalized by expressing the peak intensities in each bin as a percentage of the total area under the curve for the 0–6 ppm region of the spectrum. Data sets were analyzed by principal components analysis (PCA) with XLSTAT (Addinsoft, Inc.). PCA is a data reduction technique that transforms data via a linear combination to uncorrelated orthogonal variables (principal components), allowing sources of variation in the data to be categorized (Jolliffe 2002). Individual metabolites were manually identified using the Chenomx NMR Suite (Appendix, Table A1) and then quantified by comparison to the internal DSS standard. Additional experiments using 2D NMR techniques (^{1}H-^{1}H TOCSY, ^{1}H-^{13}C HSQC, and ^{1}H-^{13}C HMBC) and spiking of samples with authentic standards were used to verify each metabolite identified in this study (data not shown). Spectral regions representing galactitol (3.660–3.695, and 3.945–3.985 ppm) and acetate (1.900-1.960 ppm) were removed from the principal components analysis because these

compounds were present in large and highly variable quantities that were unduly influential in terms of their effects on each sample's profile. Instead, these metabolites were manually annotated and quantified for statistical evaluation. Two-tailed, parametric *z*-tests were performed using XLSTAT.

3.2.4 Metabolomic analysis of potassium cyanide, amphotericin B, and cycloheximide treated 103Q and 25Q yeast. Stage I and stage II were prepared as described in the experimental procedures, with the exception that stage II cultures were treated with either potassium cyanide (Way 1984), amphotericin B (Palacios, et al. 2007), or cycloheximide (Obrig, et al. 1971) at concentrations of 46 µM, 38 nM, and 98 nM, respectively. Concentrations of toxins were chosen that inhibited 25Q yeast growth to 30% of the growth of untreated controls. Data was collected and analyzed as described above.

3.2.5 Systematic review and comparison of published HD metabolic profiles. A systematic review of the literature was conducted to identify published data from model systems and humans that described metabolic changes associated with mutant huntingtin toxicity. The PubMed database (United States National Library of Medicine, National Institutes of Health) was utilized to perform a comprehensive search for articles published prior to August of 2009. A broad set of search criteria were utilized, which included pairing the search terms "Huntington's disease," "Huntington's chorea," "Huntington disease," "Huntingtons," and "Huntington" in combination with "biomarker," "metabolite," "metabolic," "metabolomics," "metabonomics," "metabolism," "MRI," "magenetic resonance imaging," "mass spectrometry," "neurochemical," "NMR," "nuclear magnetic resonance," and "spectroscopy."

Only studies in which m*Htt* expression was determined to be responsible for inducing HD in humans or an HD-like condition in model organisms were retained for analysis. Work employing non-m*Htt*-based systems (e.g., 3-nitropropionic acid induced neuronal toxicity) was excluded since it is uncertain the degree to which these approaches mimic HD pathogenesis (Tsang, et al. 2009). The resulting reference set was independently reviewed by two individuals and studies were retained for analysis if 1) one or more primary metabolites were identified and 2) methods for assessing changes in the concentrations of the metabolites were described. The complete list of metabolic changes observed in these studies is provided in Table A2 in the Appendixes.

The amassed data were quantitatively assessed using correspondence analysis (CA) (Greenacre 1992; 2007; Greenacre and Degos 1977). This method provides a means for analyzing qualitative data in a graphical format. Weighted profile values are calculated for tabular (row-column) data and the relative similarities between weighted profile points are described in terms of their χ^2 distances. Prior to performing CA, the data (Appendix, Table A2) were reformatted into a contingency table that was suitable for testing (Appendix, Table A3). For the purpose of this investigation, data set were structured to reflect the number of times each metabolite's concentration was reported to have changed significantly in yeast, mice, and humans in response to mutant huntingtin toxicity. CA was performed and visualized using XLSTAT.

3.3 Results

3.3.1 ^{1}H NMR determination of 103Q and 25Q yeast intracellular metabolites. Analysis of the ^{1}H NMR spectra generated from 103Q and 25Q yeast strains was undertaken using the Chenomx NMR Suite v 5.0 library of primary

metabolites. This facilitated the detection of 29 compounds whose identities were confirmed by comparisons with 1D (Appendix, Table A1) and 2D NMR data generated from authentic standards. Even with no sample cleanup prior to ^{1}H NMR analysis, the observed signal detection was excellent, which enabled the confident assignment of proton resonances that were subject to considerable signal overlap (Figure 3.1). Biomolecules were identified which represent a wide range of metabolically and chemically distinct classes including amino acids (4-aminobutyrate, alanine, arginine, asparagine, aspartate, glutamate, glutamine, histidine, isoleucine, leucine, methionine, phenylalanine, proline, threonine, tryptophan, tyrosine, and valine), a nucleoside (adenosine), a cofactor (NAD^{+}), and osmolytes (glycerol, trehalose), as well as

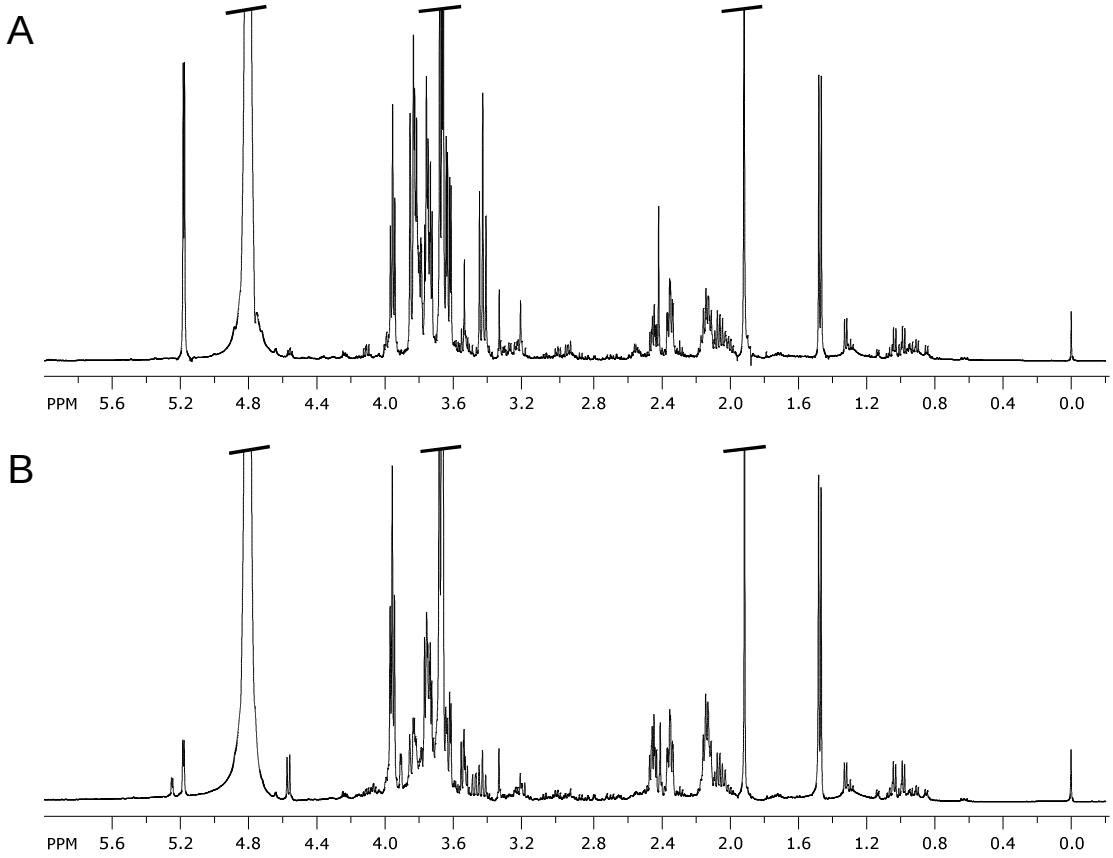

Figure 3.1. Representative ^{1}H NMR spectra (δ_H 0–6 ppm) of A) 25Q and B) 103Q HD yeast extracts acquired at 500 MHz in D_2O with 0.2% w/v sodium azide, 10 mM imidazole, and 0.5 mM DSS.

metabolites associated with energy metabolism (ATP, acetate, formate, galactose, propylene glycol, succinate) and stress response (glutathione). Galactitol was also identified, but its definitive biochemical role(s) in yeast is not well defined.

3.3.2 Expression of m*Htt* alters the metabolome of 103Q yeast. The application of principal components analysis (PCA) was tested as a multivariate statistical method for reducing the dimensionality of the metabolomics data. It was anticipated that this would enable the identification of changes in the metabolic profiles of HD yeast attributable to mutant huntingtin's toxicity. Examination of the ^{1}H NMR data by PCA revealed well-defined clusters for the metabolite profiles of 103Q and 25Q yeast (Figure 3.2). Remarkably, these data represent an accumulation of 61 replicates per strain, which were collected by three individuals from 17 independent experiments carried out over a non-consecutive 17 week period. The notable clustering of these data, despite the relatively challenging conditions used for this experiment, demonstrates the robustness and reproducibility of this metabolomics approach.

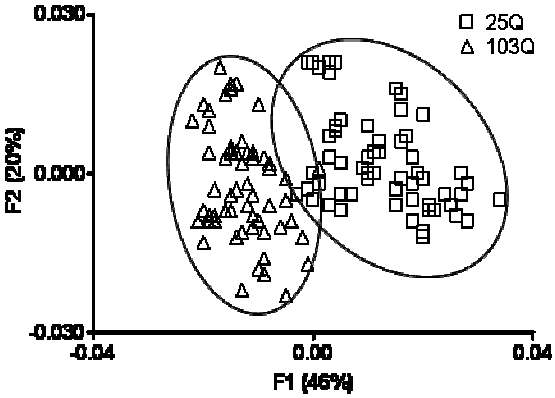

Figure 3.2. PCA scores plot of ^{1}H NMR data for 25Q (□) and 103Q (△) yeast. Data points represents single experimental replicates (n = 61 for each strain). The data were obtained from 17 different experiments performed on different days and show notable consistency. Substantial differentiation between the 25Q and 103Q yeast metabolomes is reflected in the distinct clustering among replicates of the two HD yeast strains.

Inspection of the loadings plot from the F1 axis (Figure 3.3) revealed several regions in the ^{1}H NMR spectra that substantially contributed to the metabolic differences between yeast expressing normal versus mutant *Htt* fragments. In view of the fact that the

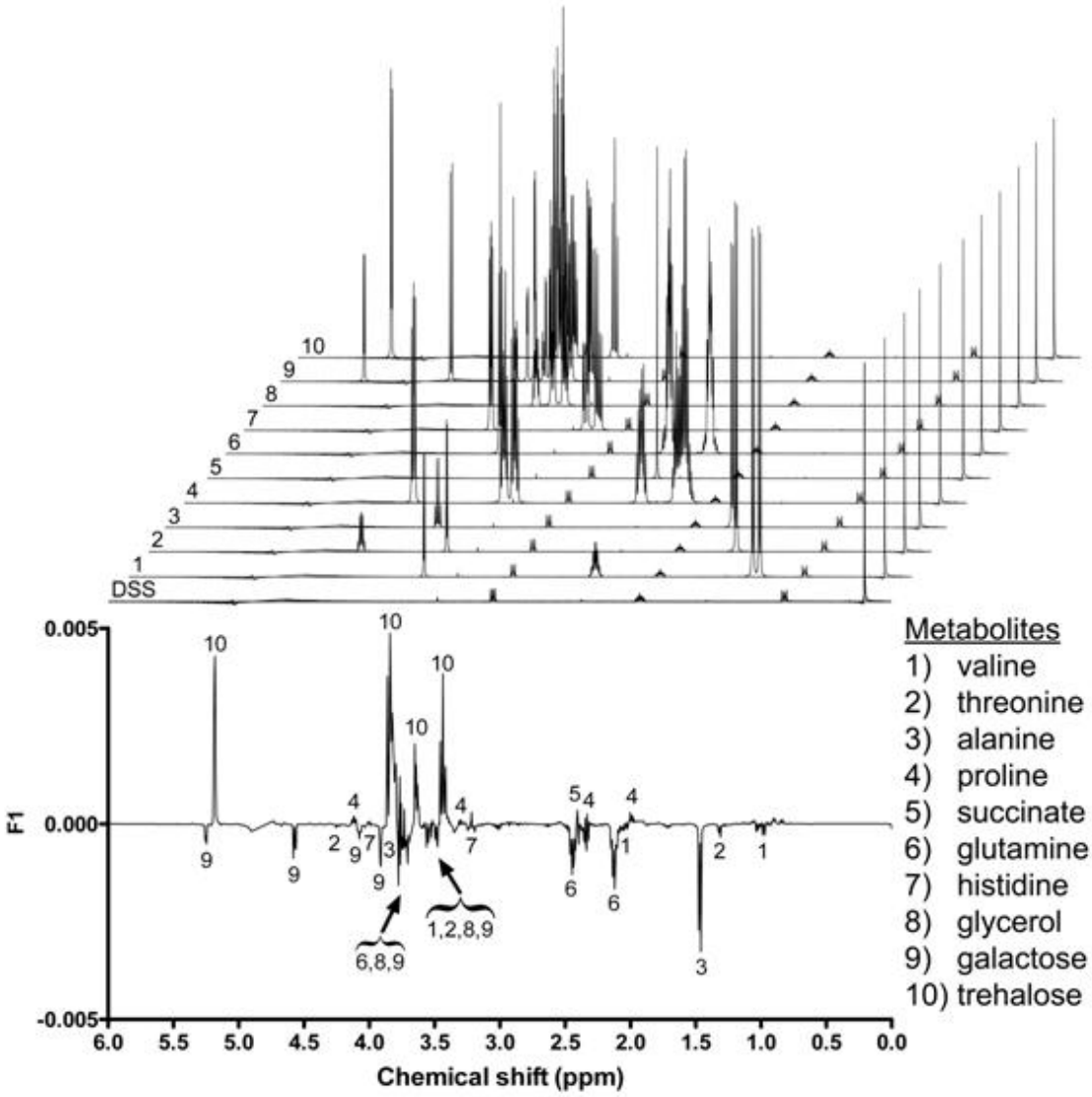

Figure 3.3. Loadings plot of the F1 axis from the PCA of 25Q and 103Q yeast metabolomes. The loadings plot was used to identify sources of variability that contributed to the differentiation between 25Q and 103Q yeast. Regions of high variability that corresponded to decreased (phased upward) or increased (phased downward) concentrations of primary metabolites in 103Q yeast are labeled. Modeled spectral data for each metabolite (and DSS standard) are stacked above the loadings plot for reference.

sole difference between 25Q and 103Q yeast was the number of CAG repeats present in

their respective *Htt* gene fragments, this enabled the use of the loadings plot data to search for metabolic changes that were attributable to mutant huntingtin's toxicity. These data assisted in the identification of 11 metabolites that exhibited substantial variations in their respective concentrations between the two yeast strains (Figure 3.3). The significantly altered metabolites included alanine, galactose, glutamine, glycerol, threonine, and valine, which were more abundant in 103Q yeast, while acetate, histidine, proline, succinate, and trehalose were markedly decreased (note: although acetate levels significantly decreased in 103Q yeast (Figure 3.4), they were removed from PCA analysis (Figure 3.3) due to their disproportionate and overwhelming influence during the initial statistical analysis). Using a quantitative method based on an internal DSS standard (Weljie, et al. 2006), the concentrations for each of the 11 metabolites in the 25Q and 103Q samples (Figure 3.4) were determined. No attempt was made to ascertain the recoveries for the 11 substances; therefore, this data does not represent their absolute cellular concentrations in yeast. However, the recovery efficiencies can be assumed to be equivalent because

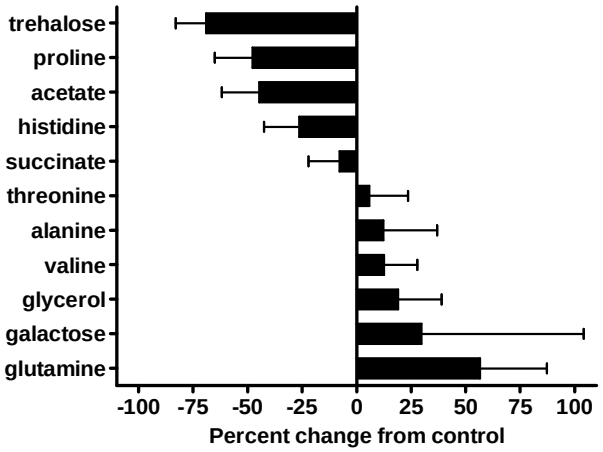

Figure 3.4. Changes in the relative concentrations of metabolites identified by PCA of 25Q and 103Q yeast. The sample concentrations of the metabolites were determined by quantifying the integrals attributed to each of the non-exchangeable proton resonances in all 25Q and 103Q samples and expressing them relative to an internal DSS standard. Data are expressed as the percent change in metabolite concentration in 103Q yeast relative to control 25Q yeast. A two-tailed, parametric *z*-test ($\alpha = 0.05$) was used to determine the significance of the change in relative concentrations for each metabolite ($n = 61$). Bars represent the mean relative metabolite concentration and standard deviations. All values were significantly different from zero with $P \leq 0.0001$ except for galactose ($P = 0.0018$) and threonine ($P = 0.0096$).

all of the sample extractions were carried out under identical conditions, thus enabling the determination of the relative percent change in the quantity of each primary metabolite. Using this approach, the relative concentrations of the 11 metabolites identified from the F1 loadings plot were shown to be significantly (two-tailed parametric *z*-test, $\alpha = 0.05$) altered in yeast expressing a human m*Htt* fragment (Figure 3.4).

Although the changes in the relative concentrations of primary metabolites had been ascribed to the toxic effect of mutant huntingtin, the possibility that some or all of the variation observed might be reflective of a generalized 'toxic' response in yeast could not be ruled out. Therefore, the impact of several small molecule toxins on the yeast metabolome was explored. The compounds potassium cyanide (inhibits complex IV of the mitochondrial electron transport chain), amphotericin B (forms pores in cellular membranes leading to the release of electrolytes), and cycloheximide (inhibits ribosomal protein biosynthesis) were screened against 25Q yeast at concentrations that caused decreases in cell proliferation equivalent to the ~30% reduction in 103Q versus 25Q cell growth following galactose-induced expression of the m*Htt* fragment. Examination of the ^{1}H NMR data by PCA revealed that each of the toxins caused restructuring of the yeast metabolome in a manner that was distinct from the 103Q yeast profile (Appendix, Figure A2). Moreover, the individual metabolites (along with their respective changes in concentrations) that contributed to the toxin-induced metabolic profiles were different from those distinguishing 103Q versus 25Q yeast (data not shown). This supported the conclusion that changes in the yeast metabolome induced by m*Htt* fragment expression are reflective of a specific gain-of-toxic function response stemming from mutant huntingtin's toxicity.

3.3.3 Comparison of conserved HD metabolic features in humans, mice, and yeast. It became clear through the course of this work that a multispecies comparison of metabolomics datasets would facilitate the identification of primary metabolites that are candidate conserved biomarkers for mutant huntingtin's gain-of-toxic function properties. Identifying these biomarkers is important since huntingtin's effects in humans are speculated to result from a combination of both loss-of-function and gain-of-toxic-function properties (Cattaneo, et al. 2005; Imarisio, et al. 2008). A systematic review of published studies documenting the metabolic changes exhibited in HD patients (Nicoli, et al. 1993; Reynolds, et al. 2005; Taylor-Robinson, et al. 1996; Underwood, et al. 2006) and transgenic mice expressing m*Htt* (Jenkins, et al. 2005; Jenkins, et al. 2000; Tkac, et al. 2007; Tsang, et al. 2006; Underwood, et al. 2006) was conducted in order to 1) identify which cellular metabolites were present in the mouse model and humans with HD and 2) determine which of these metabolites changed in response to disease. Correspondence analysis (CA), a descriptive multivariate statistical technique that is used for creating maps depicting the underlying relationships among categories of tabularized data, was selected as a statistical tool for this study. This technique enabled the direct comparison of results from the HD yeast model with data obtained from metabolomics experiments performed in mice and humans. In this case, CA was used to probe for primary metabolites whose concentration changes in yeast, mice, and humans were indicative of a generalized metabolic response to m*Htt* toxicity.

The metabolic changes reported in mice and humans were combined with results derived from HD yeast and the data were arranged in a contingency table identifying 1) the frequency with which each metabolite's concentration was reported to have changed significantly and 2) the specific biological system in which metabolic changes occurred (Appendix, Table A3). Examination of the multispecies dataset by CA resulted in the separation of the variables into two categories (organism and metabolite) along the principal axes, which accounted for all of the variation (inertia) in the data set (Figure 3.5). The CA plot revealed that the overall metabolic patterns of yeast, mice, and humans were distinguishable from one another. Interestingly, the metabolomes of mice and humans were clearly separated from yeast along the first principal (F1) axis; however, the profiles of yeast and mice were distinct from humans in the second principal (F2) dimension. Further inspection of the CA plot revealed that several metabolites responded similarly in two or more HD systems, which suggested that these metabolites could be potential biomarkers for toxicity associated with m*Htt* expression. Therefore, focused attention was placed on examining the relationships among these metabolites in reference to their source organisms.

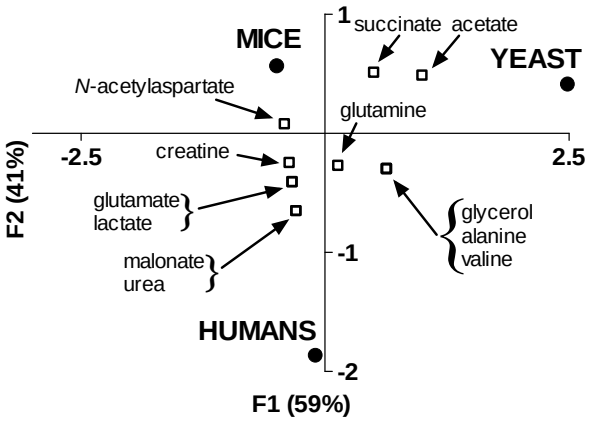

Figure 3.5 Asymmetric plot from CA of metabolic changes reported for cells in which m*Htt* expression occurs. For CA, column profiles represent the different biological systems (humans, mice, yeast), while row profiles represent the metabolites identified as having undergone significant changes. Metabolites that were reported from a single HD model occupy coordinates that superimpose upon the source organism. For clarity, these metabolites have been removed from this diagram, but they can be found in Supporting Information, Table 3.

Examination of the CA plot revealed that the four metabolites, alanine, glutamine, glycerol and valine exhibited similar changes in model organisms and humans expressing *mHtt* (Figure 3.5). The occurrence of these four metabolites in the CA plot in a region that was central to both the F1 (separating mice and humans) and F2 (separating mice and yeast) dimensions indicates that alanine, glutamine, glycerol and valine might be important multispecies biomarkers for gauging mutant huntingtin's gain-of-toxic effects. Other notable trends that were observed in the CA plot included the co-localization of creatine, glutamate, lactate, malonate, *N*-acetylaspartate, and urea with mice and humans in the F1 dimension. This indicates that these six metabolites behaved similarly in both mammalian systems. We also noted that succinate and acetate clustered in the F2 dimension of the CA plot with mice and yeast, which indicated that these metabolites responded similarly in the two model organisms. Besides alanine, glutamine, glycerol and valine, no additional metabolites were observed that were unique solely to yeast and humans.

3.4 Discussion

Metabolomics is concerned with determining the identities, concentrations, and distributions of small molecules in living systems with the presumption that the resulting metabolic profiles are reflective of an organism's physiological status. Therefore, perturbation to an organism's biological processes should result in distinct changes to its steady-state metabolome, making metabolomics a powerful multi-parameter profiling technique that is well suited for identifying disease-dependent metabolic aberrations (Dunckley, et al. 2005; Gowda, et al. 2008; Kaddurah-Daouk and Krishnan 2008; Powers 2009). A metabolomics approach has been applied as a tool for discerning the unique

gain-of-toxic function effects attributable to mutant huntingtin's toxicity in a HD yeast model and these results have been compared to the metabolic restructuring that occurs in human HD patients and transgenic mice.

Using a yeast model to map metabolites that exhibited significant shifts in their relative intracellular concentrations showed that disruptions are detected in the steady-state concentrations of small molecules whose metabolic pathways are seemingly independent (Figure 3.6). For example, the biochemically distinct compounds trehalose,

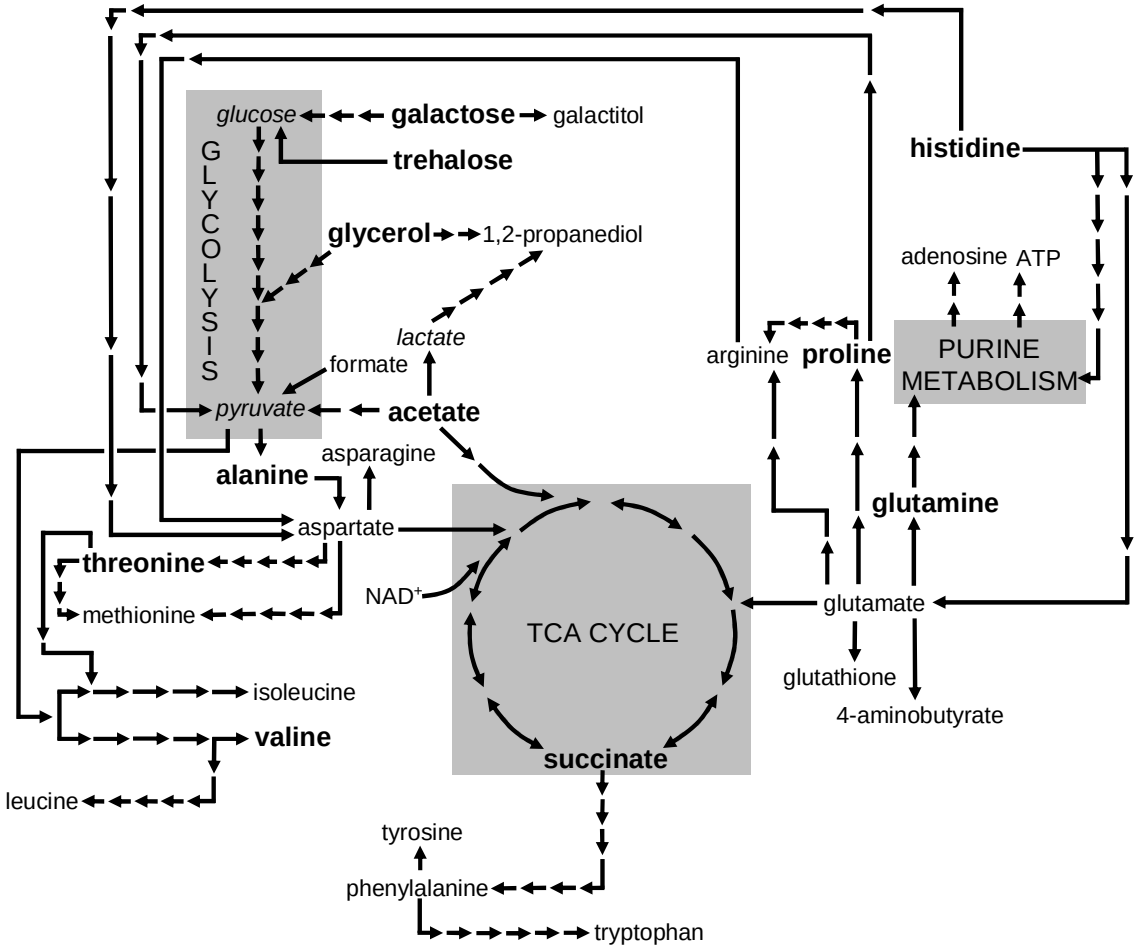

Figure 3.6. Map illustrating the biochemical linkages among the primary metabolites identified in HD yeast. Only the most predominant metabolic pathways are shown for simplicity. Metabolites shown in bold underwent significant concentration changes in 25Q versus 103Q yeast. Arrows represent individual metabolic (enzymatic) steps required for biotransformation (note – italicized metabolites were not observed in yeast extracts, but represent known and important metabolic links).

proline, glutamine, galactose, and acetate exhibited large changes in their respective concentrations following m*Htt* expression. However, if these metabolites are considered in terms of their major cellular roles – energy storage/generation (acetate, galactose and trehalose) and maintenance of intracellular nitrogen pools (glutamine and proline) – then potential links among these small molecules begin to emerge. Consequently, metabolomics can be used to provide evidence for errant or disrupted regulatory processes that are involved in HD-related cell death. However, caution should be used in applying this form of interpretation to these findings since inferences based simply on assigning gross biochemical roles to individual metabolites can be deceptive of their true functions within complex metabolic networks (Steuer 2006).

Several conserved metabolic changes have been observed that are shared among HD yeast, mice, and humans (Figure 3.7), and this has revealed what appears to be a core set of phenotypic (metabolic) markers related to m*Htt* expression. The metabolites alanine, glutamine, glycerol, and valine show substantial promise as biomarkers for gauging mutant huntingtin's gain-of-toxic function effects. It is anticipated that metabolomics and other '-omics'-based strategies will have important applications that may be applied to discerning the cellular mechanisms of HD. However, at the present time, it is not immediately apparent how altered levels of alanine, glutamine, glycerol, and valine are linked to mutant huntingtin's toxicity. Further experiments will be needed to probe the relationships among cellular pathways that are impacted by mutant huntingtin.

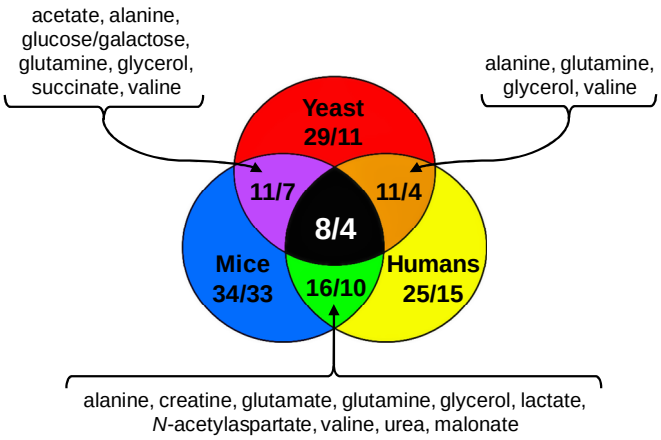

Figure 3.7. Venn diagram illustrating similarities among the metabolomes of humans, mice, and yeast expressing m*Htt*. Pairs of integers represent the number of metabolites identified within a given organism or set of organisms (first integer) versus the number of biomolecules that are reported to undergo significant concentration changes (second integer). Among the eight metabolites that are reported from all three HD systems, four (alanine, glutamine, glycerol, and valine) undergo significant shifts in concentrations following mutant huntingtin expression. The metabolites listed in the diagram are those found significantly altered in the three pair-wise comparisons (clockwise from left side: yeast and mice, mice and humans, and yeast and humans). A complete list of all metabolites is provided in Supporting Information, Table 2.

Despite the passing of nearly two decades since the genetic basis of HD was defined (MacDonald, et al. 1993), no clinically-approved therapeutic agents have been developed that allay the toxicity component of this disorder (Fecke, et al. 2009). One exciting potential application of the multispecies approach described above to investigating mutant huntingtin's toxicity is this method's capacity for sifting through large biomarker sets so that metabolic perturbations arising from the disruption of conserved biological features can be identified. These pathways are anticipated to provide focused insight into the biochemical networks that may be involved in HD and respond positively to therapeutic modulation. Currently, several of these pathways are being explored further as part of a comprehensive effort to develop novel therapeutic approaches for treating the underlying toxicity component of mutant huntingtin. It is anticipated that these efforts toward this endeavor will be reported in due course.

The material in Chapter 3 is adapted from Joyner et al. Journal of Proteome Research ***2010,*** 9 *(1), 404-412*.

Chapter 4 Alteration of the cellular response to toxicity associated with protein aggregation through the modulation of trehalose metabolism

4.1 Introduction

The recent metabolomic examination of the baker's yeast (*Saccharomyces cerevisiae*) model of Huntington's disease (HD) demonstrated the practicality of using metabolic profiling to investigate the metabolic aberrations associated with HD (Joyner, et al. 2010). Huntington's disease (HD) is a progressive neurodegenerative disorder arising from a CAG trinucleotide repeat expansion mutation in the *huntingtin* (*Htt*) gene (Imarisio, et al. 2008; Walker 2007). Individuals carrying mutant forms of *huntingtin* (m*Htt*) encoding for ≥35 glutamine repeats are at risk of developing HD, and the number of polyglutamine-encoding CAG repeats in m*Htt* strongly influences the age of disease onset, symptom severity, and rate of HD progression (Langbehn, et al. 2010). The recent metabolomic examination of the yeast HD model revealed that the metabolite which showed the greatest change in concentration in response to m*Htt* expression was trehalose (Joyner, et al. 2010).

Trehalose is a disaccharide which is found in a variety of microbes, plants and insects (Elbein, et al. 2003). The trehalose cycle in yeast is primarily maintained by seven proteins, encoded for by the genes *TPS1*, *TPS2*, *TPS3*, *TSL1*, *NTH1*, *NTH2* and *ATH1* (Figure 4.1) (Francois and Parrou 2001; Voit 2003). The protein products of *TPS1*, *TPS2*, *TPS3* and *TSL1* combine to form the trehalose synthase complex, which catalyzes in two steps the formation of trehalose from glucose-6-phosphate and UDP-glucose. Trehalose is hydrolyzed by the products of *NTH1* and *ATH1*. In contrast to the

other proteins in the trehalose cycle, the function of the protein product of *NTH2* is not well understood.

Biomolecules can be protected from many types of stress, including desiccation and heat, by the presence of trehalose (Crowe 2007; Jain and Roy 2009; Kaushik and Bhat 2003). It has been shown that trehalose can also prevent the aggregation of misfolded proteins both *in vitro* and *in vivo*, which lends support to its putative role as a chemical chaperone (Singer and Lindquist 1998). These results have inspired the exploration of the use of trehalose to inhibit the aggregation of disease-related proteins in a handful of neurodegenerative disorders, including Alzheimer's disease, prion diseases and HD (Beranger, et al. 2008; Fung, et al. 2005; Liu, et al. 2005; Qi, et al. 2009; Tanaka, et al. 2005).

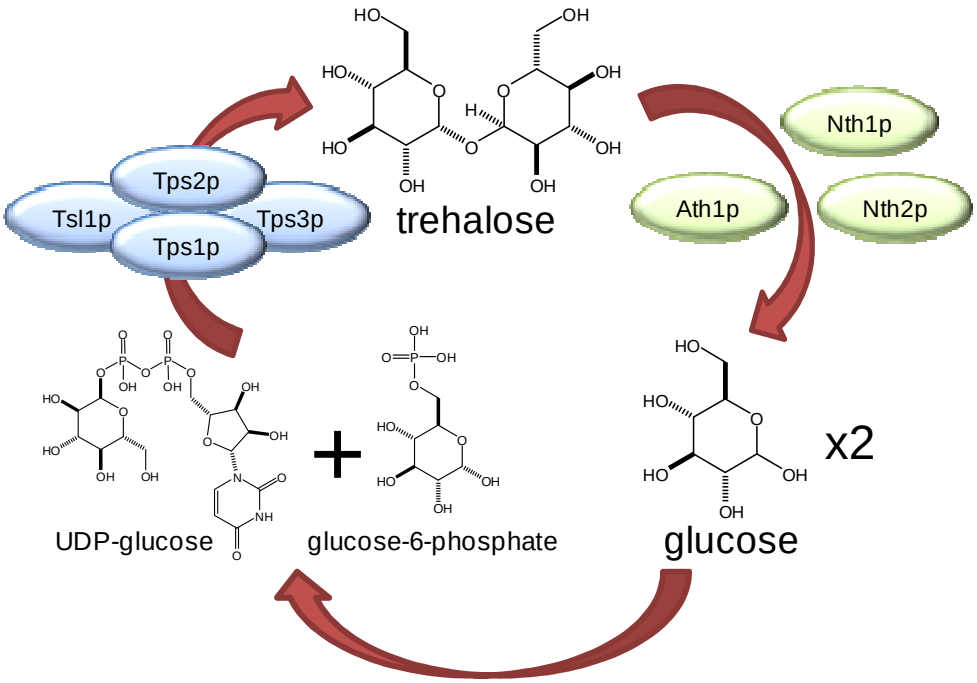

Figure 4.1 The trehalose metabolic cycle in yeast. Trehalose is biosynthesized from UDP-glucose and glucose-6-phosphate in a two-step process by the trehalose synthase complex (Tps1p, Tps2p, Tps3p, and Tsl1p). Trehalose can be hydrolyzed to form glucose by the neutral trehalases (Nth1p and Nth2p) and by acid trehalase (Ath1p).

In this study, a series of yeast strains with gene knockouts for each of the genes which participate in the trehalose cycle were engineered to express either normal *Htt* or m*Htt*. The deletion of *ATH1* leads to the elevation of intracellular concentrations of trehalose and the alleviation of the reduced cell growth caused by m*Htt* expression. The metabolic profiles of each strain were also analyzed, showing that the metabolic aberrations associated with the expression of m*Htt* can be decoupled from the toxicity of the mutant huntingtin protein. Finally, the mechanism of protection against mutant huntingtin toxicity by trehalose was explored using a series of protein degradation inhibitors.

4.2 Experimental Procedures

4.2.1 Yeast strains, plasmids and transformations. Seven *Saccharomyces cerevisiae* knockout strains prepared in the background BY4742 (MATα *his3Δ1 leu2Δ0 lys2Δ0 ura3Δ0*) were used in this study (Table 1). The plasmids containing the huntingtin construct were prepared and used as described previously (Williams, et al. 2007). Briefly, constructs containing the *N*-terminal fragment of human *Htt* followed by CAG codon repeats encoding for either 103 or 25 glutamine (Q) repeats fused at the *C*-terminus to enhanced green fluorescent protein (EGFP) reporters were placed under the control of GAL1 promoters (Zhang, et al. 2005). Transformations were performed using the lithium acetate-heat shock method (Gietz and Schiestl 2007). Transformation success was confirmed by observation of fluorescing huntingtin-EGFP and by reverse transcriptase (RT) PCR amplification of huntingtin-EGFP mRNA. Strains expressing the construct with 103 glutamine repeats or 25 glutamine repeats were designated “103Q” and “25Q”, respectively. The 103Q and 25Q lines of each strains were maintained on

uracil-free (plasmid selective marker) synthetic complex media (SC) supplemented with 2% (w/v) glucose.

Table 4.1 *S. cerevisiae* strains used in this study

Strain	Genotype
BY4742	MATα *his3Δ1 leu2Δ0 lys2Δ0 ura3Δ0*
Δ*tps1*	isogenic to BY4742, Δ*tps1::KanMX*
Δ*tps3*	isogenic to BY4742, Δ*tps3:: KanMX*
Δ*tsl1*	isogenic to BY4742, Δ*tsl1:: KanMX*
Δ*ath1*	isogenic to BY4742, Δ*ath1:: KanMX*
Δ*nth1*	isogenic to BY4742, Δ*nth1:: KanMX*
Δ*nth2*	isogenic to BY4742, Δ*nth2:: KanMX*

4.2.2 Yeast growth assays (spot tests). Yeast cultures were grown for 24 hours in SC media supplemented with 2% (w/v) glucose. Prior to performing the assays, the optical density of each culture was determined and the cultures were diluted to ensure that each assay began with a uniform number of cells. Cells were spotted onto SC agar media supplemented with 2% (w/v) galactose in four five-fold dilutions and incubated at 30˚ C.

4.2.3 Fluorescent microscopy and image processing. All microscopic images were collected using an Olympus BH-2 microscope (Olympus America Inc.) with an Olympus DApo100x oil-immersion objective, a BH2-RFL-T3 high pressure mercury burner and SPOT Insight 2 MP digital camera (Diagnostic Instruments, Inc.). Images were uniformly cropped to remove empty space in the image and adjusted for contrast and brightness.

4.2.4 Confirmation of gene transcription using RT-PCR. Expression of the *Htt*-EGFP constructs was confirmed using reverse transcriptase (RT) PCR. Total RNA was isolated from yeast cultures using an RNEasy Mini Kit (Qiagen, Inc.) and reverse transcriptase and PCR reactions were carried out in a single tube for each sample. Amplified products were analyzed using agarose gel electrophoresis.

4.2.5 Metabolomic characterization of yeast strains. Collection and analysis of metabolomics data from the yeast model of HD has been described previously by our group (Joyner, et al. 2010). Briefly, yeast were grown using a two-stage (I and II) culture process at 30 °C. Stage I cultures were grown in 50 mL SC media supplemented with 2% (w/v) glucose for 24 h. Stage II cultures were prepared by centrifuging stage I cultures, decanting the supernatant, and suspending the cell pellet in SC media supplemented with 2% (w/v) galactose to induce *Htt* gene fragment expression. After 16.5 h, stage II cultures were centrifuged, the supernatant was decanted, and the cell pellet was immediately suspended in methanol. After 3 h of extraction, cell suspensions were centrifuged and the methanol was decanted. The solvent in the resulting extracts was evaporated *in vacuo* and the samples were prepared for NMR by adding 666 µL of a solution containing deuterium oxide with a pH indicator (10 mM imidazole) and an internal standard (0.5 mM 2,2-dimethyl-2-silapentane-5-sulfonate (DSS)) to each sample. No additional sample clean-up was performed prior to NMR analysis. ^{1}H NMR spectra were collected on a 500 MHz Varian VNMRS-500 spectrometer with a triple resonance probe at 20 °C.

4.2.6 Metabolomics data analysis. Data were analyzed as described previously with minor modifications (Joyner, et al. 2010). Briefly, all ^{1}H NMR FIDs were imported into Chenomx NMR Suite v 5.0 (Chenomx, Inc.) for processing and binning. The 0–6 ppm region of each spectrum was divided into 0.005 ppm bins and the regions containing the signals for residual water (4.750–4.900 ppm) and methanol (3.335–3.350 ppm) were removed from further analysis.

All processed ^{1}H NMR data sets were normalized to the total area under the curve for the 0–6 ppm region of the spectrum prior to statistical analyses. Chenomx NMR Suite was used to manually identify metabolites and quantify their respective concentrations based upon comparisons to an internal DSS standard. Principal components analysis (PCA) was used to analyze the data sets with the software package XLSTAT (Addinsoft, Inc.). Two-tailed, parametric *t*-tests were performed using XLSTAT.

4.2.7 Protein degradation inhibition assay. Yeast strains were grown in SC media supplemented with 2% (w/v) glucose for 24 h and standardized aliquots were taken from each culture, centrifuged, and re-suspended in 50 mL 0.85% (w/v) sodium chloride solution. Ten-fold dilutions were made from the sodium chloride-yeast suspension into SC media supplemented with 2% (w/v) galactose and 200 µL aliquots were transferred into the wells of a 96-well microplate. The protein degradation inhibitors phenylmethylsulfonyl fluoride (PMSF), tunicamycin and salinosporamide were then added to individual wells of the microplate at final concentrations of 1 mM, 0.25 µg/mL and 1 µM, respectively.

4.3 Results

4.3.1 Transformation of yeast knockout strains and comparison of their growth profiles. A series of yeast knockout strains deficient for genes involved in trehalose metabolism were engineered to express either a normal *Htt* fragment (25Q) or m*Htt* fragment (103Q). Successful transformations were completed for the wild type strain (BY4742) and five of the seven knockouts, which were designated WT-25Q, WT-

103Q, Δ*tps1*-25Q, Δ*tps1*-103Q, Δ*tps3*-25Q, Δ*tps3*-103Q, Δ*nth1*-25Q, Δ*nth1*-103Q, Δ*nth2*-25Q, Δ*nth2*-103Q, Δ*ath1*-25Q and Δ*ath1*-103Q.

The growth profiles of all 10 transformants were compared using spot cultures on agar plates (Figure 4.2). Remarkably, the Δ*ath1*-103Q line grew almost as well as the Δ*ath1*-25Q line. This enhanced growth strongly suggested that the lack of functional Ath1p resulted in a reduction in the toxic effects of the mutant huntingtin protein. The growth profiles of the WT, Δ*nth1*, Δ*nth2* and Δ*tps3* strains were almost identical, with the 103Q lines for each of these strains growing significantly less than the 25Q lines due to the toxic effects of mutant huntingtin (Figure 4.2). The Δ*tps1* lines grew much less than the others, which was not unexpected since these lines should not be able to produce any trehalose, thus leading to a reduction in growth. However, the Δ*tps1*-25Q line still grew more than the Δ*tps1*-103Q line, indicating that even in this background mutant huntingtin exhibits toxicity.

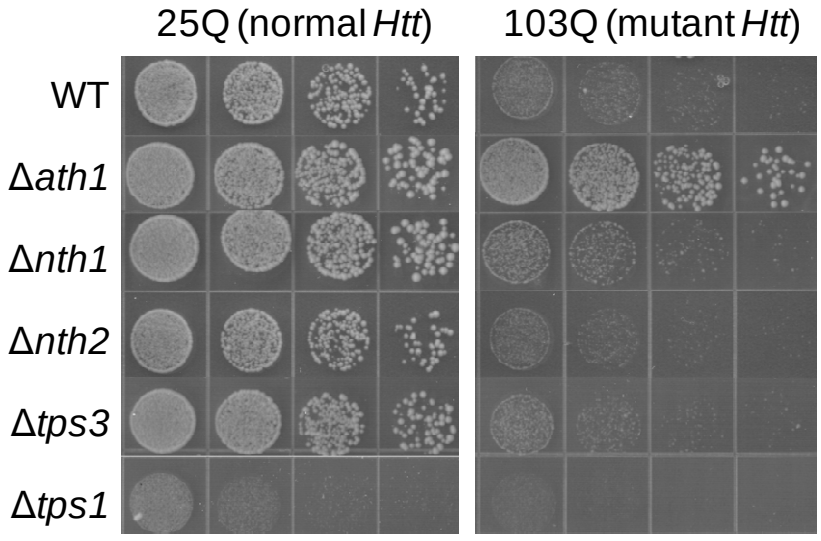

Figure 4.2 Yeast cell growth assay of 25Q and 103Q lines of yeast knockout strains. The Δ*ath1*-103Q line was the only line with enhanced growth while expressing m*Htt*.

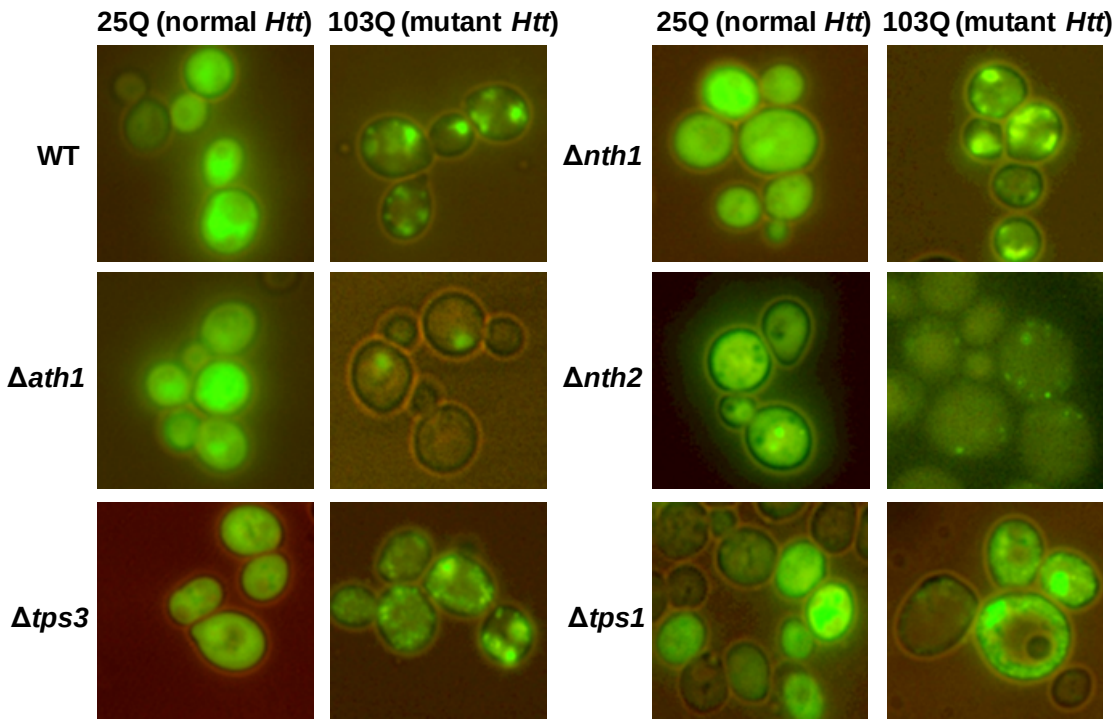

Figure 4.3 Fluorescence microscope images of yeast knockout strains expressing human *Htt* fragments. Images of the 25Q and 103Q line of each knockout are shown. Aggregates are visible in all of the 103Q lines except Δ*ath1*-103Q. No aggregates are visible in any of the 25Q lines. All images are shown at equivalent magnifications.

4.3.2 Comparison of mutant huntingtin aggregation in yeast knockout strains. Fusion of the huntingtin fragments at the *C*-terminus to enhanced green fluorescent protein (EGFP) enabled us to visualize the huntingtin fragment in all 10 transformants (Figure 4.3). All of the 25Q lines exhibited similar appearances, showing that the normal huntingtin was diffused throughout the cells. In contrast to the 25Q lines, the WT-103Q line exhibited a series of pronounced aggregates distributed throughout the cells. Both the Δ*nth1*-103Q and Δ*tps3*-103Q lines had similar phenotypes to the WT-103Q line. Interestingly, the Δ*nth2*-103Q line displayed a different phenotype from the other 103Q lines, with only very small aggregates visible in the cells and in much fewer numbers. The Δ*tps1*-103Q line was similar to both the WT-103Q and Δ*nth2*-103Q lines

in that it contained aggregates, but differed from the other strains in that it contained a large number of very small aggregates that were distributed evenly throughout the cell.

The Δ*ath1*-103Q line exhibited a very different phenotype in which the huntingtin-EGFP was localized to what appeared to be a single compartment. Although the low fluorescent intensity observed in the Δ*ath1*-103Q line suggested that the amount of transgenic protein in the cell was very low, RT-PCR confirmed that the m*Htt*-EGFP construct was being expressed at similar levels as in the WT-103Q line.

4.3.3 Metabolic profiling of yeast knockout strains and measurement of intracellular trehalose concentration. The metabolic profiles of the transformants were determined by ^{1}H NMR metabolomics. PCA was used to analyze these data and to investigate changes in the metabolite profile of each strain. As previously observed (Joyner, et al. 2010), the metabolic profiles of the WT-25Q and WT-103Q lines were distinct and did not overlap, indicating severe perturbations in primary metabolic functions in response to the expression of the m*Htt* fragment (Figure 4.4).

The metabolic profile of the Δ*ath1*-103Q line was indistinguishable from those of the Δ*ath1*-25Q and WT-25Q lines (Figure 4.4a). These similarities suggested that the Δ*ath1* deletion conferred protection from mutant huntingtin toxicity, which is in agreement with the enhanced growth observed in the spot test assay (Figure 4.2). Surprisingly, the profile of the Δ*nth1*-103Q line was also indistinguishable from those of the Δ*nth1*-25Q and WT-25Q lines (Figure 4.4b), even though no growth enhancement was observed in the spot test assay. The metabolic profiles of the Δ*nth2* lines mimicked those of the WT lines, with both of the 103Q lines clustering together and both of the

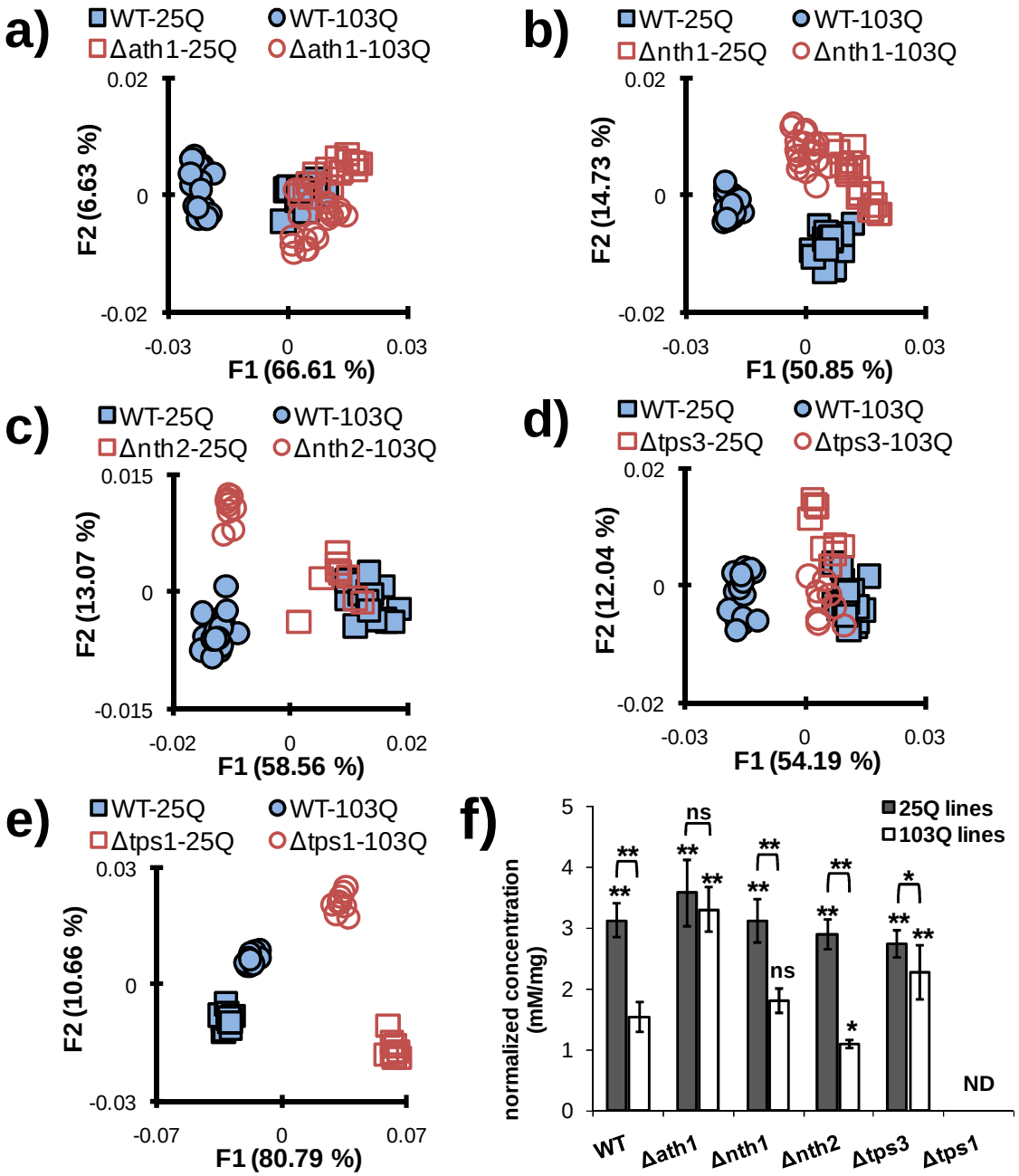

Figure 4.4 Scatter plot from PCA of metabolic data for 25Q and 103Q lines of WT (*n* = 18) vs a) Δ*ath1* (*n* = 18), b) Δ*nth1* (*n* = 18), c) Δ*nth2* (*n* = 9), d) Δ*tps3* (*n* = 9), and e) Δ*tps1* (*n* = 9). The percentage value in each axis lable represents the total amount of independent variation in the data set which is captured by that axis. f) The intracellular concentration of trehalose in yeast knockouts as determined from yeast extracts generated for metabolomic analysis. Asterisks over bars indicate significance of difference from WT-103Q based on a Dunnet's 2-sided test. Asterisks over brackets indicate significance of difference between values in 25Q and 103Q lines of each strain based on a Student's *t*-test (** $P < 0.0001$, * $P \leq 0.01$, ns = not significant, ND = not detected).

25Q lines clustering together (Figure 4.4c). Similar to the Δ*nth1* lines, the profile of the Δ*tps3*-103Q line was indistinguishable from those of the Δ*tps3*-25Q and WT-25Q lines

(Figure 4.4d). These similarities in metabolic profile between the 103Q and 25Q lines of Δ*nth1* and Δ*tps3* stand in stark contrast to the growth profile of these transformants (Figure 4.2). The metabolic profile of the Δ*tps1*-25Q and Δ*tps1*-103Q lines were quite unique, with a dramatic separation from the WT lines in the F1 axis (Figure 4.4e). Examination of the F1 loadings plot from the PCA showed that this large separation was primarily due to the extreme difference in trehalose concentrations between the Δ*tps1* and WT lines (4.4f).

The relative intracellular concentration of trehalose was also determined for each transformant (Figure 4.4f). Trehalose concentrations in the 103Q lines were generally much lower than in the 25Q lines, particularly for the WT, Δ*nth1* and Δ*nth2* lines. However, the concentration of trehalose was indistinguishable between the Δ*ath1*-25Q and Δ*ath1*-103Q lines. Trehalose was detected in higher concentrations in the Δ*tps3*-103Q line than in most of the other 103Q lines, but it was still significantly lower than in the Δ*tps3*-25Q line and much lower than the observed trehalose concentration in the Δ*ath1* lines. No trehalose was detected in any of the Δ*tps1* lines, which is in agreement with previous observations (Bell, et al. 1998).

4.3.4 Inhibition of protein degradation in yeast HD model. In view of the emerging link between the protective role of trehalose in cells and its impact on protein processing and degradation, we examined a series of protein degradation inhibitors in the WT and Δ*ath1* strains. Three inhibitors were selected which target different protein degradation pathways in yeast: PMSF, salinosporamide and tunicamycin. PMSF disrupts autophagy by inhibiting serine proteases involved in the degradation of autophagic bodies, leading to a severe reduction in autophagy (Jones 1991; Takeshige, et al. 1992).

Salinosporamide is a potent inhibitor of the 20S proteasome, reducing the functionality of the ubiquitin-proteasome system (Feling, et al. 2003). Tunicamycin inhibits protein glycosylation, leading to the accumulation of unfolded proteins in the endoplasmic reticulum (ER) which induces ER stress. The concentration of each inhibitor was determined based upon published examinations of the activity of these compounds in yeast systems.

The effects of the three protein degradation inhibitors were determined by measuring the relative amount of huntingtin per cell as well as the total growth of the

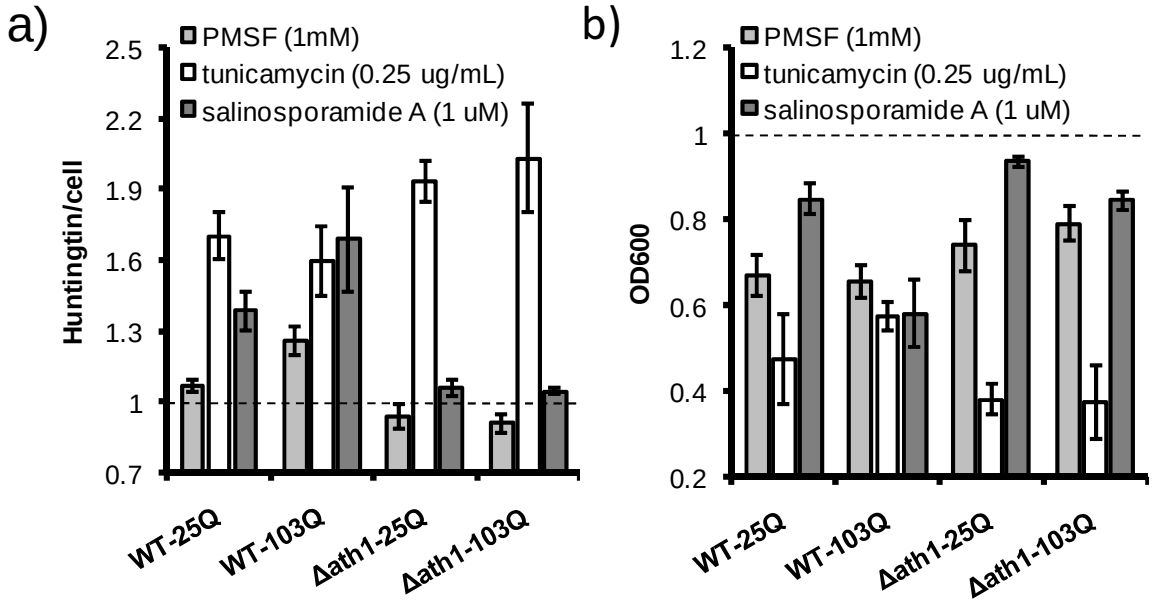

Figure 4.5 Treatment of yeast expressing m*Htt* with protein degradation inhibitors. PMSF inhibits autophagy, tunicamycin disrupts ERAD, and salinosporamide inhibits the proteasome. a)The ratio of huntingtin/cell as determined by fluorescent measurements and OD_{600} measurements of cell cultures treated with inhibitors of protein degradation. The significance of the difference between the huntingtin/cell values in the 25Q and 103Q lines of each strain were determined using a Students *t* test: WT PMSF ($P < 0.0001$), WT tunicamycin ($P = 0.0540$), WT salinosporamide ($P < 0.0001$), Δ*ath1* PMSF ($P = 0.3240$), Δ*ath1* tunicamycin ($P = 0.3605$), Δ*ath1* salinosporamide ($P = 0.2168$). b) The OD_{600} of cultures treated with protein degradation inhibitors. The significance of the difference between the OD_{600} values in the 25Q and 103Q lines of each strain were determined using a Students *t* test: WT PMSF ($P = 0.4128$), WT tunicamycin ($P = 0.0049$), WT salinosporamide ($P < 0.0001$), Δ*ath1* PMSF ($P = 0.1095$), Δ*ath1* tunicamycin ($P = 0.8802$), Δ*ath1* salinosporamide ($P < 0.0001$). All data was normalized to vehicle treated controls. Dashed lines shows the relative value of vehicle treated cultures.

WT-25Q, WT-103Q, Δ*ath1*-25Q and Δ*ath1*-103Q lines after treatment with these compounds (Figure 4.5). The relative amount of huntingtin per cell was determined by measuring the total fluorescence from EGFP in a culture and normalizing this value to the OD_{600} of the culture. Treatment of the WT-103Q line resulted in an increase in huntingtin levels for each inhibitor tested. However, only treatment with tunicamycin and salinosporamide caused an increase in huntingtin levels in the WT-25Q line. Tunicamycin was the only inhibitor which caused an increase in huntingtin in the Δ*ath1*-25Q and Δ*ath1*-103Q lines.

The effects of the protein degradation inhibitors on the growth of the WT-25Q, WT-103Q, Δ*ath1*-25Q and Δ*ath1*-103Q lines were also determined. Tunicamycin caused the most severe reduction in growth in the WT-25Q line, but in the WT-103Q line all three inhibitors had approximately the same effect. PMSF and salinosporamide caused very little reduction in growth of the Δ*ath1*-25Q and Δ*ath1*-103Q lines, but tunicamycin treatment severely impeded the growth of both lines.

4.5 Discussion

A metabolomics-based approach has been employed in this study in combination with yeast knockout strains deficient in trehalose metabolic pathways in order to investigate the role of trehalose in protecting cells against the toxicity of m*Htt*. There is substantial evidence that trehalose functions as a chemical chaperone and that its activity is due to the disruption of hydrogen bonding between the water molecules surrounding a protein (Jain and Roy 2009). It is hypothesized that interactions between water and trehalose molecules alters the thermodynamic folding landscape for misfolded proteins, causing them to remain in isolated misfolded conformations rather than form aggregates

(Liu, et al. 2008). This hypothesis may explain the ability of trehalose to increase the accessibility of misfolded proteins to molecular chaperones (Singer and Lindquist 1998).

Interestingly, only the deletion of the acid trehalase (Δ*ath1*) resulted in increased trehalose concentrations and protection against mutant huntingtin toxicity. There is currently considerable debate regarding the role of acid trehalase in cells (Fecke, et al. 2009; Garre, et al. 2009; Huang, et al. 2007), which makes interpretation of these results difficult. Even more surprising was the observation that neutral trehalase does not afford protection against mutant huntingtin toxicity. While the deletion of the neutral trehalase was expected to have a significant effect on intracellular trehalose levels, only a very modest effect was observed.

Intracellular concentrations of trehalose were not predictive of the metabolic response of the knockouts to m*Htt* expression. The metabolic aberrations associated with m*Htt* expression were completely alleviated in the Δ*ath1*-103Q line; this line also exhibited a significant increase in intracellular trehalose levels. However, the metabolic aberrations associated with m*Htt* expression were also assuaged in the Δ*nth1*-103Q line, which did not show an increase in intracellular trehalose, and in the Δ*tps3*-103Q line, which exhibited only a small increase in trehalose (Figure 4.4). Neither the Δ*nth1*-103Q line nor the Δ*tps3*-103Q line showed any increase in growth compared to the WT-103Q line, suggesting that the metabolic dysfunction caused by m*Htt* can be decoupled from the reduction in growth associated with its expression.

The variation in aggregation patterns observed in this series of yeast transformants confirms previous observations that aggregation of mutant huntingtin is not

necessarily linked to its toxicity (Duennwald, et al. 2006). Intriguingly, it has recently been shown that misfolded proteins can be sequestered into distinct cellular compartments in yeast (Kaganovich, et al. 2008). The destination of the misfolded protein depends on whether the protein is destined for degradation via the proteasome or if it is simply being sequestered to protect the cell from potential toxicity associated with misfolded proteins. The localization of the mutant huntingtin in the Δ*ath1*-103Q line appears similar to the compartmentalization described by Kaganovich et al., but the data collected in this study are insufficient to determine which compartment is being utilized by the cell.

Considering the lack of toxicity observed in the Δ*ath1*-103Q transformant, the increase in intracellular trehalose in this line, the lack of aggregation of mutant huntingtin and the alleviation of the metabolic defects associated with m*Htt* expression, it appears that trehalose protects yeast from mutant huntingtin toxicity via a chemical chaperone mechanism. This conclusion is supported by the fact that inhibition of autophagy has no effect on the clearance of mutant huntingtin from the cells with elevated trehalose concentrations (Figure 4.5). These results are in contrast to a previous observation that trehalose can enhance the clearance of protein aggregates from cells by inducing autophagy (Sarkar, et al. 2007a).

Although trehalose has been repeatedly shown to be one of the most effective osmolytes for preventing the aggregation of amyloidogenic proteins, other osmolytes have demonstrated similar properties (Singer and Lindquist 1998; Tanaka, et al. 2004). It is possible that molecular systems which function as chemical chaperones in a similar fashion to trehalose may be present in humans. If such a process is identified, it may

hold potential as a therapy for many protein misfolding diseases, including HD and other neurodegenerative diseases.

The information in Chapter 4 has been adapted from a manuscript which is in preparation for publication in the FEBS Journal.

Chapter 5 Ichthyotoxicity and Metabolic Transformation of Select Briarane Diterpenes

5.1 Introduction

Briarane diterpenes constitute a unique class of marine-derived secondary metabolites that are composed of a conserved bicyclo[8.4.0] system and fused γ-lactone. Since the first briarane diterpene, briareine A, was reported in 1977 from a gorgonian coral by Burks and colleagues at the University of Oklahoma (Burks, et al. 1977), >500 related metabolites have been described from various corals, and other marine invertebrates (Sung, et al. 2005; Sung and Chen 2002; Sung, et al. 2008; Sung, et al. 2002). A notable feature of the structural diversity within this compound family is that functionalization, ring opening/closure, and epimerization is observed throughout all 20 positions of the briarane carbon skeleton. The extraordinary biosynthetic adaptability of the briaranes to structural variation has made these metabolites an attractive subject for assessing how their naturally-occurring chemical variation influences the biological activities of this compound class.

While the majority of bioassays performed on these compounds have focused on the potential applications of briaranes to human health and diseases (e.g., cancer cell cytotoxicity, anti-inflammatory, and antiviral activities), a subset of the investigations were designed to query the ecological roles of briaranes (Changyun, et al. 2008). These studies have evaluated the antifouling properties of briaranes, as well as their toxicity and antifeedant activities against marine invertebrates and fish. For example, a fraction enriched in erythrolides A, B, and D from the encrusting gorgonian octacoral

Erythropodium caribaeorum deterred reef fish from feeding on agar baits infused with the briarane mixture; however, the antifeedant effects of the purified erythrolides were substantially diminished (Fenical and Pawlik 1991). Whereas erythrolide A was completely inactive as a feeding deterrent, the antifeedant effects of purified erythrolides B and D were rather marginal. In another example, renillins A–D were shown to inhibit feeding on baits presented to lesser blue crabs (*Callinectes similis*); however, only renillins C and D showed antifeedant activity against mummichog fish (*Fundulus heteroclitus*) (Barsby and Kubanek 2005).

In addition to the observed antifeedant properties of briaranes, it is worth considering other ecologically-relevant functions that these compounds may serve for their biogenic hosts. One possibility is that the briaranes may function as acute biotoxins, which would help prevent predation. Although toxins are generally believed to convey a competitive advantage to the host organism, there is little evidence that these types of compounds are capable of directly modulating the palatability of potential food items (Molyneux and Ralphs 1992). Moreover, it has been proposed that compounds capable of eliciting a toxic response have a greater impact on substantially limiting the dietary adaptation of predators to potential food sources than compounds which act only as feeding deterrents (Glendinning, et al. 2001). Therefore, it is reasonable to deduce that defensive toxins should play an important role in community-scale interactions between chemically-protected prey and their prospective predators (Swihart, et al. 2009). While a substantial number of putative marine-derived defensive diterpenes have been shown to be lethal to fish (Albericci, et al. 1978; Cimino, et al. 1990; Cimino, et al. 1988; De Petrocellis, et al. 1991; Gavagnin, et al. 1992; Iwagawa, et al. 1995; Iwagawa, et al. 1996;

McPhail and Davies-Coleman 1997; Miyamoto, et al. 1995; Schlenk and Gerwick 1987; Uchio, et al. 1985), we are aware of only a single ichthyotoxicity study involving a metabolite bearing a briarane-skeleton (Uchio, et al. 1989). In this particular example, it was reported that compound **1** was toxic to *Gambusia affinis* at concentrations ranging from 2–5 ppm.

The hypothesis of this investigation is that in comparison to the modest feeding deterrent activity exhibited by some briaranes, the toxicity of these compounds might play an important role in mounting an effective defensive strategy against predation. This conjecture is supported by the observation that although briaranes often accumulate at relatively substantial levels in certain corals, only a limited subset of these compounds exhibit efficacy toward deterring foraging behavior. In order to test this hypothesis, the chemical diversity of a *Briarium* sp. collected in Vanuatu has been explored. This examination led to the purification and subsequent structure determination of three new briaranes RAMs A–C (**2**-**4**). The ichthyotoxicity and brine shrimp toxicity of the RAMs were assessed against a reporter fish strain (*Pimephales promelas*) and *Artemia salina*. This research has also afforded the unique opportunity to analyze a heretofore unexplored aspect of the interaction of briaranes with biological systems – the metabolic transformation of briaranes by fish. The major RAM metabolites were also subjected to bioassay testing against *Artemia salina*. Based on this study, the theory is proposed that briarane toxicity plays a defensive role by providing protection to certain corals against predatory fish. Furthermore, these data demonstrate that the metabolism of briarane toxins by fish leads to further expansion of the already remarkable structural diversity exhibited by the briaranes.

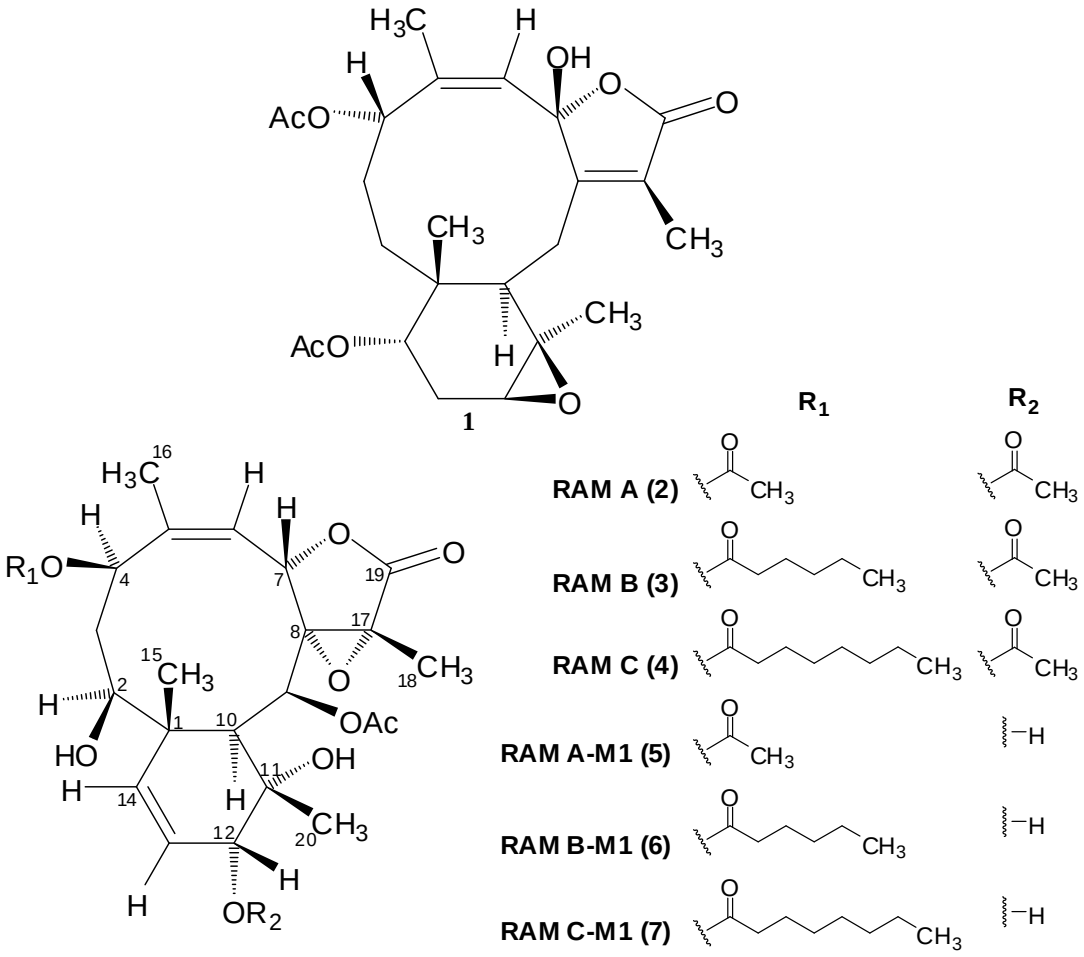

5.2 Experimental Procedures

5.2.1 General Experimental Procedures. NMR data were obtained on Varian VNMR spectrometers (400 and 500 MHz for ^{1}H, 100 and 125 MHz for ^{13}C) with broad band and triple resonance probes at 20 ± 0.5 °C. Electrospray-ionization mass spectrometry data was performed on a LCT Premier (Waters Corp.) time-of-flight instrument. Optical rotations were measured on a Rudolph Research Autopol III automatic polarimeter. HPLC separations were performed on a Shimadzu system using a SCL-10A VP system controller and Gemini 5µm C_{18} column, (110Å, 250 x 21.2 mm) with a flow rate of 10 mL/min. X-ray diffraction data were collected on a Bruker-AXS

with an APEX CCD area detector with a Cu X-ray source. All solvents were of ACS grade or better.

5.2.2 Animal Material and Sample Preparation. The *Briarium* sp. used for this project was obtained from the National Cancer Institute's Natural Products Repository of marine invertebrates (identification number C020997-A/20). The sample was collected in the Republic of Vanuatu at a depth of 10 meters. The sample had been extracted using 1:1 dichloromethane–methanol and then water. The material extracted using the 1:1 mixture of dichloromethane–methanol was selected for this study.

5.2.3 Purification of the RAMs A–C (2–4). The extract was suspended in water and partitioned against ethyl acetate. The ethyl acetate soluble material (4 g) was prepared for HPLC by passing it through a C_{18} SPE cartridge and eluting it with methanol. The extract was subjected to preparative-scale HPLC by passing the material over a C_{18} column with a mobile phase of 40–100% acetonitrile–water over 50 minutes. The first substantial peak to elute from the column (965 mg) was determined to be pure **2**. The second major peak to elute from the preparative HPLC was determined by ESIMS and ^{1}H NMR to be a mixture of structurally related metabolites. The mixture was further purified by subjecting the material to a second round of C_{18} HPLC, but this time an isocratic elution scheme utilizing 68% acetonitrile in water was used. This provided 520 mg of **3**. The third fraction to elute from preparative HPLC (96 mg) was determined to be a mixture and it was subsequently purified by C_{18} HPLC with a 45–65% acetonitrile–water gradient, which yielded 54 mg of **4**.

5.2.4 RAM A (2) : colorless crystalline solid from methanol; $[\alpha]^{21}_{D}$ –109.0 (*c* 0.001, acetone); HRESIMS *m/*z 545.2004, $C_{26}H_{34}NaO_{11}$ ($[M + Na]^+$, clad. 545.1999); ^1H NMR, see Table 2; ^{13}C NMR see Table 1.

5.2.5 RAM B (3) : white powder; $[\alpha]^{21}_{D}$ –100.8 (*c* 0.0024, chloroform); HRESIMS *m/*z 601.2616, $C_{30}H_{42}NaO_{11}$ ($[M + Na]^+$, calcd. 601.2625); ^1H NMR, see Table 2; ^{13}C NMR see Table 1.

5.2.6 RAM C (4) : white powder; $[\alpha]^{21}_{D}$ –102.0 (*c* 0.0024, chloroform); HRESIMS *m/*z 629.2938, $C_{32}H_{46}NaO_{11}$ ($[M + Na]^+$, calcd 629.2938); ^1H NMR, see Table 2; ^{13}C NMR see Table 1.

5.2.7 Ichthyotoxicity Assay. The ichthyotoxicity of RAMs A and B were determined as specified in EPA-821-R-02-012 (US EPA, 2002) (with the modifications noted below) and were approved by the University of Oklahoma Institutional Animal Care and Use Committee. For each assay, 90 mL clear glass jars were filled with 50 mL of filtered and aged tap water and 10-14 day old *Pimephales promelas* fry (three per jar) were added and allowed to acclimatize for 1 h. The jars were randomized and samples dissolved in 0.5 mL methanol were added to the jars. The RAM A (**2**) sample used in this experiment appeared to contain < 1% (by mass) contaminants as determined by ^1H NMR and HPLC. The RAM B (**3**) sample used in the assay was determined to contain ~5% (by mass) RAM C (**4**) as determined by ^1H NMR and HPLC. Controls consisting of vehicle-only were included in each experiment. Fish were maintained under 12 h light/12 h dark photoperiods at 24 ºC. Samples were tested in triplicate and the results were expressed as the LC_{50} (the concentration lethal to 50% of fish) ± standard deviation at 48

h. The LC_{50} values were determined in SigmaPlot v10 (Systat Software Inc) using sigmoidal dose-response regression analyses with variable slope parameters. All fish were euthanized at the conclusion of each experiment.

5.2.8 Purification of the RAMs A-M1, B-M1, and C-M1 (5–7). The water from all treatment groups for compounds **2** and **3** were pooled separately and the samples were partitioned against ethyl acetate. The ethyl acetate soluble materials from the two samples were subjected to preparative-scale HPLC by passing the material over a C_{18} column with a mobile phase of 50–100% methanol–water over 60 minutes. The samples pooled from the ichthyotoxicity test of **2** yielded one major new metabolite that was designated RAM A-M1 (**5**) (12 mg), while the samples from the ichthyotoxicity test of **3** yielded one new major metabolite designated RAM B-M1 (**6**) (5 mg) and one minor new metabolite designated RAM C-M1 (**7**) (3 mg). The chromatograms generated during the purification of the metabolites are illustrated in Figure 4.

5.2.9 RAM A-M1 (5) : colorless crystalline solid from methanol; $[\alpha]^{21}_{D}$ –45.0 (*c* 0.0024, methanol); HRESIMS *m/*z 503.1895, $C_{24}H_{32}NaO_{10}$ ($[M + Na]^+$, calcd 503.1893); ^{1}H NMR, see Table 2; ^{13}C NMR see Table 1.

5.2.10 RAM B-M1 (6) : white powder; $[\alpha]^{21}_{D}$ –13.0 (*c* 0.0024, methanol); HRESIMS *m/*z 559.2529, $C_{28}H_{40}NaO_{10}$ ($[M + Na]^+$, calcd 559.2519); ^{1}H NMR, see Table 2; ^{13}C NMR see Table 1.

5.2.11 RAM C-M1 (7) : white powder; $[\alpha]^{21}_{D}$ –2.9 (*c* 0.0024, methanol); HRESIMS *m/*z 587.2818, $C_{30}H_{44}NaO_{10}$ ($[M + Na]^+$, calcd 587.2832); ^{1}H NMR, see Table 2; ^{13}C NMR see Table 1.

HRESIMS and NMR (^{1}H and ^{13}C NMR, HSQC, HMBC, COSY, and NOESY) data for compounds **2**–**7** and crystallographic data for **2** and **5** are included in the Appendix.

5.3 Results and Discussion

The methanol extract of the *Briareum* sp. was partitioned between water and ethyl acetate. The ethyl acetate layer was retained and the solvent removed under vacuum. The resulting organic residue was analyzed by gradient C_{18} HPLC, which revealed three major metabolites that were targeted for isolation. Compound **2** eluted first from the C_{18} column and it exhibited a pseudomolecular ion $[M+Na]^{+}$ with a *m/*z of 545.2004 under HRESIMS conditions. This corresponded to a molecular formula of $C_{26}H_{34}NaO_{11}$ (calcd 545.1999) for the metabolite. Inspection of the ^{13}C NMR data for **2** (Table 5.1) revealed a total of 26 unique carbon atoms, which included four carbonyls (δ_C 168.3, 169.8, 170.3 and 170.4), four olefinic carbons (δ_C 121.9, 122.5, 142.0, and 144.2), and eight sp^3 hybridized carbons attached to oxygens (δ_C 64.8, 65.1, 71.3, 72.4, 72.8, 73.5, 73.6, and 77.4). The remaining carbon resonances appeared between δ_C 9.7 to 48.2 and $^{1}J_{H\text{-}C}$ HSQC data enabled the determination that seven of the carbons were methyls (δ_C 9.7, 14.0, 20.9, 21.0, 21.2, 21.6, and 26.5). Given the biogenic source of compound **2**, both the HRESIMS and HSQC data were consistent with what was expected for briarane-diterpene-type metabolites that are commonly encountered in these organisms. Structure determination efforts focused on dereplicating compound **2** ultimately proved fruitless, however, we did observe notable similarities between the data for **2** and those reported by Wu et al. for briaexcavatolide S ($C_{26}H_{34}O_{11}$) (Wu, et al. 2003). Consequently, attention

Table 5.1 ^{13}C NMR Data ($CDCl_3$) for RAMs A, B, C, A-M1, B-M1 and C-M1 (**2**–**7**)

position	δ_C, number of attached protons[a]					
	2[b]	**3**[c]	**4**[c]	**5**[c]	**6**[c]	**7**[c]
1	48.2, C	48.2, C	48.2, C	48.0, C	48.0, C	48.0, C
2	77.4, CH	77.5, CH	77.5, CH	77.7, CH	77.6, CH	77.7, CH
3	40.1, CH_2	40.2, CH_2	40.2, CH_2	40.1, CH_2	40.1, CH_2	40.1, CH_2
4	72.8, CH	72.5, CH	72.5, CH	72.9, CH	72.8, CH	72.7, CH
5	144.2, C	144.3, C	144.4, C	144.2, C	144.3, C	144.3, C
6	122.5, CH	122.4, CH	122.4, CH	122.4, CH	122.3, CH	122.3, CH
7	73.6, CH	73.6, CH	73.6, CH	73.9, CH	73.8, CH	73.7, CH
8	71.3, C	71.4, C	71.4, C	71.4, C	71.4, C	71.4, C
9	65.1, CH	65.2, CH	65.2, CH	65.6, CH	65.6, CH	65.6, CH
10	44.6, CH	44.7, CH	44.7, CH	44.0, CH	44.0, CH	44.0, CH
11	72.4, C	72.6, C	72.6, C	77.2, C	73.9, C	73.9, C
12	73.5, CH	73.5, CH	73.5, CH	70.6, CH	70.6, CH	70.6, CH
13	121.9, CH	122.1, CH	122.0, CH	124.4, CH	124.2, CH	124.3, CH
14	142.0, CH	141.9, CH	142.0, CH	140.0, CH	140.1, CH	140.1, CH
15	14.0, CH_3	14.1, CH_3	14.1, CH_3	14.1, CH_3	14.1, CH_3	14.1, CH_3
16	26.5, CH_3	26.5, CH_3	26.5, CH_3	26.6, CH_3	26.6, CH_3	26.6, CH_3
17	64.8, C	64.9, C	64.9, C	64.9, C	64.9, C	64.9, C
18	9.7, CH_3	9.7, CH_3	9.7, CH_3	9.8, CH_3	9.8, CH_3	9.8, CH_3
19	170.4, C	170.4, C	170.4, C	170.5, C	170.5, C	170.5, C
20	21.2, CH_3	21.2, CH_3	21.2, CH_3	21.4, CH_3	21.4, CH_3	21.4, CH_3
1’		173.2, C	173.1, C		173.1, C	173.1, C
2’		34.2, CH_2	34.2, CH_2		34.2, CH_2	34.3, CH_2
3’		24.5, CH_2	24.8, CH_2		24.6, CH_2	24.9, CH_2
4’		31.2, CH_2	29.0, CH_2		31.2, CH_2	29.0, CH_2
5’		22.3, CH_2	28.9, CH_2		22.3, CH_2	28.9, CH_2
6’		13.9, CH_3	31.6, CH_2		13.9, CH_3	31.6, CH_2
7’			22.6, CH_2			22.6, CH_2
8’			14.1, CH_3			14.07, CH_3
4-O*C*OCH$_3$	170.3, C			170.2, C		
4-OCO*C*H$_3$	21.0, CH_3			21.1, CH_3		
9-O*C*OCH$_3$	168.3, C	168.3, C	168.3, C	168.3, C	168.3, C	168.3, C
9-OCO*C*H$_3$	21.6, CH_3	21.6, CH_3	21.6, CH_3	21.6, CH_3	21.6, CH_3	21.6, CH_3
12-O*C*OCH$_3$	169.8, C	169.8, C	169.8, C			
12-OCO*C*H$_3$	20.9, CH_3	20.9, CH_3	20.9, CH_3			

[a]Determined by HSQC experiment
[b]Data for ^{13}C NMR determined at 125 MHz
[c]Data for ^{13}C NMR determined at 100 MHz

was focused on using the basic briarane diterpene scaffold of briaexcavatolide S as a convenient tool for accelerating the structural characterization of **2**.

While all of the proton and carbon resonances in the cyclodecane and fused γ-lactone ring portions of **2** closely matched the data for briaexcavatolide S, some substantial differences among the carbon resonances in the vicinity of the hexene ring

system were noted. For example, the observation was made that C-20 in **2** resonated at δ_C 21.2, whereas in briaexcavatolide S this carbon was reported to appear at δ_C 28.8 (Δ -7.6 ppm). Other carbon chemical shifts in the hexene system that varied between **2** versus briaexcavatolide S included C-1 (Δ 0.2 ppm), C-10 (Δ -1.1 ppm), C-11 (Δ -1.5 ppm), C-12 (Δ -1.8 ppm), C-13 (Δ 3.1 ppm), and C-14 (Δ -3.2 ppm).

Using a $^{2-3}J_{H-C}$ HMBC experiment (Appendix, Table A4), the entire planar structure of **2** was independently confirmed. Focusing on the hexene portion of the compound, correlations were observed from H-10 → C-1, C-11, C-12, and C-20; from H-12 → C-11, C-13, C-14, C-20, and C-25; from H-13 → C-1 and C-11; from H-14 → C-1, C-10, C-12, and C-15; from H-20 → C-10; and from H-26 → C-25. This established that the hexene ring systems in **2** and briaexcavatolide S shared the same planar configuration and that the compounds must be stereoisomers that differed in the configuration of one or more asymmetric centers. Using NOESY to probe this portion of **2** (Appendix, Table A4), a series of informative correlations were observed that enabled the investigation of the relative configuration of the four asymmetric carbons. Whereas the H-15 methyl protons exhibited NOE correlations with H-14 and H-20, the H-10 proton was only correlated with H-2. The H-20 protons also exhibited additional correlations that included H-9, H-12, and OH-2. An additional set of correlations were detected between OH-11 and H-9 and H-12. In view of these data, compound **2** was determined to be the C-11, C-12 diastereomer of briaexcavatolide S.

While in the process of establishing the relative configuration of **2**, crystals of the new metabolite were successfully prepared for X-ray diffraction studies. A thermal ellipsoid plot generated from these data is shown in Figure 5.1. The data from this

experiment not only supported the proposed relative configuration of **2**, but it also enabled the unequivocal determination of the absolute configuration of the metabolite as 1*S*,2*S*,4*R*,7*S*,8*S*,9*S*,10*S*,11*S*,12*R*,17*R*.

The HRESIMS analysis of compound **3** provided a pseudomolecular ion $[M + Na]^+$ at *m/*z 601.2616 that was consistent with a molecular formula of $C_{30}H_{42}NaO_{11}$ (calcd 601.2625). Upon examination of the ^{1}H NMR data, it became apparent that compound **3** was structurally similar to **2** (Tables 5.1 and 5.2). Two notable changes in the ^{1}H NMR spectrum of **3** were that an acetate methyl singlet that had appeared in **2** was replaced by a methyl triplet (δ_H 0.9, t, J = 7.0 Hz) in **3** and that eight new protons were detected at δ_H 2.32 (t, J = 7.5 Hz, 2H), 1.64 (m, 2H), and 1.32 (m, 4H). In addition, the ^{13}C NMR (Table 5.1) and $^1J_{H\text{-}C}$ HSQC spectra of **3** exhibited four new methylene carbon resonances at δ_C 22.3, 24.5, 31.2, and 34.2 that accounted for all eight of the new protons. Given the substantial quantity of **3** that was available (>500 mg), the opportunity to perform a ^{13}C–^{13}C INADEQUATE experiment was capitalized on (Figure 5.2). Based on the results from this study, it was concluded that the aforementioned methylenes were part of a pendant hexanoate that began with an ester carbonyl (δ_C 173.2) and terminated in a methyl group (δ_C 13.9).

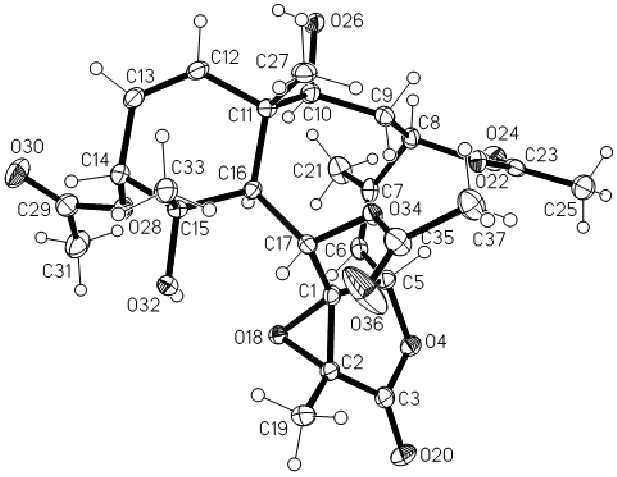

Figure 5.1 Thermal ellipsoid plot drawing for the X-ray crystal structure of **2**.

Table 5.2 ^{1}H NMR Data ($CDCl_3$) for RAMs A, B, C, A-M1, B-M1 and C-M1 (**2**–**7**)

position	δ_H, multiplicity (*J* in Hz)					
	2[a]	**3**[b]	**4**[a]	**5**[a]	**6**[a]	**7**[a]
2	3.25, dd (5.5, 7.0)	3.27, dd (5.0, 7.0)	3.26, t (7.5)	3.32, d (7.7)	3.32, d (7.3)	3.33, d (7.0)
3a	2.00, m	2.00, m	2.00, m	2.00, m	2.00, m	2.00, m
3b	2.84, t (13.0)	2.84, dd (13.0, 14.3)	2.85, dd (12.7, 14.3)	2.83, dd (12.5, 14.0)	2.83, dd (12.4, 14.5)	2.83, dd (12.5, 14.0)
4	5.16, ddd (1.0, 5.5, 13.0)	5.17, dd (5.0, 7.0, 13.0)	5.17, ddd (1.0, 5.5, 12.7)	5.17, ddd (12.5, 5.5, 1.0)	5.17, dd (5.4, 12.4)	5.17, dd (5.4, 12.5)
6	5.41, dt (1.3, 9.5)	5.41, dt (1.3, 9.5)	5.40, dt (1.5, 9.5)	5.39, dt (9.5, 1.5)	5.38, dt (9.5, 1.2)	5.38, d (9.4)
7	5.78, d (9.5)	5.78, d (9.5)	5.78, d (9.5)	5.78, d (9.5)	5.76, d (9.5)	5.76, d (9.4)
9	5.92, d (4.0)	5.92, d (3.8)	5.92, d (4.0)	5.92, d (3.4)	5.92, d (3.5)	5.92, d (3.0)
10	2.46, d (4.0)	2.47, d (3.8)	2.47, d (4.0)	2.40, d (3.4)	2.40, d (3.5)	2.40, d (3.0)
12	4.73, d (6.0)	4.75, d (6.0)	4.74, d (6.0)	3.75, d (6.0)	3.75, d (6.0)	3.75, d (6.0)
13	5.96, dd (6.0, 10.3)	5.97, dd (6.0, 10.3)	5.96, dd (6.0, 10.3)	5.90, dd (10.3, 6.0)	5.90, dd (6.0, 10.2)	5.90, dd (6.0, 10.4)
14	5.89, d (10.3)	5.89, d (10.3)	5.89, d (10.3)	5.83, d (10.3)	5.84, d (10.2)	5.84, d (10.4)
15	1.13, s	1.13, s	1.13, s	1.13, s	1.13, s	1.13, s
16	2.04, d (1.3)	2.05, d (1.3)	2.05, d (1.5)	2.04, d (1.5)	2.04, d (1.2)	2.04, s
18	1.67, s	1.69, s	1.68, s	1.71, s	1.70, s	1.71, s
20	1.21, s	1.22, s	1.22, s	1.17, s	1.16, s	1.17, s
2’		2.32, t (7.5)	2.32, t (7.5)		2.32, t, 7.4	2.32, t (7.5)
3’		1.64, m	1.62, m		1.63, m, 7.4	1.63, m
4’		1.32, m	1.31		1.32, m	1.31, m
5’		1.32, m	1.31		1.32, m	1.31, m
6’		0.90, t (7.0)	1.29		0.90, t (7.0)	1.27, m
7’			1.28			1.29, m
8’			0.88, t (7.0)			0.88, t (7.5)
4-$OCOCH_3$	2.08, s			2.09, s		
9-$OCOCH_3$	2.24, s	2.24, s	2.24, s	2.25, s	2.24, s	2.24, s
12-$OCOCH_3$	2.06, s	2.07, s	2.06, s			
2-OH	2.14, d (5.5)	4.87, br s	2.63, br s			
11-OH	2.38, s	2.39, br s	2.39, br s	2.65, br s	2.67, br. s	2.67, br. s

[a]Data for ^{1}H NMR determined at 500 MHz
[b]Data for ^{1}H NMR determined at 400 MHz

Rather than further optimizing the $^{13}C–^{13}C$ INADEQUATE experiment to capture all possible $^{1}J_{C\text{-}C}$ correlations, these data were supplemented with information from a $^{2\text{-}3}J_{H\text{-}C}$ HMBC experiment and this enabled the confirmation that the only variation in the planar structures of **2** and **3** was the type of ester substituent attached at the C-4 position (Figure 5.2). NOESY data collected for **3** (Appendix, Table A5) exhibited a strikingly similar pattern of proton correlations with **2** (Appendix, Table A4) and this enabled the conclusion to be made that **3** shared the same relative configuration. While the preparation of a crystal suitable for X-ray analysis of **3** was not successful, it is proposed that the absolute configuration of **3** is also 1*S*,2*S*,4*R*,7*S*,8*S*,9*S*,10*S*,11*S*,12*R*,17*R* based on its shared biogenic origins and similar optical rotation data ($[\alpha]^{21}_{D}$ –109.0 and –100.8 for **2** and **3**, respectively)

Compound **4** yielded a pseudomolecular ion (HRESIMS $[M + Na]^{+}$) at *m/*z 629.2938 consistent with a molecular formula of $C_{32}H_{46}NaO_{11}$ (calcd 629.2938). Compared to **3**, the molecular formula of **4** represented an increase in C_2H_4, from which the speculation was made that this was due to the addition of two methylenes. Examination of the ^{1}H NMR integration data for **4** revealed four new protons in the region spanning from δ_H 1.28 to 1.31 (Table 5.2). HSQC confirmed that these protons were associated to two new methylenes (δ_C 28.9 and 29.0), while HMBC established

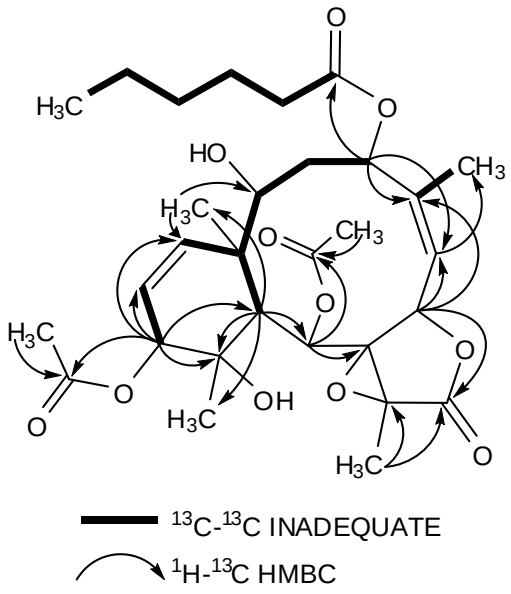

Figure 5.2 ^{13}C-^{13}C INADEQUATE and selected ^{1}H-^{13}C HMBC data that were used to establish the structure of **3**.

that these carbons were situated among a group of four other methylenes (δ_C 22.6, 24.8, 31.6, and 34.2), a carbonyl (δ_C 173.1), and a methyl group (δ_C 14.1) (Appendix, Table A6). Together, these carbons formed an octanoate ester. Consideration of the remaining HMBC correlations and NOESY data for **4** (Appendix, Table A6) confirmed that the compound shared the same briarane skeleton that had previously been established for **2** and **3**. The only difference in the new metabolite was that **4** bore a C-4 octanoate ester whereas **2** and **3** possessed C-4 acetate and hexanoate groups, respectively. In light of the fact that all three compounds have the same biogenic source and exhibit similar optical rotations values ($[\alpha]^{21}_D$ –102.0 for **4**), it is proposed that the absolute configuration of **4** is 1*S*,2*S*,4*R*,7*S*,8*S*,9*S*,10*S*,11*S*,12*R*,17*R*.

Given the substantial quantity of **2** (> 99% purity based on HPLC) and **3** (mixture of approximately 95% of **3** with 5% of **4**) that was obtained, the investigation of the ichthyotoxicity of these compounds was initiated. The flathead minnow (*Pimephales promelas*) was employed for this study since it is a widely used and well accepted model for determining the acute toxicity of a broad range of chemicals against aquatic vertebrates (EPA-821-R-02-012 2002). After a preliminary assessment of the toxicity of **2** and **3**, both compounds were tested across a series seven concentrations (each concentration was tested in triplicate sets of three fish) that spanned the estimated LC_{50} range of the toxin. Based on these experiments, **3** was found to be quite toxic to fish with an LC_{50} of 0.3 mM, while **2** was 4.7 times less potent with an LC_{50} of 1.4 mM (Figure 5.3).

At the conclusion of the ichthyotoxicity studies, the water from each vessel that had supported the fish throughout the assay was collected and pooled separately for all doses of **2** and **3**. Although the RAMs demonstrate remarkable stability with no detectable signs of degradations for periods of up to one month in aqueous and organic-based solvents, the surprising finding was made that < 30% of the RAMs used in the ichthyotoxicity test were left in the assay water. Instead, it was noted that the samples from the two treatment groups each contained new metabolites (Figure 5.4). The separation of the metabolites was carried out by gradient C_{18} HPLC resulting in the isolation of **5**-**7**.

The assumption that **5** (RAM A-M1) had been derived from **2** was confirmed by comparative inspection of the ^{1}H NMR data for both compounds (Table 5.2). The spectra of **2** and **5** looked remarkably similar with two notable exceptions: the C-12 acetate methyl singlet was missing for **5** and H-12 had shifted upfield from δ_H 4.73 (d, J = 6.0 Hz, 1H) in **2** to δ_H 3.75 (d, J = 6.0 Hz, 1H) in **5**. The HRESIMS analysis of compound **5** provided a pseudomolecular ion $[M + Na]^+$ at *m/*z 503.1895 that was consistent with a molecular formula of $C_{24}H_{32}NaO_{10}$ (calcd 503.1893). This represented a loss of C_2H_3O, which could be readily accounted for if an acetate had been lost through hydrolytic cleavage. In addition to the ^{1}H NMR and HRESIMS data that supported the loss of an

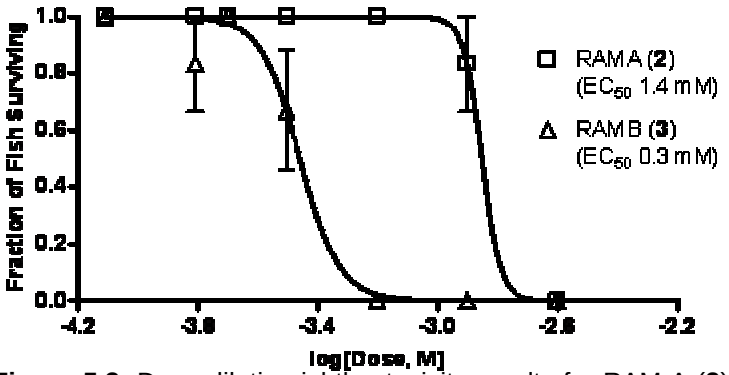

Figure 5.3 Dose-dilution ichthyotoxicity results for RAM A (**2**) and RAM B (**3**) against *P. promelas* fry.

acetate from **2**, the ^{13}C NMR data further substantiated this proposal showing the loss of methyl and carbonyl resonances in **5**, as well as the upfield shift of C-12 from δ_C 73.5 in **2** to δ_C 70.6 in **5** (Table 5.1). In addition, compound **5** was successfully crystallized from chloroform and the crystal was analyzed by X-ray diffraction spectroscopy. The thermal ellipsoid plot diagram of **5** illustrated in Figure 5.5 supported the loss of the C-12 acetate and confirmed that the rest of the briarane structure remained intact with a relative configuration of 1*S*,2*S*,4*R*,7*S*,8*S*,9*S*,10*S*,11*S*,12*R*,17*R*. Given the relative stability previously noted for **2**, the proposal was made that **5** was the product of metabolic transformation of **2** by the fish and therefore retained the absolute configuration of **2**. The fish were not directly ingesting the compounds under the assay conditions; therefore the uptake of **2** may have occurred through the gill membrane. Following its deacetylation, it is postulated that **5** was excreted back into the water either through the gills or urine.

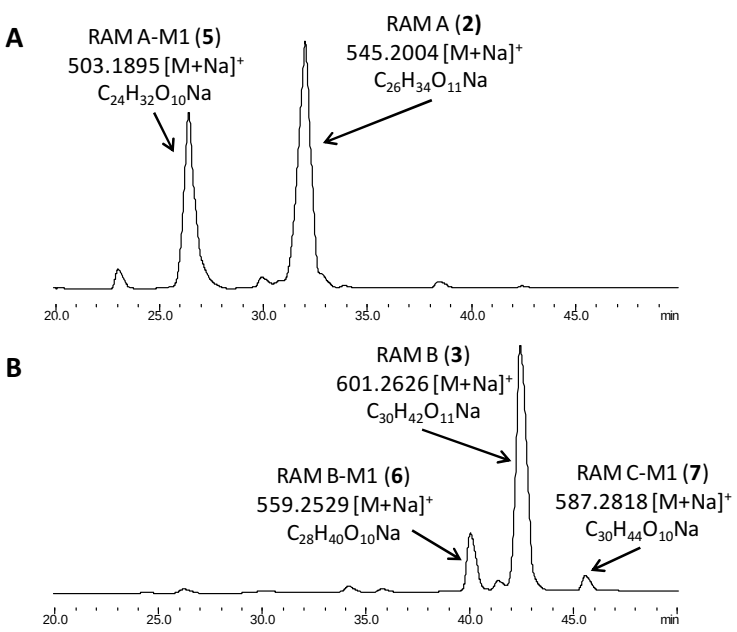

Figure 5.4 New metabolites that were generated from treating fish (*P. promelas* fry) with RAMs A-C (**2**-**4**). **A**) Fish treated with RAM A (**2**) resulted in the formation of the RAM A-M1 (**5**). **B**) Fish treated with a mixture of RAM B (**3**) and RAM C (**4**) (~95:5 mixture) led to the formation of RAM B-M1 (**6**) and RAM C-M1 (**7**). Only the sections of the HPLC chromatogram where the RAMs and their metabolite eluted (20-50 minutes) when passed over C_{18} (50–100% MEOH over 60 minutes) are shown for clarity. The structures of compounds corresponding to the other minor abundance peaks were not determined.

Compound **6** (RAM B-M1) yielded a pseudomolecular ion (HRESIMS [M + Na]$^+$) at *m/*z 559.2529 that was consistent with a molecular formula of $C_{24}H_{32}NaO_{10}$ (calcd 559.2519). The loss of C_2H_3O in **6** compared to **3** suggested that this compound was also the product of a deacetylation process. This was quickly confirmed by comparisons ^{1}H (loss of methyl singlet and upfield shift of the H-12 doublet from δ_H 4.75 in **3** to δ_H 3.75 in **6**) (Table 5.2) and ^{13}C (loss of methyl and carbonyl resonances in **6** and upfield shift of C-12 from δ_C 73.5 in **3** to δ_C 70.6 in **6**) (Table 5.1) NMR data for both compounds. HMBC and NOESY experiments (Appendix, Table A8) confirmed that the remainder of **6** shared the same planar structure and relative configuration as **3** and it is proposed that this metabolite also shares the same absolute configuration.

HRESIMS analysis of compound **7** (RAM C-M1) provided a pseudomolecular ion [M + Na]$^+$ at *m/*z 587.2818 that was consistent with a molecular formula of $C_{24}H_{32}NaO_{10}$ (calcd 587.2832). Although the relationship of this metabolite to **3** was at first perplexing, the recollection was made that approximately 5% by mass of **3** used in the fish assay had been contaminated with **4**. Reconsideration of the possibility that the residual quantity of **4** could have been metabolically transformed into **7** led to the reexamination of the HRESIMS data where it was noted that this metabolite had likely arisen as the result of **4** being deacetylated. Inspection of the ^{1}H NMR (loss of methyl singlet and upfield shift of the

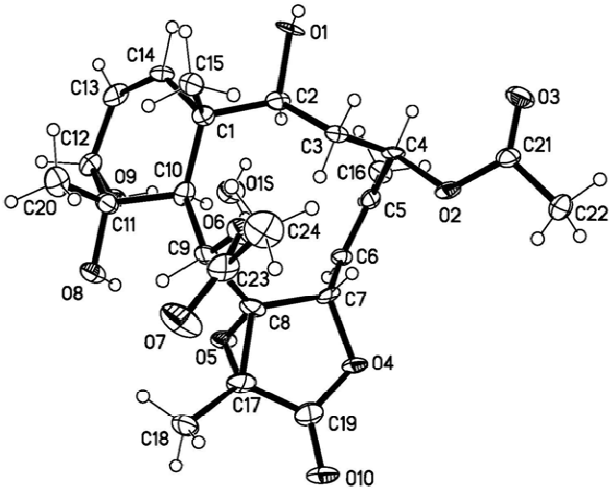

Figure 5.5 Thermal ellipsoid plot drawing for the X-ray crystal structure of **5**.

H-12 doublet from δ_H 4.74 in **4** to δ_H 3.75 in **7**) (Table 5.2) and ^{13}C NMR (loss of methyl and carbonyl resonances in **7** and upfield shift of C-12 from δ_C 73.5 in **4** to δ_C 70.6 in **7**) (Table 5.1) data for **7** quickly confirmed that this metabolite was derived from **4**. Examination of the HMBC and NOESY data (Appendix, Table A9) showed that other than the loss of the C-12 acetate, the remaining portion of the structure for **7** was identical to the parent compound. Consequently, it is proposed that **7** also shared the same absolute configuration with the rest of the briarane diterpenes and metabolic transformation products obtained in this study.

Although insufficient material was available to test the relative ichthyotoxic properties of the RAM metabolites (**5**–**7**), the toxicity of these compounds and **2**–**4** were evaluated against *Artemia salina*. However, even at doses ranging up to 2 mM, no brine shrimp toxicity was observed for any of the compounds. These data suggest that the ichthyotoxic effects of briaranes likely contribute to a toxic defensive strategy used by certain corals and marine invertebrates to protect against foraging fish predators, but may be inactive against other invertebrate species. It has also been shown for the first time that these compounds are subjected to structural modification via metabolic transformation in fish. These data serve as a cautionary reminder of the role that metabolic transformations can play when testing natural products in vivo.

The information in Chapter 5 has been adapted from a manuscript which is in preparation for publication in the Journal of Natural Products.

References

Abin-Carriquiry, J. A.; Costa, G.; Urbanavicius, J.; Cassels, B. K.; Rebolledo-Fuentes, M.; Wonnacott, S.; Dajas, F. In vivo modulation of dopaminergic nigrostriatal pathways by cytisine derivatives: Implications for Parkinson's Disease. *Eur. J. Pharmacol.* **2008,** *589* (1-3), 80-84.

Abu-Salah, K. M. Amphotericin B: an update. *Br. J. Biomed. Sci.* **1996,** *53* (2), 122-33.

Albericci, M.; Braekman, J. C.; Daloze, D.; Tursch, B.; Declercq, J. P.; Gemain, G.; Van Meerssche, M. Chemical studies of marine invertebrates. XXXV. Sarcoglaucol, a novel cembrane diterpene from the soft coral Sarcophyton glaucum (Coelenterata, Octocorallia). *Bull. Soc. Chim. Belg.* **1978,** *87* (6), 487-92.

Allain, H.; Bentué-Ferrer, D.; Akwa, Y. Disease-modifying drugs and Parkinson's disease. *Prog. Neurobiol.* **2008,** *84* (1), 25-39.

Amor, S.; Puentes, F.; Baker, D.; van der Valk, P. Inflammation in neurodegenerative diseases. *Immunology* **2010,** *129*, 154-169.

Anand, P.; Thomas, S. G.; Kunnumakkara, A. B.; Sundaram, C.; Harikumar, K. B.; Sung, B.; Tharakan, S. T.; Misra, K.; Priyadarsini, I. K.; Rajasekharan, K. N.; Aggarwal, B. B. Biological activities of curcumin and its analogues (Congeners) made by man and Mother Nature. *Biochem. Pharmacol.* **2008,** *76* (11), 1590-1611.

Asai, M.; Iwata, N.; Yoshikawa, A.; Aizaki, Y.; Ishiura, S.; Saido, T. C.; Maruyama, K. Berberine alters the processing of Alzheimer's amyloid precursor protein to decrease Aβ secretion. *Biochem. Biophys. Res. Commun.* **2007,** *352* (2), 498-502.

Barbosa Filho, J. M.; Medeiros, K. C. P.; Diniz, M. d. F. F. M.; Batista, L. M.; Athayde-Filho, P. F.; Silva, M. S.; Cunha, E. V. L. d.; Almeida, J. R. G. S.; Quintans-Júnior, L. J. Natural products inhibitors of the enzyme acetylcholinesterase. *Rev. Bras. Farmacogn.* **2006,** *16*, 258-285.

Barsby, T.; Kubanek, J. Isolation and Structure Elucidation of Feeding Deterrent Diterpenoids from the Sea Pansy, Renilla reniformis. *J. Nat. Prod.* **2005,** *68* (4), 511-516.

Bastianetto, S.; Brouillette, J.; Quirion, R. Neuroprotective Effects of Natural Products: Interaction with Intracellular Kinases, Amyloid Peptides and a Possible Role for Transthyretin. *Neurochem. Res.* **2007,** *32* (10), 1720-1725.

Bateman, D. A.; Chakrabartty, A. Interactions of Alzheimer amyloid peptides with cultured cells and brain tissue, and their biological consequences. *Biopolymers* **2004,** *76* (1), 4-14.

Bell, W.; Sun, W.; Hohmann, S.; Wera, S.; Reinders, A.; De Virgilio, C.; Wiemken, A.; Thevelein, J. M. Composition and Functional Analysis of the Saccharomyces cerevisiae Trehalose Synthase Complex. *J. Biol. Chem.* **1998,** *273* (50), 33311-33319.

Beranger, F.; Crozet, C.; Goldsborough, A.; Lehmann, S. Trehalose impairs aggregation of PrPSc molecules and protects prion-infected cells against oxidative damage. *Biochem. Biophys. Res. Commun.* **2008,** *374* (1), 44-48.

Bloom, G. S.; Ren, K.; Glabe, C. G. Cultured cell and transgenic mouse models for tau pathology linked to β-amyloid. *BBA-Mol. Basis Dis.* **2005,** *1739* (2-3), 116-124.

Branco, J.; Al-Ramahi, I.; Ukani, L.; Perez, A. M.; Fernandez-Funez, P.; Rincon-Limas, D.; Botas, J. Comparative analysis of genetic modifiers in Drosophila points to

common and distinct mechanisms of pathogenesis among polyglutamine diseases. *Hum. Mol. Genet.* **2008,** *17* (3), 376-90.

Brown, G. C. Mechanisms of inflammatory neurodegeneration: iNOS and NADPH oxidase. *Biochem. Soc. Trans.* **2007,** *35* (Pt 5), 1119-21.

Brundin, P.; Jia-Yi, L.; Holton, J. L.; Lindvall, O.; Revesz, T. Research in motion: the enigma of Parkinson's disease pathology spread. *Nat. Rev. Neurosci.* **2008,** *9* (10), 741-745.

Burks, J. E.; Van der Helm, D.; Chang, C. Y.; Ciereszko, L. S. The crystal and molecular structure of briarein A, a diterpenoid from the gorgonian Briareum asbestinum. *Acta Crystallogr. B* **1977,** *B33* (3), 704-709.

Butler, M. S. The Role of Natural Product Chemistry in Drug Discovery *J. Nat. Prod.* **2004,** *67* (12), 2141-2153.

Carmichael, J.; Sugars, K. L.; Bao, Y. P.; Rubinsztein, D. C. Glycogen Synthase Kinase-3β Inhibitors Prevent Cellular Polyglutamine Toxicity Caused by the Huntington's Disease Mutation. *J. Biol. Chem.* **2002,** *277* (37), 33791-33798.

Cattaneo, E.; Zuccato, C.; Tartari, M. Normal huntingtin function: an alternative approach to Huntington's disease. *Nat. Rev. Neurosci.* **2005,** *6* (12), 919-30.

Caughey, B.; Raymond, L. D.; Raymond, G. J.; Maxson, L.; Silveira, J.; Baron, G. S. Inhibition of Protease-Resistant Prion Protein Accumulation In Vitro by Curcumin. *J. Virol.* **2003,** *77* (9), 5499-5502.

Changyun, W.; Haiyan, L.; Changlun, S.; Yanan, W.; Liang, L.; Huashi, G. Chemical defensive substances of soft corals and gorgonians. *Acta Ecolog. Sin.* **2008,** *28* (5), 2320-2328.

Cheng, Y.; Schneider, B.; Riese, U.; Schubert, B.; Li, Z.; Hamburger, M. Farinosones A-C, neurotrophic alkaloidal metabolites from the entomogenous deuteromycete Paecilomyces farinosus. *J. Nat. Prod.* **2004,** *67* (11), 1854-8.

Cheng, Y.; Schneider, B.; Riese, U.; Schubert, B.; Li, Z.; Hamburger, M. (+)-N-Deoxymilitarinone A, a neuritogenic pyridone alkaloid from the insect pathogenic fungus Paecilomyces farinosus. *J. Nat. Prod.* **2006,** *69* (3), 436-8.

Cimino, G.; Crispino, A.; Gavagnin, M.; Sodano, G. Diterpenes from the nudibranch Chromodoris luteorosea. *J. Nat. Prod.* **1990,** *53* (1), 102-6.

Cimino, G.; Gavagnin, M.; Sodano, G.; Puliti, R.; Mattia, C. A.; Mazzarella, L. Verrucosin-A and -B. Ichthyotoxic diterpenoic acid glycerides with a new carbon skeleton from the dorid nudibranch Doris verrucosa. *Tetrahedron* **1988,** *44* (8), 2301-10.

Clement, J. A.; Yoder, B. J.; Kingston, D. G. I. Natural Products as a Source of CNS-Active Agents. *Mini Rev. Org. Chem.* **2004,** *1* (2), 183-208.

Colby, D. W.; Chu, Y.; Cassady, J. P.; Duennwald, M.; Zazulak, H.; Webster, J. M.; Messer, A.; Lindquist, S.; Ingram, V. M.; Wittrup, K. D. Potent inhibition of huntingtin aggregation and cytotoxicity by a disulfide bond-free single-domain intracellular antibody. *Proc. Natl. Acad. Sci. U.S.A.* **2004,** *101* (51), 17616?17621-17616?17621.

Colosimo, C.; Fabbrini, G.; Berardelli, A. Drug Insight: new drugs in development for Parkinson's disease. *Nat. Clin. Pract. Neurol.* **2006,** *2* (11), 600-610.

Connor, B.; Dragunow, M. The role of neuronal growth factors in neurodegenerative disorders of the human brain. *Brain. Res. Rev.* **1998,** *27* (1), 1-39.

Cornelis, S.; Kersse, K.; Festjens, N.; Lamkanfi, M.; Vandenabeele, P. Inflammatory Caspases: Targets for Novel Therapies. *Curr. Pharm. Des.* **2007,** *13* (4), 367-385.

Crowe, J. H., Trehalose as a "chemical chaperone": Fact and fantasy. In *Molecular Aspects of the Stress Response: Chaperones, Membranes and Networks*, Springer-Verlag Berlin: Berlin, 2007; Vol. 594, pp 143-158.

Davies, J.; Sarkar, S.; Rubinsztein, D. The ubiquitin proteasome system in Huntington's disease and the spinocerebellar ataxias. *BMC Biochem.* **2007,** *8* (Suppl 1), S2-S2.

Davies, J. E.; Sarkar, S.; Rubinsztein, D. C. Trehalose reduces aggregate formation and delays pathology in a transgenic mouse model of oculopharyngeal muscular dystrophy. *Hum. Mol. Genet.* **2006,** *15* (1), 23-31.

De Petrocellis, L.; Di Marzo, V.; Arca, B.; Gavagnin, M.; Minei, R.; Cimino, G. The effect of diterpenoidic diacylglycerols on tentacle regeneration in Hydra vulgaris. *Comp. Biochem. Physiol., C: Comp. Pharmacol. Toxicol.* **1991,** *100C* (3), 603-7.

Desai, U. A.; Pallos, J.; Ma, A. A.; Stockwell, B. R.; Thompson, L. M.; Marsh, J. L.; Diamond, M. I. Biologically active molecules that reduce polyglutamine aggregation and toxicity. *Hum. Mol. Genet.* **2006,** *15* (13), 2114-24.

Dheen, S. T.; Kaur, C.; Ling, E. A. Microglial activation and its implications in the brain diseases. *Curr. Med. Chem.* **2007,** *14* (11), 1189-97.

Diekmann, H.; Anichtchik, O.; Fleming, A.; Futter, M.; Goldsmith, P.; Roach, A.; Rubinsztein, D. C. Decreased BDNF levels are a major contributor to the embryonic phenotype of huntingtin knockdown zebrafish. *J. Neurosci.* **2009,** *29* (5), 1343-9.

Dong, X.-x.; Wang, Y.; Qin, Z.-h. Molecular mechanisms of excitotoxicity and their relevance to pathogenesis of neurodegenerative diseases. *Acta Pharmacol. Sin.* **2009,** *30* (4), 379-387.

Duennwald, M. L.; Jagadish, S.; Muchowski, P. J.; Lindquist, S. Flanking sequences profoundly alter polyglutamine toxicity in yeast. *Proc. Natl. Acad. Sci. U.S.A.* **2006,** *103* (29), 11045-50.

Dunckley, T.; Coon, K. D.; Stephan, D. A. Discovery and development of biomarkers of neurological disease. *Drug Discov. Today* **2005,** *10* (5), 326-34.

Durairajan, S. S. K.; Yuan, Q.; Xie, L.; Chan, W.-S.; Kum, W.-F.; Koo, I.; Liu, C.; Song, Y.; Huang, J.-D.; Klein, W. L.; Li, M. Salvianolic acid B inhibits Aβ fibril formation and disaggregates preformed fibrils and protects against Aβ-induced cytotoxicty. *Neurochem. Int. 52* (4-5), 741-750.

El Sayed, K. A.; Kelly, M.; Kara, U. A. K.; Ang, K. K. H.; Katsuyama, I.; Dunbar, D. C.; Khan, A. A.; Hamann, M. T. New Manzamine Alkaloids with Potent Activity against Infectious Diseases. *J. Am. Chem. Soc.* **2001,** *123* (9), 1804-1808.

Elbein, A. D.; Pan, Y. T.; Pastuszak, I.; Carroll, D. New insights on trehalose: a multifunctional molecule. *Glycobiology* **2003,** *13* (4), 17R-27.

EPA-821-R-02-012, *Methods for Measuring the Acute Toxicity of Effluents and Receiving Waters to Freshwater and Marine Organisms*. 5th ed.; U.S. Environmental Protection Agency: Washington, DC., 2002.

Faber, P. W.; Alter, J. R.; MacDonald, M. E.; Hart, A. C. Polyglutamine-mediated dysfunction and apoptotic death of a Caenorhabditis elegans sensory neuron. *Proc. Natl. Acad. Sci. U.S.A.* **1999,** *96* (1), 179-184.

Faber, P. W.; Voisine, C.; King, D. C.; Bates, E. A.; Hart, A. C. Glutamine/proline-rich PQE-1 proteins protect Caenorhabditis elegans neurons from huntingtin polyglutamine neurotoxicity. *Proc. Natl. Acad. Sci. U.S.A.* **2002,** *99* (26), 17131-6.

Fang, J.; Liu, R.; Tian, Q.; Hong, X. P.; Wang, S. H.; Cao, F. Y.; Pan, X. P.; Wang, J. Z. Dehydroevodiamine attenuates calyculin A-induced tau hyperphosphorylation in rat brain slices. *Acta Pharmacol. Sin.* **2007,** *28* (11), 1717-23.

Farooqui, T.; Farooqui, A. A. Aging: an important factor for the pathogenesis of neurodegenerative diseases. *Mech. Ageing Dev.* **2009,** *130* (4), 203-15.

Fecke, W.; Gianfriddo, M.; Gaviraghi, G.; Terstappen, G. C.; Heitz, F. Small molecule drug discovery for Huntington's Disease. *Drug Discov. Today* **2009,** *14* (9-10), 453-464.

Feling, R. H.; Buchanan, G. O.; Mincer, T. J.; Kauffman, C. A.; Jensen, P. R.; Fenical, W. Salinosporamide A: a highly cytotoxic proteasome inhibitor from a novel microbial source, a marine bacterium of the new genus salinospora. *Angew. Chem. Int. Ed. Engl.* **2003,** *42* (3), 355-7.

Fenical, W.; Pawlik, J. R. Defensive properties of secondary metabolites from the Caribbean gorgonian coral Erythropodium caribaeorum. *Mar. Ecol. Prog. Ser.* **1991,** *75* (1), 1-8.

Fontaine, S. N.; Brown, D. R. Mechanisms of Prion Protein Aggregation. *Protein Pept. Lett.* **2009,** *16* (1), 14-26.

Forloni, G.; Salmona, M.; Marcon, G.; Tagliavini, F. Tetracyclines and Prion Infectivity. *Infect. Disord. Drug Targets* **2009,** *9* (1), 23-30.

Francois, J.; Parrou, J. L. Reserve carbohydrates metabolism in the yeast Saccharomyces cerevisiae. *FEMS Microbiol. Rev.* **2001,** *25* (1), 125-45.

Fung, J.; Darabie, A. A.; McLaurin, J. Contribution of simple saccharides to the stabilization of amyloid structure. *Biochem. Biophys. Res. Commun.* **2005,** *328* (4), 1067-1072.

Garre, E.; Perez-Torrado, R.; Gimeno-Alcaniz, J. V.; Matallana, E. Acid trehalase is involved in intracellular trehalose mobilization during postdiauxic growth and severe saline stress in Saccharomyces cerevisiae. *FEMS Yeast Res.* **2009,** *9* (1), 52-62.

Gavagnin, M.; Vardaro, R. R.; Avila, C.; Cimino, G.; Ortea, J. Ichthyotoxic diterpenoids from the Cantabrian nudibranch Chromodoris luteorosea. *J. Nat. Prod.* **1992,** *55* (3), 368-71.

Geissen, M.; Krasemann, S.; Matschke, J.; Glatzel, M. Understanding the natural variability of prion diseases. *Vaccine* **2007,** *25* (30), 5631-5636.

Giese, K. P. GSK-3: a key player in neurodegeneration and memory. *IUBMB Life* **2009,** *61* (5), 516-21.

Gietz, R. D.; Schiestl, R. H. High-efficiency yeast transformation using the LiAc/SS carrier DNA/PEG method. *Nat. Protoc.* **2007,** *2* (1), 31-4.

Gilgun-Sherki, Y.; Melamed, E.; Offen, D. Anti-Inflammatory Drugs in the Treatment of Neurodegenerative Diseases: Current State. *Curr. Pharm. Des.* **2006,** *12* (27), 3509-3519.

Giorgini, F.; Muchowski, P. J., Exploiting Yeast Genetics to Inform Therapeutic Strategies for Huntington's Disease. In *Yeast Functional Genomics and Proteomics*, Stagljar, I., Ed. Humana Press: New York, 2009; Vol. 548, pp 161-174.

Glendinning, J. I.; Domdom, S.; Long, E. Selective adaptation to noxious foods by a herbivorous insect. *J. Exp. Biol.* **2001,** *204* (19), 3355-3367.

Gold, B. G.; Villafranca, J. E. Neuroimmunophilin ligands: the development of novel neuroregenerative/ neuroprotective compounds. *Curr. Top. Med. Chem.* **2003,** *3* (12), 1368-75.

Gomes, N. G.; Campos, M. G.; Orfao, J. M.; Ribeiro, C. A. Plants with neurobiological activity as potential targets for drug discovery. *Prog. Neuropsychopharmacol. Biol. Psychiatry* **2009,** *33* (8), 1372-89.

Gowda, G. A.; Zhang, S.; Gu, H.; Asiago, V.; Shanaiah, N.; Raftery, D. Metabolomics-based methods for early disease diagnostics. *Expert Rev. Mol. Diagn.* **2008,** *8* (5), 617-33.

Graziani, E. I. Recent advances in the chemistry, biosynthesis and pharmacology of rapamycin analogs. *Nat. Prod. Rep.* **2009,** *26* (5), 602-9.

Greenacre, M. Correspondence analysis in medical research. *Stat. Methods Med. Res.* **1992,** *1* (1), 97-117.

Greenacre, M., *Correspondence analysis in practice*. 2nd ed.; Chapman & Hall/CRC Taylor & Francis Group: Boca Raton, 2007.

Greenacre, M. J.; Degos, L. Correspondence analysis of HLA gene frequency data from 124 population samples. *Am. J. Hum. Genet.* **1977,** *1* (1), 60-75.

Gunasekera, S. P.; McCarthy, P. J.; Longley, R. E.; Pomponi, S. A.; Wright, A. E.; Lobkovsky, E.; Clardy, J. Discorhabdin P, a new enzyme inhibitor from a deep-water Caribbean sponge of the genus Batzella. *J. Nat. Prod.* **1999,** *62* (1), 173-5.

Hamann, M.; Alonso, D.; Martin-Aparicio, E.; Fuertes, A.; Perez-Puerto, M. J.; Castro, A.; Morales, S.; Navarro, M. L.; Del Monte-Millan, M.; Medina, M.; Pennaka, H.; Balaiah, A.; Peng, J.; Cook, J.; Wahyuono, S.; Martinez, A. Glycogen synthase kinase-3 (GSK-3) inhibitory activity and structure-activity relationship (SAR) studies of the manzamine alkaloids. Potential for Alzheimer's disease. *J. Nat. Prod.* **2007,** *70* (9), 1397-405.

Heinrich, M.; Lee Teoh, H. Galanthamine from snowdrop--the development of a modern drug against Alzheimer's disease from local Caucasian knowledge. *J. Ethnopharmacol.* **2004,** *92* (2-3), 147-62.

Hernandez, F.; Avila, J. The role of glycogen synthase kinase 3 in the early stages of Alzheimers' disease. *FEBS Lett.* **2008,** *582* (28), 3848-54.

Hong, S.; Yong, Y.; Kang, K.; Shin, S. Y.; Lee, Y. H.; Lim, Y. NF-κB Activation by compounds found in Platycodon grandiflorum extract. *J. Microbiol. Biotechnol.* **2009,** *19* (6), 556-9.

Houghton, P. J.; Howes, M. J. Natural products and derivatives affecting neurotransmission relevant to Alzheimer's and Parkinson's disease. *Neurosignals* **2005,** *14* (1-2), 6-22.

Huang, J.; Reggiori, F.; Klionsky, D. J. The transmembrane domain of acid trehalase mediates ubiquitin-independent multivesicular body pathway sorting. *Mol. Biol. Cell* **2007,** *18* (7), 2511-24.

Igarashi, S.; Morita, H.; Bennett, K. M.; Tanaka, Y.; Engelender, S.; Peters, M. F.; Cooper, J. K.; Wood, J. D.; Sawa, A.; Ross, C. A. Inducible PC12 cell model of Huntington's disease shows toxicity and decreased histone acetylation. *Neuroreport* **2003,** *14* (4), 565-8.

Iijima, K.; Iijima-Ando, K. Drosophila Models of Alzheimer's Amyloidosis: The Challenge of Dissecting the Complex Mechanisms of Toxicity of Amyloid-β 42. *J. Alzheimers Dis.* **2008,** *15* (4), 523-540.

Imarisio, S.; Carmichael, J.; Korolchuk, V.; Chen, C.-W.; Saiki, S.; Rose, C.; Krishna, G.; Davies, J. E.; Ttofi, E.; Underwood, B. R.; Rubinsztein, D. C. Huntington's disease: from pathology and genetics to potential therapies. *Biochem. J.* **2008,** *412* (2), 191-209.

Iwagawa, T.; Nakamura, S.; Masuda, T.; Okamura, H.; Nakatani, M.; Siro, M. Irregular cembranoids containing a 13-membered carbocyclic skeleton isolated from a soft coral, Sarcophyton species. *Tetrahedron* **1995,** *51* (18), 5291-8.

Iwagawa, T.; Nakamura, S.; Okamura, H.; Nakatani, M. New cembranoids from Sarcophyton sp. collected at Bonotsu, Kagoshima prefecture. 3. Ichthyotoxic cembranoids from the soft coral, Sarcophyton sp. *Bull. Chem. Soc. Jpn.* **1996,** *69* (12), 3543-3549.

Jackson, G. R.; Salecker, I.; Dong, X.; Yao, X.; Arnheim, N.; Faber, P. W.; MacDonald, M. E.; Zipursky, S. L. Polyglutamine-Expanded Human Huntingtin Transgenes Induce Degeneration of Drosophila Photoreceptor Neurons. *Neuron* **1998,** *21* (3), 633-642.

Jain, N. K.; Roy, I. Effect of trehalose on protein structure. *Protein Sci.* **2009,** *18* (1), 24-36.

Jayaprakasam, B.; Padmanabhan, K.; Nair, M. G. Withanamides in Withania somnifera fruit protect PC-12 cells from β-amyloid responsible for Alzheimer's disease. *Phytother. Res.* **2009**.

Jenkins, B. G.; Andreassen, O. A.; Dedeoglu, A.; Leavitt, B.; Hayden, M.; Borchelt, D.; Ross, C. A.; Ferrante, R. J.; Beal, M. F. Effects of CAG repeat length, HTT protein length and protein context on cerebral metabolism measured using magnetic resonance spectroscopy in transgenic mouse models of Huntington's disease. *J. Neurochem.* **2005,** *95* (2), 553-62.

Jenkins, B. G.; Klivenyi, P.; Kustermann, E.; Andreassen, O. A.; Ferrante, R. J.; Rosen, B. R.; Beal, M. F. Nonlinear decrease over time in N-acetyl aspartate levels in the absence of neuronal loss and increases in glutamine and glucose in transgenic Huntington's disease mice. *J. Neurochem.* **2000,** *74* (5), 2108-19.

Jenner, P. Functional models of Parkinson's disease: A valuable tool in the development of novel therapies. *Ann. Neurol.* **2008,** *64* (S2), S16-S29.

Jeong, H.; Then, F.; Melia, T. J., Jr.; Mazzulli, J. R.; Cui, L.; Savas, J. N.; Voisine, C.; Paganetti, P.; Tanese, N.; Hart, A. C.; Yamamoto, A.; Krainc, D. Acetylation targets mutant huntingtin to autophagosomes for degradation. *Cell* **2009,** *137* (1), 60-72.

Jolliffe, I. T., *Principal Component Analysis*. Springer-Verlag: 2002.

Jones, E. W. Tackling the protease problem in Saccharomyces cerevisiae. *Meth. Enzymol.* **1991,** *194*, 428-53.

Joyner, P. M.; Matheke, R. M.; Smith, L. M.; Cichewicz, R. H. Probing the metabolic aberrations underlying mutant huntingtin toxicity in yeast and assessing their degree of preservation in humans and mice. *J. Proteome Res.* **2010,** *9* (1), 404-12.

Jung, H. A.; Min, B.-S.; Yokozawa, T.; Lee, J.-H.; Kim, Y. S.; Choi, J. S. Anti-Alzheimer and Antioxidant Activities of Coptidis Rhizoma Alkaloids. *Biol. Pharm. Bull.* **2009,** *32* (8), 1433-1438.

Jung, M.; Park, M. Acetylcholinesterase inhibition by flavonoids from Agrimonia pilosa. *Molecules* **2007,** *12* (9), 2130-9.

Kaddurah-Daouk, R.; Krishnan, K. R. R. Metabolomics: A Global Biochemical Approach to the Study of Central Nervous System Diseases. *Neuropsychopharmacology* **2008,** *34* (1), 173-186.

Kaddurah-Daouk, R.; Kristal, B. S.; Weinshilboum, R. M. Metabolomics: A Global Biochemical Approach to Drug Response and Disease. *Annu. Rev. Pharmacol. Toxicol.* **2008,** *48* (1), 653-683.

Kaganovich, D.; Kopito, R.; Frydman, J. Misfolded proteins partition between two distinct quality control compartments. *Nature* **2008,** *454* (7208), 1088-1095.

Kang, C. B.; Hong, Y.; Dhe-Paganon, S.; Yoon, H. S. FKBP family proteins: immunophilins with versatile biological functions. *Neurosignals* **2008,** *16* (4), 318-25.

Kang, S. Y.; Lee, K. Y.; Sung, S. H.; Kim, Y. C. Four new neuroprotective dihydropyranocoumarins from Angelica gigas. *J. Nat. Prod.* **2005,** *68* (1), 56-9.

Kaushik, J. K.; Bhat, R. Why is trehalose an exceptional protein stabilizer? An analysis of the thermal stability of proteins in the presence of the compatible osmolyte trehalose. *J. Biol. Chem.* **2003,** *278* (29), 26458-26465.

Kim, S. R.; Lee, K. Y.; Koo, K. A.; Sung, S. H.; Lee, N. G.; Kim, J.; Kim, Y. C. Four new neuroprotective iridoid glycosides from Scrophularia buergeriana roots. *J. Nat. Prod.* **2002,** *65* (11), 1696-9.

Kim, S. U.; de Vellis, J. Stem cell-based cell therapy in neurological diseases: a review. *J. Neurosci. Res.* **2009,** *87* (10), 2183-200.

Kocisko, D. A.; Baron, G. S.; Rubenstein, R.; Chen, J.; Kuizon, S.; Caughey, B. New Inhibitors of Scrapie-Associated Prion Protein Formation in a Library of 2,000 Drugs and Natural Products. *J. Virol.* **2003,** *77* (19), 10288-10294.

Kossuga, M. H.; Nascimento, A. M.; Reimao, J. Q.; Tempone, A. G.; Taniwaki, N. N.; Veloso, K.; Ferreira, A. G.; Cavalcanti, B. C.; Pessoa, C.; Moraes, M. O.; Mayer, A. M.; Hajdu, E.; Berlinck, R. G. Antiparasitic, antineuroinflammatory, and cytotoxic polyketides from the marine sponge Plakortis angulospiculatus collected in Brazil. *J. Nat. Prod.* **2008,** *71* (3), 334-9.

Krammer, C.; Vorberg, I.; Schatzl, H. M.; Gilch, S. Therapy in Prion Diseases: From Molecular and Cellular Biology to Therapeutic Targets. *Infect. Disord. Drug Targets* **2009,** *9* (1), 3-14.

Krobitsch, S.; Lindquist, S. Aggregation of huntingtin in yeast varies with the length of the polyglutamine expansion and the expression of chaperone proteins. *Proc. Natl. Acad. Sci. U.S.A.* **2000,** *97* (4), 1589-94.

Kwon, H. C.; Lee, K. C.; Cho, O. R.; Jung, I. Y.; Cho, S. Y.; Kim, S. Y.; Lee, K. R. Sphingolipids from Bombycis Corpus 101A and their neurotrophic effects. *J. Nat. Prod.* **2003,** *66* (4), 466-9.

Langbehn, D. R.; Hayden, M. R.; Paulsen, J. S. and The Predict-H.D. Investigators of the Huntington Study Group CAG-repeat length and the age of onset in Huntington disease (HD): A review and validation study of statistical approaches. *Am. J. Med. Genet. B Neuropsychiatr. Genet.* **2010,** *153B* (2), 397-408.

Lee, K. Y.; Sung, S. H.; Kim, Y. C. Neuroprotective bibenzyl glycosides of Stemona tuberosa roots. *J. Nat. Prod.* **2006,** *69* (4), 679-81.

Lees, A. J.; Hardy, J.; Revesz, T. Parkinson's disease. *Lancet* **2009,** *373* (9680), 2055-66.

Lemke, A.; Kiderlen, A. F.; Kayser, O. Amphotericin B. *Appl. Microbiol. Biotechnol.* **2005,** *68* (2), 151-62.

Lin, L.; Lee, K.-H.; Atta-ur, R., Structure-activity relationships of curcumin and its analogs with different biological activities. In *Studies in Natural Products Chemistry*, Elsevier: 2006; Vol. Volume 33, Part 13, pp 785-812.

Liu, F. F.; Dong, X. Y.; Sun, Y. Molecular mechanism for the effects of trehalose on β-hairpin folding revealed by molecular dynamics simulation. *J. Mol. Graph. Model.* **2008,** *27* (4), 421-429.

Liu, J. W.; Tian, S. J.; de Barry, J.; Luu, B. Panaxadiol glycosides that induce neuronal differentiation in neurosphere stem cells. *J. Nat. Prod.* **2007,** *70* (8), 1329-34.

Liu, R.; Barkhordarian, H.; Emadi, S.; Park, C. B.; Sierks, M. R. Trehalose differentially inhibits aggregation and neurotoxicity of β-amyloid 40 and 42. *Neurobiol. Dis.* **2005,** *20* (1), 74-81.

Lleo, A. Current Therapeutic Options for Alzheimer's Disease. *Curr. Genomics* **2007,** *8* (8), 550-558.

Loizzo, M. R.; Tundis, R.; Menichini, F. Natural products and their derivatives as cholinesterase inhibitors in the treatment of neurodegenerative disorders: an update. *Curr. Med. Chem.* **2008,** *15* (12), 1209-28.

Lumsden, A. L.; Henshall, T. L.; Dayan, S.; Lardelli, M. T.; Richards, R. I. Huntingtin-deficient zebrafish exhibit defects in iron utilization and development. *Hum. Mol. Genet.* **2007,** *16* (16), 1905-20.

MacDonald, M. E.; Ambrose, C. M.; Duyao, M. P.; Myers, R. H.; Lin, C.; Srinidhi, L.; Barnes, G.; Taylor, S. A.; James, M.; Groot, N.; MacFarlane, H.; Jenkins, B.; Anderson, M. A.; Wexler, N. S.; Gusella, J. F.; Bates, G. P.; Baxendale, S.; Hummerich, H.; Kirby, S.; North, M.; Youngman, S.; Mott, R.; Zehetner, G.; Sedlacek, Z.; Poustka, A.; Frischauf, A.-M.; Lehrach, H.; Buckler, A. J.; Church, D.; Doucette-Stamm, L.; O'Donovan, M. C.; Riba-Ramirez, L.; Shah, M.; Stanton, V. P.; Strobel, S. A.; Draths, K. M.; Wales, J. L.; Dervan, P.; Housman, D. E.; Altherr, M.; Shiang, R.; Thompson, L.; Fielder, T.; Wasmuth, J. J.; Tagle, D.; Valdes, J.; Elmer, L.; Allard, M.; Castilla, L.; Swaroop, M.; Blanchard, K.; Collins, F. S.; Snell, R.; Holloway, T.; Gillespie, K.; Datson, N.; Shaw, D.; Harper, P. S. A novel gene containing a trinucleotide repeat that is expanded and unstable on Huntington's disease chromosomes. *Cell* **1993,** *72* (6), 971-983.

Mange, A.; Nishida, N.; Milhavet, O.; McMahon, H. E. M.; Casanova, D.; Lehmann, S. Amphotericin B Inhibits the Generation of the Scrapie Isoform of the Prion Protein in Infected Cultures. *J. Virol.* **2000,** *74* (7), 3135-3140.

Masuda, N.; Peng, Q.; Li, Q.; Jiang, M.; Liang, Y.; Wang, X.; Zhao, M.; Wang, W.; Ross, C. A.; Duan, W. Tiagabine is neuroprotective in the N171-82Q and R6/2 mouse models of Huntington's disease. *Neurobiol. Dis.* **2008,** *30* (3), 293-302.

Mayer, A. M.; Hall, M. L.; Lynch, S. M.; Gunasekera, S. P.; Sennett, S. H.; Pomponi, S. A. Differential modulation of microglia superoxide anion and thromboxane B2 generation by the marine manzamines. *BMC Pharmacol.* **2005,** *5*, 6.

McPhail, K.; Davies-Coleman, M. T. New spongian diterpenes from the east African nudibranch Chromodoris hamiltoni. *Tetrahedron* **1997,** *53* (13), 4655-4660.

Mechlinski, W.; Schaffner, C. P.; Ganis, P.; Avitabile, G. Structure and absolute configuration of the polyene macrolide antibiotic amphotericin B. *Tetrahedron Lett.* **1970,** *11* (44), 3873-3876.

Meijer, L.; Thunnissen, A. M.; White, A. W.; Garnier, M.; Nikolic, M.; Tsai, L. H.; Walter, J.; Cleverley, K. E.; Salinas, P. C.; Wu, Y. Z.; Biernat, J.; Mandelkow, E. M.; Kim, S. H.; Pettit, G. R. Inhibition of cyclin-dependent kinases, GSK-3β and CK1 by hymenialdisine, a marine sponge constituent. *Chem. Biol.* **2000,** *7* (1), 51-63.

Menalled, L.; El-Khodor, B. F.; Patry, M.; Suarez-Farinas, M.; Orenstein, S. J.; Zahasky, B.; Leahy, C.; Wheeler, V.; Yang, X. W.; MacDonald, M.; Morton, A. J.; Bates, G.; Leeds, J.; Park, L.; Howland, D.; Signer, E.; Tobin, A.; Brunner, D. Systematic behavioral evaluation of Huntington's disease transgenic and knock-in mouse models. *Neurobiol. Dis.* **2009,** *35* (3), 319-36.

Meriin, A. B.; Zhang, X.; He, X.; Newnam, G. P.; Chernoff, Y. O.; Sherman, M. Y. Huntington toxicity in yeast model depends on polyglutamine aggregation mediated by a prion-like protein Rnq1. *J. Cell Biol.* **2002,** *157* (6), 997-1004.

Miyamoto, T.; Takenaka, Y.; Yamada, K.; Higuchi, R. Bioactive diterpenoids from octocorallia, 2. Deoxyxeniolide B, a novel ichthyotoxic diterpenoid from the soft coral Xenia elongata. *J. Nat. Prod.* **1995,** *58* (6), 924-8.

Molyneux, R. J.; Ralphs, M. H. Plant Toxins and Palatability to Herbivores. *J. Range Manage.* **1992,** *45* (1), 13-18.

Nakasato, T.; Asada, S.; Marui, K. Dehydroevodiamine, main alkaloid from the leaves of Evodia rutaecarpa. *Yakugaku Zasshi* **1962,** *82*, 619-626.

Naoi, M.; Maruyama, W.; Yi, H.; Inaba, K.; Akao, Y.; Shamoto-Nagai, M. Mitochondria in neurodegenerative disorders: regulation of the redox state and death signaling leading to neuronal death and survival. *J. Neural Transm.* **2009,** *116* (11), 1371-1381.

Newman, D. J. Natural Products as Leads to Potential Drugs: An Old Process or the New Hope for Drug Discovery? *J. Med. Chem.* **2008,** *51* (9), 2589-2599.

Newman, D. J.; Cragg, G. M. Natural products as sources of new drugs over the last 25 years. *J. Nat. Prod.* **2007,** *70* (3), 461-77.

Nicoli, F.; Vion-Dury, J.; Maloteaux, J. M.; Delwaide, C.; Confort-Gouny, S.; Sciaky, M.; Cozzone, P. J. CSF and serum metabolic profile of patients with Huntington's chorea: a study by high resolution proton NMR spectroscopy and HPLC. *Neurosci. Lett.* **1993,** *154* (1-2), 47-51.

Nicoll, A. J.; Collinge, J. Preventing Prion Pathogenicity by Targeting the Cellular Prion Protein. *Infect. Disord. Drug Targets* **2009,** *9* (1), 48-57.

NINDS National Institute of Neurological Disorders and Stroke, National Institutes of Health. http://www.ninds.nih.gov/index.htm (February 2010),

Obrig, T. G.; Culp, W. J.; McKeehan, W. L.; Hardesty, B. The mechanism by which cycloheximide and related glutarimide antibiotics inhibit peptide synthesis on reticulocyte ribosomes. *J. Biol. Chem.* **1971,** *246* (1), 174-81.

Ohizumi, Y.; Yamakuni, T.; Li, Y. Search for Constituents with Neurotrophic Factor Activity from Medicinal Plants and their Application to Drug Development. *J. Appl. Pharmacol.* **2004,** *12*, 195-197.

Orhan, G.; Orhan, I.; Subutay-Oztekin, N.; Ak, F.; Sener, B. Contemporary anticholinesterase pharmaceuticals of natural origin and their synthetic analogues for the treatment of Alzheimer's disease. *Recent Pat. CNS Drug Discov.* **2009,** *4* (1), 43-51.

Oura, M.; Sternberg, T. H.; Wright, E. T. A new antifungal antibiotic, amphotericin B. *Antibiot. Annu.* **1955,** *3*, 566-73.

Outeiro, T. F.; Giorgini, F. Yeast as a drug discovery platform in Huntington's and Parkinson's diseases. *Biotechnol. J.* **2006,** *1* (3), 258-69.

Ouyang, Y. H.; Xu, Q. H.; Mitsui, K.; Motizuki, M.; Xu, Z. J. Human trehalase is a stress responsive protein in Saccharomyces cerevisiae. *Biochem. Biophys. Res. Commun.* **2009,** *379* (2), 621-625.

Palacios, D. S.; Anderson, T. M.; Burke, M. D. A post-PKS oxidation of the amphotericin B skeleton predicted to be critical for channel formation is not required for potent antifungal activity. *J. Am. Chem. Soc.* **2007,** *129* (45), 13804-5.

Pallas, M.; Camins, A. Molecular and Biochemical Features in Alzheimer's Disease. *Curr. Pharm. Des.* **2006,** *12* (33), 4389-4408.

Panza, F.; Solfrizzi, V.; Frisardi, V.; Capurso, C.; D'Introno, A.; Colacicco, A. M.; Vendemiale, G.; Capurso, A.; Imbimbo, B. P. Disease-Modifying Approach to the Treatment of Alzheimer's Disease: From α-Secretase Activators to γ-Secretase Inhibitors and Modulators. *Drugs Aging* **2009,** *26* (7), 537-555.

Patel, A. K.; Rogers, J. T.; Huang, X. Flavanols, mild cognitive impairment, and Alzheimer's dementia. *Int. J. Clin. Exp. Med.* **2008,** *1* (2), 181-91.

Pattison, L. R.; Kotter, M. R.; Fraga, D.; Bonelli, R. M. Apoptotic cascades as possible targets for inhibiting cell death in Huntington's disease. *J. Neurol.* **2006,** *253* (9), 1137-42.

Peng, J.; Kudrimoti, S.; Prasanna, S.; Odde, S.; Doerksen, R. J.; Pennaka, H. K.; Choo, Y.-M.; Rao, K. V.; Tekwani, B. L.; Madgula, V.; Khan, S. I.; Wang, B.; Mayer, A. M. S.; Jacob, M. R.; Tu, L. C.; Gertsch, J. r.; Hamann, M. T. Structure-Activity Relationship and Mechanism of Action Studies of Manzamine Analogues for the Control of Neuroinflammation and Cerebral Infections. *J. Med. Chem.* **2010,** *53* (1), 61-76.

Planells-Cases, R.; Lerma, J.; Ferrer-Montiel, A. Pharmacological Intervention at Ionotropic Glutamate Receptor Complexes. *Curr. Pharm. Des.* **2006,** *12* (28), 3583-3596.

Powers, R. NMR metabolomics and drug discovery. *Magn. Reson. Chem.* **2009,** *47 Suppl 1*, S2-11.

Price, R. D.; Milne, S. A.; Sharkey, J.; Matsuoka, N. Advances in small molecules promoting neurotrophic function. *Pharmacol. Ther.* **2007,** *115* (2), 292-306.

Qi, W.; Zhang, A.; Good, T. A.; Fernandez, E. J. Two Disaccharides and Trimethylamine N-Oxide Affect Aβ Aggregation Differently, but All Attenuate Oligomer-Induced Membrane Permeability. *Biochemistry* **2009,** *48* (37), 8908-8919.

Querfurth, H. W.; LaFerla, F. M. Alzheimer's disease. *N. Engl. J. Med. 362* (4), 329-44.

Ravikumar, B.; Berger, Z.; Vacher, C.; O'Kane, C. J.; Rubinsztein, D. C. Rapamycin pre-treatment protects against apoptosis. *Hum. Mol. Genet.* **2006,** *15* (7), 1209-16.

Reynolds, N. C.; Prost, R. W.; Mark, L. P. Heterogeneity in ^{1}H-MRS profiles of presymptomatic and early manifest Huntington's disease. *Brain Res.* **2005,** *1031* (1), 82-9.

Roze, E.; Saudou, F.; Caboche, J. Pathophysiology of Huntington's disease: from huntingtin functions to potential treatments. *Curr. Opin. Neurol.* **2008,** *21* (4), 497-503.

Sarkar, S.; Davies, J. E.; Huang, Z.; Tunnacliffe, A.; Rubinsztein, D. C. Trehalose, a Novel mTOR-independent Autophagy Enhancer, Accelerates the Clearance of Mutant Huntingtin and α-Synuclein. *J. Biol. Chem.* **2007a,** *282* (8), 5641-5652.

Sarkar, S.; Krishna, G.; Imarisio, S.; Saiki, S.; O'Kane, C. J.; Rubinsztein, D. C. A rational mechanism for combination treatment of Huntington's disease using lithium and rapamycin. *Hum. Mol. Genet.* **2008,** *17* (2), 170-178.

Sarkar, S.; Perlstein, E. O.; Imarisio, S.; Pineau, S.; Cordenier, A.; Maglathlin, R. L.; Webster, J. A.; Lewis, T. A.; O'Kane, C. J.; Schreiber, S. L.; Rubinsztein, D. C. Small molecules enhance autophagy and reduce toxicity in Huntington's disease models. *Nat. Chem. Biol.* **2007b,** *3* (6), 331-338.

Satyal, S. H.; Schmidt, E.; Kitagawa, K.; Sondheimer, N.; Lindquist, S.; Kramer, J. M.; Morimoto, R. I. Polyglutamine aggregates alter protein folding homeostasis in Caenorhabditis elegans. *Proc. Natl. Acad. Sci. U.S.A.* **2000,** *97* (11), 5750-5.

Scatena, R.; Martorana, G. E.; Bottoni, P.; Botta, G.; Pastore, P.; Giardina, B. An update on pharmacological approaches to neurodegenerative diseases. *Expert. Opin. Investig. Drugs* **2007,** *16* (1), 59-72.

Schapira, A. H. V.; Bezard, E.; Brotchie, J.; Calon, F. d. r.; Collingridge, G. L.; Ferger, B.; Hengerer, B.; Hirsch, E.; Jenner, P.; Novare, N. L.; Obeso, J. A.; Schwarzschild, M. A.; Spampinato, U.; Davidai, G. Novel pharmacological targets for the treatment of Parkinson's disease. *Nat. Rev. Drug Discov.* **2006,** *5* (10), 845-854.

Schatzl, H. M. Drug Targets in Prion Diseases. *Infect. Disord. Drug Targets* **2009,** *9* (1), 1-2.

Schiffer, N. W.; Broadley, S. A.; Hirschberger, T.; Tavan, P.; Kretzschmar, H. A.; Giese, A.; Haass, C.; Hartl, F. U.; Schmid, B. Identification of anti-prion compounds as efficient inhibitors of polyglutamine protein aggregation in a zebrafish model. *J. Biol. Chem.* **2007,** *282* (12), 9195-203.

Schlenk, D.; Gerwick, W. H. Dilophic acid, a diterpenoid from the tropical brown seaweed Dilophus guineensis. *Phytochemistry* **1987,** *26* (4), 1081-4.

Schmidt, K.; Gunther, W.; Stoyanova, S.; Schubert, B.; Li, Z.; Hamburger, M. Militarinone A, a neurotrophic pyridone alkaloid from Paecilomyces militaris. *Org. Lett.* **2002,** *4* (2), 197-9.

Schmidt, K.; Riese, U.; Li, Z.; Hamburger, M. Novel tetramic acids and pyridone alkaloids, militarinones B, C, and D, from the insect pathogenic fungus Paecilomyces militaris. *J. Nat. Prod.* **2003,** *66* (3), 378-83.

Sehgal, S. N.; Baker, H.; Vezina, C. Rapamycin (AY-22,989), a new antifungal antibiotic. II. Fermentation, isolation and characterization. *J. Antibiot. (Tokyo)* **1975,** *28* (10), 727-32.

Sheldon, A. L.; Robinson, M. B. The role of glutamate transporters in neurodegenerative diseases and potential opportunities for intervention. *Neurochem. Int.* **2007,** *51* (6-7), 333-355.

Shigeta, K.; Ootaki, K.; Tatemoto, H.; Nakanishi, T.; Inada, A.; Muto, N. Potentiation of nerve growth factor-induced neurite outgrowth in PC12 cells by a Coptidis Rhizoma extract and protoberberine alkaloids. *Biosci. Biotechnol. Biochem.* **2002,** *66* (11), 2491-4.

Simola, N.; Morelli, M.; Carta, A. The 6-Hydroxydopamine model of parkinson's disease. *Neurotox. Res.* **2007,** *11* (3), 151-167.

Singer, M. A.; Lindquist, S. Multiple effects of trehalose on protein folding in vitro and in vivo. *Mol. Cell* **1998,** *1* (5), 639-48.

Skovronsky, D. M.; Lee, V. M.; Trojanowski, J. Q. Neurodegenerative diseases: new concepts of pathogenesis and their therapeutic implications. *Annu. Rev. Pathol.* **2006,** *1*, 151-70.

Stefani, M. Generic Cell Dysfunction in Neurodegenerative Disorders: Role of Surfaces in Early Protein Misfolding, Aggregation, and Aggregate Cytotoxicity. *Neuroscientist* **2007,** *13* (5), 519-531.

Steuer, R. Review: On the analysis and interpretation of correlations in metabolomic data. *Brief. Bioinformatics* **2006,** *7* (2), 151-158.

Stiller, E. T.; Vandeputte, J.; Wachtel, J. L. Amphotericins A and B, antifungal antibiotics produced by a streptomycete. II. The isolation and properties of the crystalline amphotericins. *Antibiot. Annu.* **1955,** *3*, 587-91.

Subramaniam, S.; Sixt, K. M.; Barrow, R.; Snyder, S. H. Rhes, a striatal specific protein, mediates mutant-huntingtin cytotoxicity. *Science* **2009,** *324* (5932), 1327-30.

Sung, P.-J.; Chang, P.-C.; Fang, L.-S.; Sheu, J.-H.; Chen, W.-C.; Chen, Y.-P.; Lin, M.-R. Survey of briarane-related diterpenoids-Part II. *Heterocycles* **2005,** *65* (1), 195-204.

Sung, P.-J.; Chen, M.-C. The heterocyclic natural products of gorgonian corals of genus Briareum exclusive of briarane-type diterpenoids. *Heterocycles* **2002,** *57* (9), 1705-1715.

Sung, P.-J.; Sheu, J.-H.; Wang, W.-H.; Fang, L.-S.; Chung, H.-M.; Pai, C.-H.; Su, Y.-D.; Tsai, W.-T.; Chen, B.-Y.; Lin, M.-R.; Li, G.-Y. Survey of briarane-type diterpenoids - part III. *Heterocycles* **2008,** *75* (11), 2627-2648.

Sung, P.-J.; Sheu, J.-H.; Xu, J.-P. Survey of briarane-type diterpenoids of marine origin. *Heterocycles* **2002,** *57* (3), 535-579.

Swihart, R.; DeAngelis, D.; Feng, Z.; Bryant, J. Troublesome toxins: time to re-think plant-herbivore interactions in vertebrate ecology. *BMC Ecol.* **2009,** *9* (1), 5.

Takeshige, K.; Baba, M.; Tsuboi, S.; Noda, T.; Ohsumi, Y. Autophagy in Yeast Demonstrated with Proteinase-Deficient Mutants and Conditions for Its Induction. *J. Cell Biol.* **1992,** *119* (2), 301-311.

Tanaka, M.; Machida, Y.; Niu, S.; Ikeda, T.; Jana, N. R.; Doi, H.; Kurosawa, M.; Nekooki, M.; Nukina, N. Trehalose alleviates polyglutamine-mediated pathology in a mouse model of Huntington disease. *Nat. Med.* **2004,** *10* (2), 148-54.

Tanaka, M.; Machida, Y.; Nukina, N. A novel therapeutic strategy for polyglutamine diseases by stabilizing aggregation-prone proteins with small molecules. *J. Mol. Med.* **2005,** *83* (5), 343-352.

Taylor-Robinson, S. D.; Weeks, R. A.; Bryant, D. J.; Sargentoni, J.; Marcus, C. D.; Harding, A. E.; Brooks, D. J. Proton magnetic resonance spectroscopy in Huntington's disease: evidence in favour of the glutamate excitotoxic theory. *Mov. Disord.* **1996,** *11* (2), 167-73.

Thampithak, A.; Jaisin, Y.; Meesarapee, B.; Chongthammakun, S.; Piyachaturawat, P.; Govitrapong, P.; Supavilai, P.; Sanvarinda, Y. Transcriptional

regulation of iNOS and COX-2 by a novel compound from Curcuma comosa in lipopolysaccharide-induced microglial activation. *Neurosci. Lett.* **2009,** *462* (2), 171-5.

Tkac, I.; Dubinsky, J. M.; Keene, C. D.; Gruetter, R.; Low, W. C. Neurochemical changes in Huntington R6/2 mouse striatum detected by in vivo ^{1}H NMR spectroscopy. *J. Neurochem.* **2007,** *100* (5), 1397-406.

Tohda, C.; Kuboyama, T.; Komatsu, K. Search for natural products related to regeneration of the neuronal network. *Neurosignals* **2005,** *14* (1-2), 34-45.

Triggle, D., J.; Mitchell, J., M.; Filler, R. The Pharmacology of Physostigmine. *CNS Drug Rev.* **1998,** *4* (2), 87-136.

Tsang, T. M.; Haselden, J. N.; Holmes, E. Metabonomic Characterization of the 3-Nitropropionic Acid Rat Model of Huntington's Disease. *Neurochem. Res.* **2009,** *34* (7), 1261-1271.

Tsang, T. M.; Woodman, B.; McLoughlin, G. A.; Griffin, J. L.; Tabrizi, S. J.; Bates, G. P.; Holmes, E. Metabolic characterization of the R6/2 transgenic mouse model of Huntington's disease by high-resolution MAS ^{1}H NMR spectroscopy. *J. Proteome Res.* **2006,** *5* (3), 483-92.

Uchio, Y.; Eguchi, S.; Kuramoto, J.; Nakayama, M.; Hase, T. Denticulatolide, an ichthyotoxic peroxide-containing cembranolide from the soft coral Lobophytum denticulatum. *Tetrahedron Lett.* **1985,** *26* (37), 4487-90.

Uchio, Y.; Fukazawa, Y.; Bowden, B. F.; Coll, J. C. New diterpenes from an Australian Pachyclavularia species (Coelenterata, Anthozoa, Octocorallia). *Tennen Yuki Kagobutsu Toronkai Koen Yoshishu* **1989,** *31*, 548-553

Underwood, B. R.; Broadhurst, D.; Dunn, W. B.; Ellis, D. I.; Michell, A. W.; Vacher, C.; Mosedale, D. E.; Kell, D. B.; Barker, R. A.; Grainger, D. J.; Rubinsztein, D. C. Huntington disease patients and transgenic mice have similar pro-catabolic serum metabolite profiles. *Brain* **2006,** *129* (Pt 4), 877-86.

Urbain, A.; Marston, A.; Grilo, L. S.; Bravo, J.; Purev, O.; Purevsuren, B.; Batsuren, D.; Reist, M.; Carrupt, P. A.; Hostettmann, K. Xanthones from Gentianella amarella ssp. acuta with acetylcholinesterase and monoamine oxidase inhibitory activities. *J. Nat. Prod.* **2008,** *71* (5), 895-7.

Uversky, V. N. Neuropathology, biochemistry, and biophysics of α-synuclein aggregation. *J. Neurochem.* **2007,** *103* (1), 17-37.

Vafeiadou, K.; Vauzour, D.; Spencer, J. P. E. Neuroinflammation and its Modulation by Flavonoids. *Endocr. Metab. Immune Disord. Drug Targets* **2007,** *7* (3), 211-224.

Van der Schyf, C. J.; Gal, S.; Geldenhuys, W. J.; Youdim, M. B. Multifunctional neuroprotective drugs targeting monoamine oxidase inhibition, iron chelation, adenosine receptors, and cholinergic and glutamatergic action for neurodegenerative diseases. *Expert. Opin. Investig. Drugs* **2006,** *15* (8), 873-86.

Van der Schyf, C. J.; Mandel, S.; Geldenhuys, W. J.; Amit, T.; Avramovich, Y.; Zheng, H.; Fridkin, M.; Gal, S.; Weinreb, O.; Bar Am, O.; Sagi, Y.; Youdim, M. B. Novel multifunctional anti-Alzheimer drugs with various CNS neurotransmitter targets and neuroprotective moieties. *Curr. Alzheimer Res.* **2007,** *4* (5), 522-36.

Van Raamsdonk, J. M.; Warby, S. C.; Hayden, M. R. Selective degeneration in YAC mouse models of Huntington disease. *Brain Res. Bull.* **2007,** *72* (2-3), 124-31.

Vassar, R.; Kovacs, D. M.; Yan, R.; Wong, P. C. The β-Secretase Enzyme BACE in Health and Alzheimer's Disease: Regulation, Cell Biology, Function, and Therapeutic Potential. *J. Neurosci.* **2009,** *29* (41), 12787-12794.

Viegas Jr, C.; Bolzani, V. d. S.; Barreiro, E. J.; Fraga, C. A. M. New Anti-Alzheimer Drugs from Biodiversity: The Role of the Natural Acetylcholinesterase Inhibitors. *Mini Rev. Med. Chem.* **2005,** *5* (10), 915-926.

Voit, E. O. Biochemical and genomic regulation of the trehalose cycle in yeast: review of observations and canonical model analysis. *J. Theor. Biol.* **2003,** *223* (1), 55-78.

Walker, F. O. Huntington's disease. *Lancet* **2007,** *369* (9557), 218-28.

Wang, H.-H.; Chou, C.-J.; Liao, J.-F.; Chen, C.-F. Dehydroevodiamine attenuates β-amyloid peptide-induced amnesia in mice. *Eur. J. Pharmacol.* **2001,** *413* (2-3), 221-225.

Wang, W.; Duan, W.; Igarashi, S.; Morita, H.; Nakamura, M.; Ross, C. A. Compounds blocking mutant huntingtin toxicity identified using a Huntington's disease neuronal cell model. *Neurobiol. Dis.* **2005,** *20* (2), 500-8.

Way, J. L. Cyanide intoxication and its mechanism of antagonism. *Annu. Rev. Pharmacol. Toxicol.* **1984,** *24*, 451-81.

Webster, N.; Pirrung, M. Small molecule activators of the Trk receptors for neuroprotection. *BMC Neurosci.* **2008,** *9* (Suppl 2), S1.

Weljie, A. M.; Newton, J.; Mercier, P.; Carlson, E.; Slupsky, C. M. Targeted profiling: quantitative analysis of ^{1}H NMR metabolomics data. *Anal. Chem.* **2006,** *78* (13), 4430-42.

Williams, R. B.; Gutekunst, W. R.; Joyner, P. M.; Duan, W.; Li, Q.; Ross, C. A.; Williams, T. D.; Cichewicz, R. H. Bioactivity profiling with parallel mass spectrometry reveals an assemblage of green tea metabolites affording protection against human huntingtin and alpha-synuclein toxicity. *J. Agric. Food Chem.* **2007,** *55* (23), 9450-6.

Wolfgang, W. J.; Miller, T. W.; Webster, J. M.; Huston, J. S.; Thompson, L. M.; Marsh, J. L.; Messer, A. Suppression of Huntington's disease pathology in Drosophila by human single-chain Fv antibodies. *Proc. Natl. Acad. Sci. U.S.A.* **2005,** *102* (32), 11563-8.

Wu, S.-L.; Sung, P.-J.; Su, J.-H.; Sheu, J.-H. Briaexcavatolides S-V, Four New Briaranes from a Formosan Gorgonian Briareum excavatum. *J. Nat. Prod.* **2003,** *66* (9), 1252-1256.

Yan, X.-Z. Isolation and identification of stilbene glycoside from Polygonum multiflorum Thunb. *Shanghai Diyi Yixueyuan Xuebao* **1981,** *8* (2), 123-126.

Yuan, D.; Ma, B.; Wu, C.; Yang, J.; Zhang, L.; Liu, S.; Wu, L.; Kano, Y. Alkaloids from the leaves of Uncaria rhynchophylla and their inhibitory activity on NO production in lipopolysaccharide-activated microglia. *J. Nat. Prod.* **2008,** *71* (7), 1271-4.

Yuen, E. C.; Mobley, W. C. Therapeutic potential of neurotrophic factors for neurological disorders. *Ann. Neurol.* **1996,** *40* (3), 346-354.

Zangara, A. The psychopharmacology of huperzine A: an alkaloid with cognitive enhancing and neuroprotective properties of interest in the treatment of Alzheimer's disease. *Pharmacol. Biochem. Behav.* **2003,** *75* (3), 675-686.

Zhang, L.; Xing, Y.; Ye, C.-F.; Ai, H.-X.; Wei, H.-F.; Li, L. Learning-memory deficit with aging in APP transgenic mice of Alzheimer's disease and intervention by using tetrahydroxystilbene glucoside. *Behav. Brain Res.* **2006,** *173* (2), 246-254.

Zhang, X.; Smith, D. L.; Meriin, A. B.; Engemann, S.; Russel, D. E.; Roark, M.; Washington, S. L.; Maxwell, M. M.; Marsh, J. L.; Thompson, L. M.; Wanker, E. E.; Young, A. B.; Housman, D. E.; Bates, G. P.; Sherman, M. Y.; Kazantsev, A. G. A potent small molecule inhibits polyglutamine aggregation in Huntington's disease neurons and suppresses neurodegeneration in vivo. *Proc. Natl. Acad. Sci. U.S.A.* **2005,** *102* (3), 892-7.

Appendix

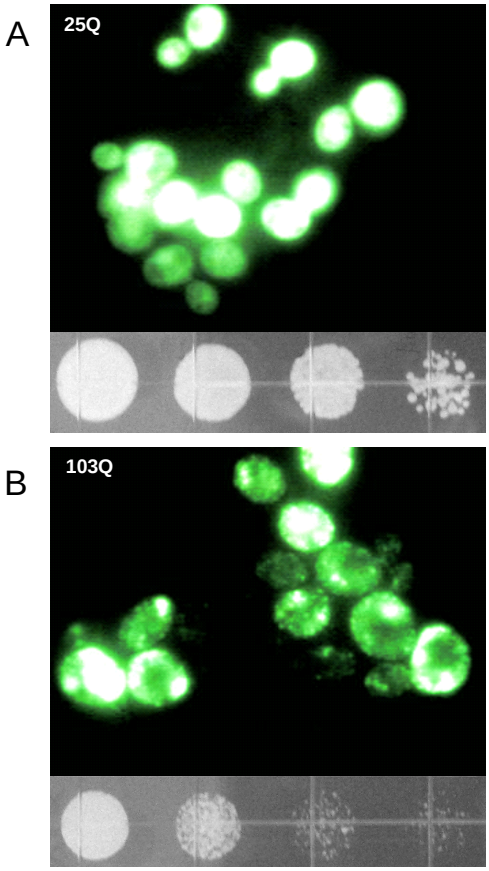

Figure A1 False-color fluorescent microscopy images of yeast cells expressing human *Htt* fragments. A) Yeast expressing *Htt* fragment with 25 glutamine repeats. B) Yeast expressing m*Htt* fragment with 103 glutamine repeats. Spot cultures (A, lower panel; B, lower panel) show a significant decrease in cell viability due to mutant huntingtin toxicity.

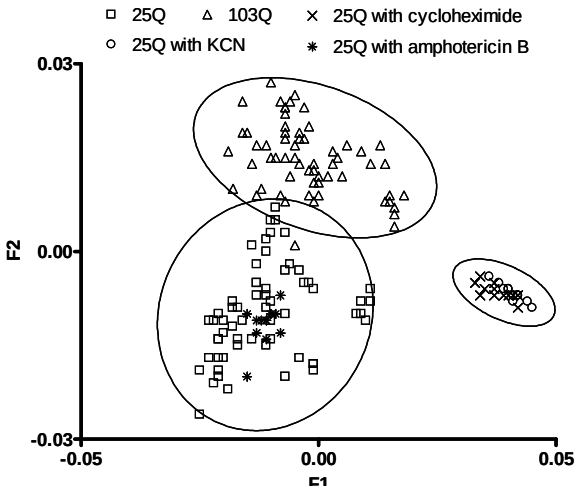

Figure A2 Comparison of metabolic changes in response to various toxins. Potassium cyanide (KCN) and cycloheximide treatment cause distinct metabolic changes in 25Q yeast that are different from the changes caused by *mHtt* toxicity.

Table A1 Structures of Metabolites with ^{1}H NMR Chemical Shifts and Multiplicities

Metabolite	Structure with ^{1}H NMR Chemical Shifts and Multiplicities
4-aminobutyrate	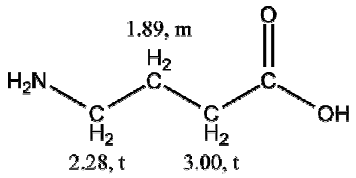
acetate	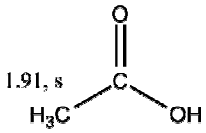
adenosine	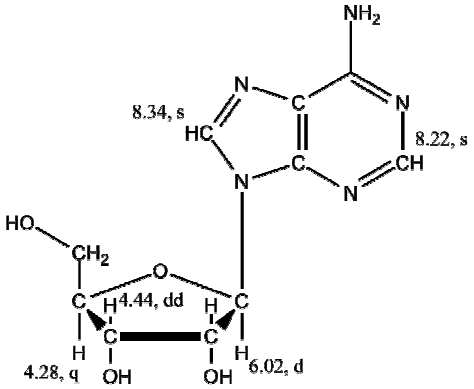
adenosine triphosphate	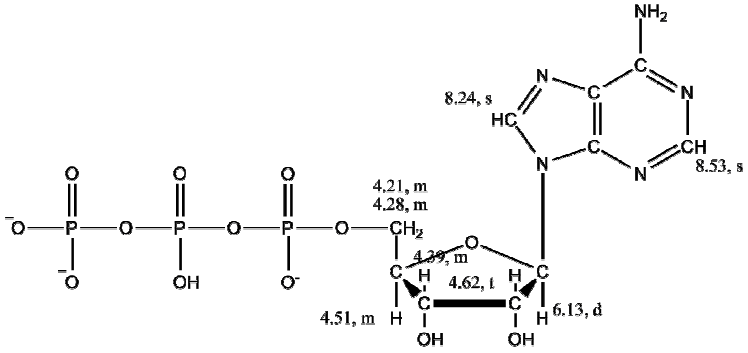
alanine	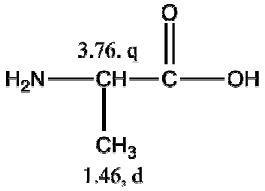
arginine	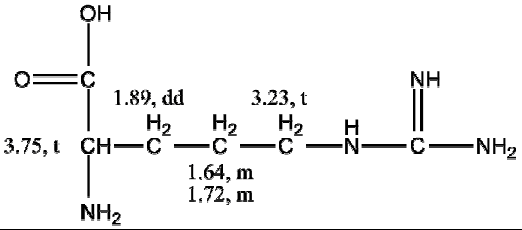

Table A1 Structures of Metabolites with ^{1}H NMR Chemical Shifts and Multiplicities (continued from page 105)

Metabolite	Structure with ^{1}H NMR Chemical Shifts and Multiplicities
asparagine	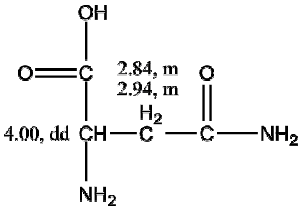
aspartate	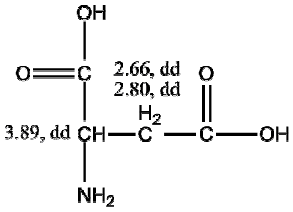
formate	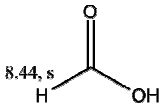
galactitol	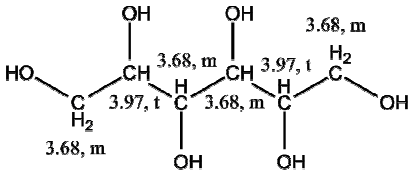
galactose	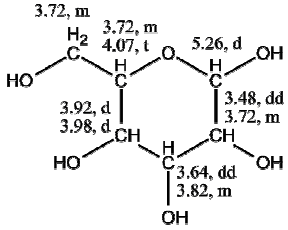
glutamate	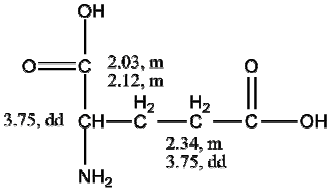
glutamine	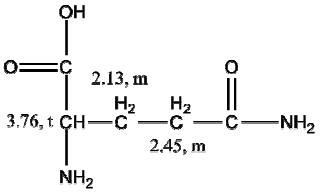
glutathione	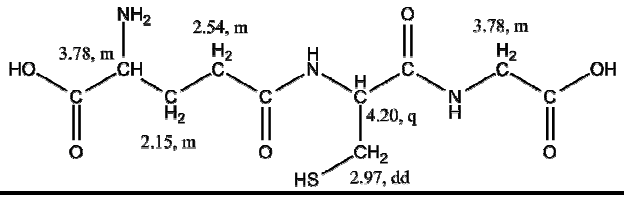

Table A1 Structures of Metabolites with ^{1}H NMR Chemical Shifts and Multiplicities

(continued from page 106)

Metabolite	Structure with ^{1}H NMR Chemical Shifts and Multiplicities
glycerol	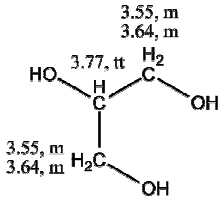
histidine	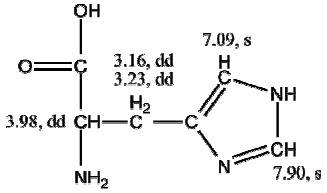
isoleucine	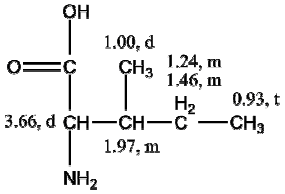
leucine	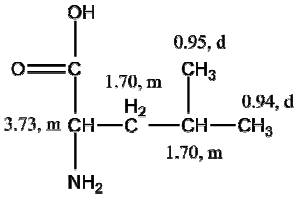
methionine	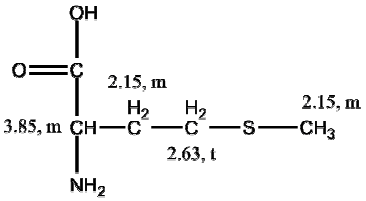
Nicotinamide adenine dinucleotide (oxidized)	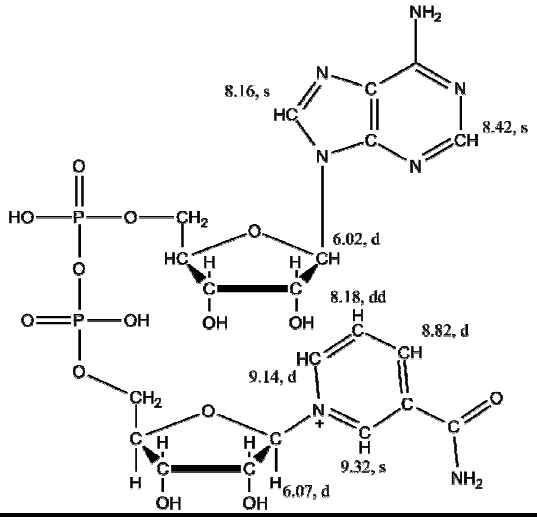

Table A1 Structures of Metabolites with ^{1}H NMR Chemical Shifts and Multiplicities

(continued from page 107)

Metabolite	Structure with ^{1}H NMR Chemical Shifts and Multiplicities
phenylalanine	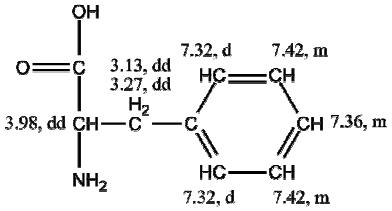
proline	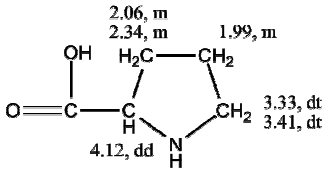
propylene glycol	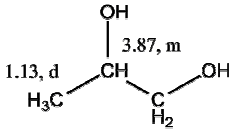
succinate	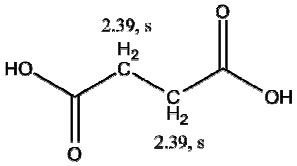
threonine	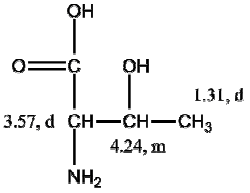
trehalose	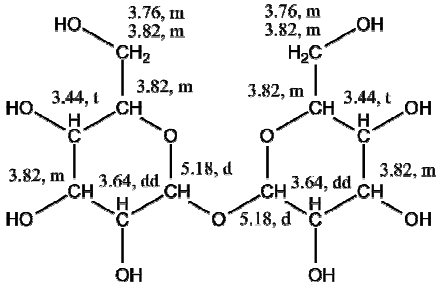
tryptophan	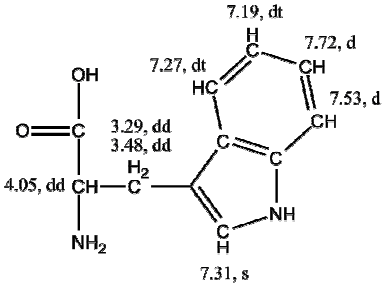

Table A1 Structures of Metabolites with ^{1}H NMR Chemical Shifts and Multiplicities

(continued from page 108)

Metabolite	Structure with ^{1}H NMR Chemical Shifts and Multiplicities
tyrosine	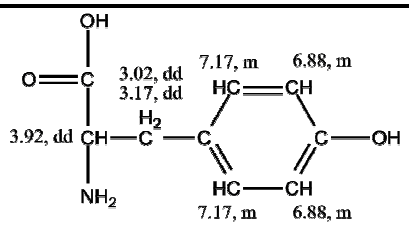
valine	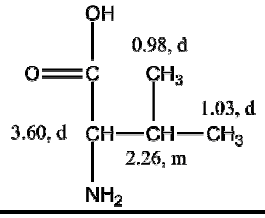

Table A2 Metabolic Profiling Data for Selected Key Metabolites Identified in Studies of Huntington's Disease Model Systems and Humans

	This study	**Nicoli et al. (1993)[4]**	**Taylor-Robinson et al. (1996)[5]**	**Reynolds et al. (2005)[6]**	**Underwood et al. (2006)[7]**	**Jenkins et al. (2000)[8]**	**Jenkins et al. (2005)[9]**	**Tsang et al. (2006)[10]**	**Tkac et al. (2007)[11]**
Organism	yeast	human [a, b]	human [c, d]	human [d]	human [b], mouse [b]	mouse [c, d, e]	mouse [c, d]	mouse [b, c, e, f]	mouse [c, d]
Data collection technique	^{1}H NMR	^{1}H NMR, HPLC	^{1}H MRS	^{1}H MRS	GC-TOF-MS	^{1}H-NMR	^{1}H MRS	^{1}H NMR, HR-MAS ^{1}H NMR	*in vivo* ^{1}H NMR
2-amino-*n*-butyrate	ND	ND	ND	ND	significant [g, h]	ND	ND	ND	ND
2-oxoglutarate	ND	ND	ND	ND	ND	ND	ND	increase	ND
4-aminobutyrate	ns	ns	ND	ND	ND	ns	ND	decrease	ns
acetate	decrease	ns	ND	ND	ND	ND	ND	decrease	ND
adenosine	ns	ND	ND	ND	ND	ND	ND	ND	ND
alanine	decrease	ns	ND	ND	significant [g, h]	ns	ND	decrease	ND
arginine	ns	ND	ND	ND	ND	ND	ND	ND	ND
ascorbate	ND	ND	ND	ND	ND	ND	ND	ND	increase
asparagine	ns	ND	ND	ND	ND	ND	ND	ND	ND
aspartate	ns	ns	ND	ND	ND	ns	ND	decrease	ND
ATP	ns	ND	ND	ND	ND	ND	ND	ND	ND
choline	ND	ND	ns	ND	ND	increase	increase	decrease	ND
citrate	ND	ns	ND	ND	ND	ND	ND	ND	ND
creatine	ND	ns	ns	decrease	ND	ns	ns	increase	increase
dimethylglycine	ND	ND	ND	ND	ND	ND	ND	decrease	ND
ethylene glycol	ND	ND	ND	ND	significant [g, h]	ND	ND	ND	ND
formate	ns	ND	ND	ND	ND	ND	ND	ND	ND
galactitol	ns	ND	ND	ND	ND	ND	ND	ND	ND
galactose	increase	ND	ND	ND	ND	ND	ND	ND	ND
glucose	ND	ND	ND	ND	significant [g, i]	increase	ND	ND	ns
glutamate	ns	ns	increase	increase	ND	decrease	ns	decrease	increase
glutamine	increase	ns	increase	increase	ND	increase	ns	increase	increase
glutathione	ns	ND	ND	ND	ND	ND	ND	ND	increase
glycerol	increase	ND	ND	ND	significant [g]	ND	ND	ND	ND
glycerophosphocholine	ND	ND	ND	ND	ND	ND	ND	increase	increase
glycine	ND	increase	ND	ND	ND	ns	ND	ns	ND

Table A2 Metabolic Profiling Data for Selected Key Metabolites Identified in Studies of Huntington's Disease Model Systems and Humans (continued from page 110)

	This study	**Nicoli et al. (1993)[4]**	**Taylor-Robinson et al. (1996)[5]**	**Reynolds et al. (2005)[6]**	**Underwood et al. (2006)[7]**	**Jenkins et al. (2000)[8]**	**Jenkins et al. (2005)[9]**	**Tsang et al. (2006)[10]**	**Tkac et al. (2007)[11]**
Organism	yeast	human [a, b]	human [c, d]	human [d]	human [b], mouse [b]	mouse [c, d, e]	mouse [c, d]	mouse [b, c, e, f]	mouse [c, d]
Data collection technique	^{1}H NMR	^{1}H NMR, HPLC	^{1}H MRS	^{1}H MRS	GC-TOF-MS	^{1}H-NMR	^{1}H MRS	^{1}H NMR, HR-MAS ^{1}H NMR	*in vivo* ^{1}H NMR
histidine	decrease	ND	ND	ND	ND	ND	ND	ND	ND
isoleucine	ns	ns	ND	ND	ND	ND	ND	ND	ND
lactate	ND	ns	ns	increase	significant [g]	decrease	ND	increase	ns
leucine	ns	ns	ND	ND	ND	ND	ND	ND	ND
lysine	ND	ns	ND	ND	ND	ND	ND	ND	ND
malonate	ND	ND	ND	ND	significant [g]	ND	ND	ND	ND
methionine	ns	ND	ND	ND	ND	ND	ND	ND	ND
myo-inositol	ND	ND	ND	ns	ND	ns	ND	increase	increase
N-acetylaspartate	ND	ND	ns	decrease	ND	decrease	decrease	decrease	decrease
N-acetylaspartate glutamate	ND	ND	ND	ND	ND	ND	ND	increase/ decrease	ns
NAD+	ns	ND	ND	ND	ND	ND	ND	ND	ND
phenylalanine	ns	ND	ND	ND	ND	ND	ND	ND	ND
phosphocholine	ND	ND	ND	ND	ND	ND	ND	decrease	ns
phosphocreatine	ND	ND	ND	ND	ND	ND	ND	ND	increase
phosphorylethanolamine	ND	ND	ND	ND	ND	ND	ND	ND	decrease
proline	decrease	ns	ND	ND	ND	ND	ND	ND	ND
propylene glycol	ns	ND	ND	ND	ND	ND	ND	ND	ND
pyroglutamate	ND	ND	ND	ND	significant g, i	ND	ND	ND	ND
pyruvate	ND	increase	ND	ND	ND	ND	ND	ND	ND
scyllo-inositol	ND	ND	ND	ND	ND	increase	ND	increase	ND
spermine	ND	ND	ND	ND	ND	ND	ND	decrease	ND
succinate	decrease	ND	ND	ND	ND	decrease	ND	decrease	ND
taurine	ND	ND	ND	ND	ND	increase	increase	increase	increase
threonine	increase	ND	ND	ND	ND	ND	ND	ND	ND
trehalose	decrease	ND	ND	ND	ND	ND	ND	ND	ND

Table A2 Metabolic Profiling Data for Selected Key Metabolites Identified in Studies of Huntington's Disease Model Systems and Humans (continued from page 111)

	This study	**Nicoli et al. (1993)[4]**	**Taylor-Robinson et al. (1996)[5]**	**Reynolds et al. (2005)[6]**	**Underwood et al. (2006)[7]**	**Jenkins et al. (2000)[8]**	**Jenkins et al. (2005)[9]**	**Tsang et al. (2006)[10]**	**Tkac et al. (2007)[11]**
Organism	yeast	human [a, b]	human [c, d]	human [d]	human [b], mouse [b]	mouse [c, d, e]	mouse [c, d]	mouse [b, c, e, f]	mouse [c, d]
Data collection technique	^{1}H NMR	^{1}H NMR, HPLC	^{1}H MRS	^{1}H MRS	GC-TOF-MS	^{1}H-NMR	^{1}H MRS	^{1}H NMR, HR-MAS ^{1}H NMR	*in vivo* ^{1}H NMR
trimethylamine	ND	ND	ND	ND	ND	ND	ND	decrease	ND
trimethylamine N-oxide	ND	ND	ND	ND	ND	ND	ND	increase	ND
tryptophan	ns	ND	ND	ND	ND	ND	ND	ND	ND
tyrosine	ns	ND	ND	ND	ND	ND	ND	ND	ND
urea	ND	ND	ND	ND	significant g	ND	ND	ND	ND
valine	increase	ND	ND	ND	significant g	ND	ND	ND	ND
α-hydroxybutyric acid	ND	ND	ND	ND	significant g, h	ND	ND	ND	ND
α-ketoisocaproate	ND	ND	ND	ND	ND	ND	ND	decrease	ND

Abbreviations: ND = Not detected or not reported, ns = not significant, MRS = magnetic resonance spectroscopy, HR-MAS = high-resolution magic angle spinning, HPLC = high performance liquid chromatography. [a] Cerebrospinal fluid. [b] Serum. [c] Results from multiple tissue types summarized in this table. [d] *In vivo* brain. [e] *In vitro* brain. [f] Urine. [g] Direction of change (increase/decrease) not reported. [h] Detected only in human serum.

Table A3 Contingency Table of Metabolic Studies of Mutant Huntingtin Toxicity

Metabolite	**Yeast**	**Human**	**Mouse**	**TOTALS**
2-amino-n-butyrate	0	1	0	1
2-oxoglutarate	0	0	1	1
4-aminobutyrate	0	0	1	1
acetate	1	0	1	2
alanine	1	1	1	3
ascorbate	0	0	1	1
aspartate	0	0	1	1
choline	0	0	3	3
creatine	0	1	2	3
dimethylglycine	0	0	1	1
ethylene glycol	0	1	0	1
galactitol	1	0	0	1
glucose	0	0	2	2
glutamate	0	2	3	5
glutamine	1	2	3	6
glutathione	0	0	1	1
glycerol	1	1	1	3
glycerophosphocholine	0	0	2	2
glycine	0	1	0	1
histidine	1	0	0	1
lactate	0	2	3	5
malonate	0	1	1	2
myo-inositol	0	0	2	2
N-acetylaspartate	0	1	4	5
phosphocholine	0	0	1	1
phosphocreatine	0	0	1	1
phosphorylethanolamine	0	0	1	1
proline	1	0	0	1
pyroglutamate	0	0	1	1
pyruvate	0	1	0	1
scyllo-inositol	0	0	2	2
spermine	0	0	1	1
succinate	1	0	2	3
taurine	0	0	4	4
threonine	1	0	0	1
trehalose	1	0	0	1
trimethylamine	0	0	1	1
trimethylamine N-oxide	0	0	1	1
urea	0	1	1	2
valine	1	1	1	3
alpha-hydroxybutyric acid	0	1	0	1
alpha-ketoisocaproate	0	0	1	1
TOTALS	11	18	52	81

Table A4 NMR Spectroscopic Data ($CDCl_3$) for RAM A (**2**)

position	δC,[a] mult.[b]	δH (J in Hz)[c]	COSY[c]	HMBC[c]	NOESY[c]
1	48.2, C				
2	77.4, CH	3.25, dd (5.5, 7.0)	3a, 2-OH	4, 10, 15	16, 10
3a	40.1, CH2	2.00, m	2, 3b, 4	2, 4, 5	3b
3b		2.84, t (13.0)	3a, 4	1, 2, 4, 5	3a, 7
4	72.8, CH	5.16, ddd (1.0, 5.5, 13.0)	3a	3, 6, 5, 16, 4-OCOCH3	16
5	144.2, C				
6	122.5, CH	5.41, dt (1.3, 9.5)	7, 16	4, 16	16
7	73.6, CH	5.78, d (9.5)	6, 12-OCOCH3	5, 6, 19	3b
8	71.3, C				
9	65.1, CH	5.92, d (4.0)	10	1, 8, 12, 17, 9-OCOCH3	18, 20
10	44.6, CH	2.46, d (4.0)	9	1, 2, 8, 9, 11, 12, 15, 20	2
11	72.4, C				
12	73.5, CH	4.73, d (6.0)	13	9, 10, 11, 13, 14, 20, 12-OCOCH3	13, 20
13	121.9, CH	5.96, dd (6.0, 10.3)	12, 14	1, 11	12
14	142.0, CH	5.89, d (10.3)	13	1, 2, 10, 12, 15	15, 2-OH
15	14.0, CH3	1.13, s		1, 2, 10, 13, 14	14, 20, 9-OCOCH3
16	26.5, CH3	2.04, d (1.3)	6	4, 5, 6	2, 4, 6
17	64.8, C				
18	9.7, CH3	1.67, s		8, 10, 17, 19	9
19	170.4, C				
20	21.2, CH3	1.21, s	11-OH	4, 10	9, 12, 15, 2-OH
4-OCOCH3	170.3, C				
4-OCOCH3	21.0, CH3	2.08, s		4-OCOCH3	
9-OCOCH3	168.3, C				
9-OCOCH3	21.6, CH3	2.24, s		9, 9-OCOCH3	15
12-OCOCH3	169.8, C				
12-OCOCH3	20.9, CH3	2.06, s	7	12-OCOCH3	
2-OH		2.14, d (5.5)	2	2, 3	14, 20
11-OH		2.38, s	20	11, 20	9 (vw), 12 (w)

[a]Data determined at 100 MHz
[b]Determined by HSQC experiment at 500 MHz
[c]Data determined at 500 MHz

Table A5 NMR Spectroscopic Data ($CDCl_3$) for RAM B (**3**)

position	δC, [a] mult.[b]	δH (J in Hz)[c]	COSY[c]	HMBC[c]	INADEQUATE[a]	NOESY[d]
1	48.2, C				2, 10, 14	
2	77.5, CH	3.27, dd (5.0, 7.0)	3a	15	1, 3	10, 16
3a	40.2, CH2	2.00, m	2, 3b	2	2, 4	3b, 4, 7, 15
3b		2.84, dd (13.0, 14.3)	3a, 4	1, 2, 5		3a, 7, 15
4	72.5, CH	5.17, dd (5.0, 7.0, 13.0)	3b	3, 5, 6, 16, 1’	3	3a
5	144.3, C				16	
6	122.4, CH	5.41, dt (1.3, 9.5)	7, 16	16		
7	73.6, CH	5.78, d (9.5)	6	5, 6, 19		3a, 3b
8	71.4, C					
9	65.2, CH	5.92, d (3.8)	10	8, 9-OCOCH3		10, 18, 20
10	44.7, CH	2.47, d (3.8)	9, 11-OH	1, 2, 8, 9, 11, 15, 20		2, 9
11	72.6, C					
12	73.5, CH	4.75, d (6.0)	13	10, 11, 13, 14, 12-OCOCH3	13	13, 20
13	122.1, CH	5.97, dd (6.0, 10.3)	12, 14	1	12	12
14	141.9, CH	5.89, d (10.3)	13	1, 10, 15		15
15	14.1, CH3	1.13, s		1, 2, 14		3a, 3b, 14, 20 9-OCOCH3
16	26.5, CH3	2.05, d (1.3)	6		5	2
17	64.9, C					
18	9.7, CH3	1.69, s		8, 17, 19		9
19	170.4, C					
20	21.2, CH3	1.22, s				9, 12, 15
1’	173.2, C				2’	
2’	34.2, CH2	2.32, t (7.5)	23	1’, 3’, 4’	1’, 3’	
3’	24.5, CH2	1.64, m	22, 24	1’, 2’, 4’, 5’	2’, 4’	
4’	31.2, CH2	1.32, m		5’	3’, 5’	
5’	22.3, CH2	1.32, m	26	4’	4’, 6’	
6’	13.9, CH3	0.90, t (7.0)	25	4’, 5’	5’	
9-OCOCH3	168.3, C					
9-OCOCH3	21.6, CH3	2.24, s		9-OCOCH3		15
12-OCOCH3	169.8, C					
12-OCOCH3	20.9, CH3	2.07, s		11, 12-OCOCH3		
11-OH		2.39, br s	10, 20	20		
2-OH		4.87, br s				

[a]Data determined at 100 MHz
[b]Determined by HSQC experiment at 400 MHz
[c]Data determined at 400 MHz
[d]Data determined at 500 MHz

Table A6 NMR Spectroscopic Data ($CDCl_3$) for RAM C (**4**)

position	δC, [a] mult.b	δH (J in Hz)c	COSYd	HMBCd	NOESYc
1	48.2, C				
2	77.5, CH	3.26, t (7.5)	3a	15, 3, 10, 1	
3a	40.2, CH2	2.00, m	2, 3b, 4	4, 2	2, 3b, 4, 7, 15
3b		2.85, dd (12.7, 14.3)	3a, 4	1, 4, 2, 5	2, 3b, 4, 6, 7, 9, 10, 15, 9-OCOCH3
4	72.5, CH	5.17, ddd (1.0, 5.5, 12.7)	3a, 3b	16, 6, 5	2, 3a, 3b, 7, 16
5	144.4, C				
6	122.4, CH	5.40, dt (1.5, 9.5)	7, 16	16, 4	10, 16
7	73.6, CH	5.78, d (9.5)	6	9, 6, 5, 19	3b, 9-OCOCH3
8	71.4, C				
9	65.2, CH	5.92, d (4.0)	10	8, 9-OCOCH3	
10	44.7, CH	2.47, d (4.0)	9	15, 20, 1, 9, 8, 11, 2	2, 6, 9
11	72.6, C				
12	73.5, CH	4.74, d (6.0)	13	20, 10, 11, 13, 14, 12-OCOCH3	10, 13, 14, 20, 11-OH
13	122.0, CH	5.96, dd (6.0, 10.3)	12, 14	1, 4	12, 15, 20
14	142.0, CH	5.89, d (10.3)	13	15, 10, 1, 12, 2	2, 12, 15, 20, 11-OH
15	14.1, CH3	1.13, s		10, 1, 2, 14	14, 16, 18, 9-OCOCH3, 12-OCOCH3
16	26.5, CH3	2.05, d (1.5)	6	4, 5, 6	
17	64.9, C				
18	9.7, CH3	1.68, s		17, 8, 19	9
19	170.4, C				
20	21.2, CH3	1.22, s	11-OH	10, 11, 12	9, 15
1’	173.1, C				
2’	34.2, CH2	2.32, t (7.5)	3’	1’, 3’, 4’	3’, 4’, 7
3’	24.8, CH2	1.62, m	2’, 4’	1’, 2’, 4’	
4’	29.0, CH2	1.31	3’	5’	
5’	28.9, CH2	1.31			
6’	31.6, CH2	1.29		8’	
7’	22.6, CH2	1.28	8’		
8’	14.1, CH3	0.88, t (7.0)	7’	6’, 7’	
9-OCOCH3	168.3, C				
9-OCOCH3	21.6, CH3	2.24, s		9-OCOCH3	15, 16, 18, 20, 12-OCOCH3, 2-OH
12-OCOCH3	169.8, C				
12-OCOCH3	20.9, CH3	2.06, s		12-OCOCH3	
11-OH		2.39, br s	20		
2-OH		2.63, br s			

[a]Data determined at 100 MHz
[b]Determined by HSQC experiment at 400 MHz.
[c]Data determined at 500 MHz
[d]Data determined at 400 MHz

Table A7 NMR Spectroscopic Data ($CDCl_3$) for RAM A-M1 (**5**)

position	δC, [a] mult.[b]	δH (J in Hz)[c]	COSY[d]	HMBC[d]	NOESY[c]
1	48.0, C				
2	77.7, CH	3.32, d (7.7)	3a	15	10, 16
3a	40.1, CH2	2.00	2, 3b, 4	4, 2, 5	3b, 15
3b		2.83, dd (12.5, 14.0)	3a, 4	1, 4	3a, 7, 15
4	72.9, CH	5.17, ddd (12.5, 5.5, 1.0)	3a, 3b	16, 3, 6, 5, 4-OCOCH3	16
5	144.2, C				
6	122.4, CH	5.39, dt (9.5, 1.5)	7, 16	16, 4	7, 16
7	73.9, CH	5.78, d (9.5)	6	5, 19	3b, 6
8	71.4, C				
9	65.6, CH	5.92, d (3.4)	10	10, 1, 17, 12, 8, 7, 9-OCOCH3	18, 20, 11-OH
10	44.0, CH	2.40, d (3.4)	9	15, 20, 1, 9, 8, 7, 2	2, 11-OH
11	77.2, C				
12	70.6, CH	3.75, d (6.0)	13	10, 13, 14	13, 20
13	124.4, CH	5.90, dd (10.3, 6.0)	12, 14	1, 12, 7	12
14	140.0, CH	5.83, d (10.3)	13	15, 10, 1, 12, 2	15
15	14.1, CH3	1.13, s		10, 1, 2, 14	3a, 3b, 14, 9-OCOCH3
16	26.6, CH3	2.04, d (1.5)	6	4, 6, 5	2, 4, 6
17	64.9, C				
18	9.8, CH3	1.71, s		17, 8, 19	9
19	170.5, C				
20	21.4, CH3	1.17, s		10, 12, 7	9, 12
4-OCOCH3	170.2, C				
4-OCOCH3	21.1, CH3	2.09, s		4-OCOCH3	
9-OCOCH3	168.3, C				
9-OCOCH3	21.6, CH3	2.25, s		9-OCOCH3	15
11-OH		2.65, br s		20	9, 10

[a]Data determined at 100 MHz
[b]Determined by HSQC experiment at 400 MHz.
[c]Data determined at 500 MHz
[d]Data determined at 400 MHz

Table A8 NMR Spectroscopic Data ($CDCl_3$) for RAM B-M1 (**6**)

position	δC,[a] mult.[b]	δH (J in Hz)[c]	COSY[d]	HMBC[c]	NOESY[c]
1	48.0, C				
2	77.6, CH	3.32, d (7.3)	3a	3, 4, 10, 15	10, 16
3a	40.1, CH2	2.00 m	3b, 2, 4	2, 4, 5	3b
3b		2.83, dd (12.4, 14.5)	3a, 4	1, 4	3a, 7, 15
4	72.8, CH	5.17, dd (5.4, 12.4)	3a, 3b	5, 6, 16, 1’	16
5	144.3, C				
6	122.3, CH	5.38, dt (9.5, 1.2)	16, 7	4, 16	7, 16
7	73.8, CH	5.76, d (9.5)	6	5, 6, 19	3b, 6
8	71.4, C				
9	65.6, CH	5.92, d (3.5)	10	1, 7, 8, 10, 9-OCOCH3	10, 18, 20, 11-OH
10	44.0, CH	2.40, d (3.5)	20, 9	1, 2, 7, 8, 9, 15, 20	2, 9, 11-OH
11	73.9, C				
12	70.6, CH	3.75, d (6.0)	13	10, 11, 13, 14, 20	13, 14, 20
13	124.2, CH	5.90, dd (6.0, 10.2)	12, 14	11, 12	12, 14
14	140.1, CH	5.84, d (10.2)	13	1, 10, 12, 15	12, 13, 15
15	14.1, CH3	1.13, s			3b, 14, 9-OCOCH3
16	26.6, CH3	2.04, d (1.2)	6	4,5, 6	2, 4, 6
17	64.9, C				
18	9.8, CH3	1.70, s		8, 17, 19	9
19	170.5, C				
20	21.4, CH3	1.16, s	10	10, 11, 12	9, 12
1’	173.1, C				
2’	34.2, CH2	2.32, t, 7.4	3’	1’, 3’, 4’	3’
3’	24.6, CH2	1.63, m, 7.4	2’, 4’	1’, 2’, 4’, 5’	2’, 4’
4’	31.2, CH2	1.32, m	3’	5’	3’
5’	22.3, CH2	1.32, m	6’	4’	6’
6’	13.9, CH3	0.90, t (7.0)	5’	4’, 5’	5’
9-OCOCH3	168.3, C				
9-OCOCH3	21.6, CH3	2.24, s		9-OCOCH3	
11-OH		2.67, br. s		11, 20	9, 10

[a]Data determined at 100 MHz
[b]Determined by HSQC experiment at 500 MHz.
[c]Data determined at 500 MHz
[d]Data determined at 400 MHz

Table A9 NMR Spectroscopic Data ($CDCl_3$) for RAM C-M1 (**7**)

position	δC,[a] mult.[b]	δH (J in Hz)[c]	COSY[d]	HMBC[c]	NOESY[c]
1	48.0, C				
2	77.7, CH	3.33, d (7.0)	3a	4, 15	10, 16
3a	40.1, CH2	2.00, m	2, 3b, 4	2, 4, 5	3b, 15
3b		2.83, dd (12.5, 14.0)	3a, 4	1, 2, 4	3a, 7, 15
4	72.7, CH	5.17, dd (5.4, 12.5)	3a, 3b	3a, 5, 6, 16, 1’	16
5	144.3, C				
6	122.3, CH	5.38, d (9.4)	7, 16	4, 16	7, 16
7	73.7, CH	5.76, d (9.4)	6	5, 6, 19	3b, 6
8	71.4, C				
9	65.6, CH	5.92, d (3.0)	10	8, 11	18, 20, 11-OH
10	44.0, CH	2.40, d (3.0)	9	1, 2, 8, 11, 15, 20	
11	73.9, C				
12	70.6, CH	3.75, d (6.0)	13	10, 11, 13, 14, 20	20
13	124.3, CH	5.90, dd (6.0, 10.4)	12, 14	9-OCOCH3	14
14	140.1, CH	5.84, d (10.4)	13	1, 10, 12	13, 15
15	14.1, CH3	1.13, s		1, 2, 10, 14	3a, 3b, 14, 9-OCOCH3
16	26.6, CH3	2.04, s	6	4, 5, 6	2, 4, 6
17	64.9, C				
18	9.8, CH3	1.71, s		8, 17, 19	9
19	170.5, C				
20	21.4, CH3	1.17, s		10, 11, 12	9, 12
1’	173.1, C				
2’	34.3, CH2	2.32, t (7.5)	3’	1’, 3’, 4’	3’
3’	24.9, CH2	1.63, m	2’,4’	1’, 2’, 4’	2’
4’	29.0, CH2	1.31, m	3’	5’	
5’	28.9, CH2	1.31, m			
6’	31.6, CH2	1.27, m			
7’	22.6, CH2	1.29, m	8’	8’	8’
8’	14.07, CH3	0.88, t (7.5)	7’	6’, 7’	7’
9-OCOCH3	168.3, C				
9-OCOCH3	21.6, CH3	2.24, s		9-OCOCH3	
11-OH		2.67, br. s		11, 20	

[a]Data determined at 100 MHz
[b]Determined by HSQC experiment at 500 MHz.
[c]Data determined at 500 MHz
[d]Data determined at 400 MHz

Table A10 Crystallographic data and structure refinement for RAM A (**2**). Data was collected and interpreted by Dr. Douglas Powell in the Department of Chemistry and Biochemistry at the University of Oklahoma.

Empirical formula	$C_{26}\ H_{34}\ O_{11}$
Formula weight	522.53
Crystal system	Monoclinic
Space group	$P2_1$
Unit cell dimensions	a = 9.724(2) Å α= 90° b = 14.873(3) Å β= 115.539(8)° c = 10.233(2) Å γ= 90°
Volume	1335.3(5) $Å^3$
Z, Z'	2, 1
Density (calculated)	1.300 Mg/m^3
Wavelength	0.71073 Å
Temperature	100(2) K
F(000)	556
Absorption coefficient	Semi-empirical from equivalents
Max. and min. transmission	0.979 and 0.961
Theta range for data collection	2.21 to 26.00°
Reflections collected	11814
Independent reflections	5239 [R(int) = 0.0258]
Data / restraints / parameters	5239 / 1 / 340
$wR(F^2$ all data)	$wR2$ = 0.0766
R(F obsd data)	$R1$ = 0.0331
Goodness-of-fit on F^2	1.005
Observed data [I > 2σ(I)]	4977
Absolute structure parameter	0.3(6)
Largest and mean shift / s.u.	0.000and 0.000
Largest diff. peak and hole	0.177 and -0.175 $e/Å^3$

$wR2 = (\Sigma [w(F_o^2 - F_c^2)^2] / \Sigma [w(F_o^2)^2])^{1/2}$

$R1 = \Sigma ||F_o| - |F_c|| / \Sigma |F_o|$

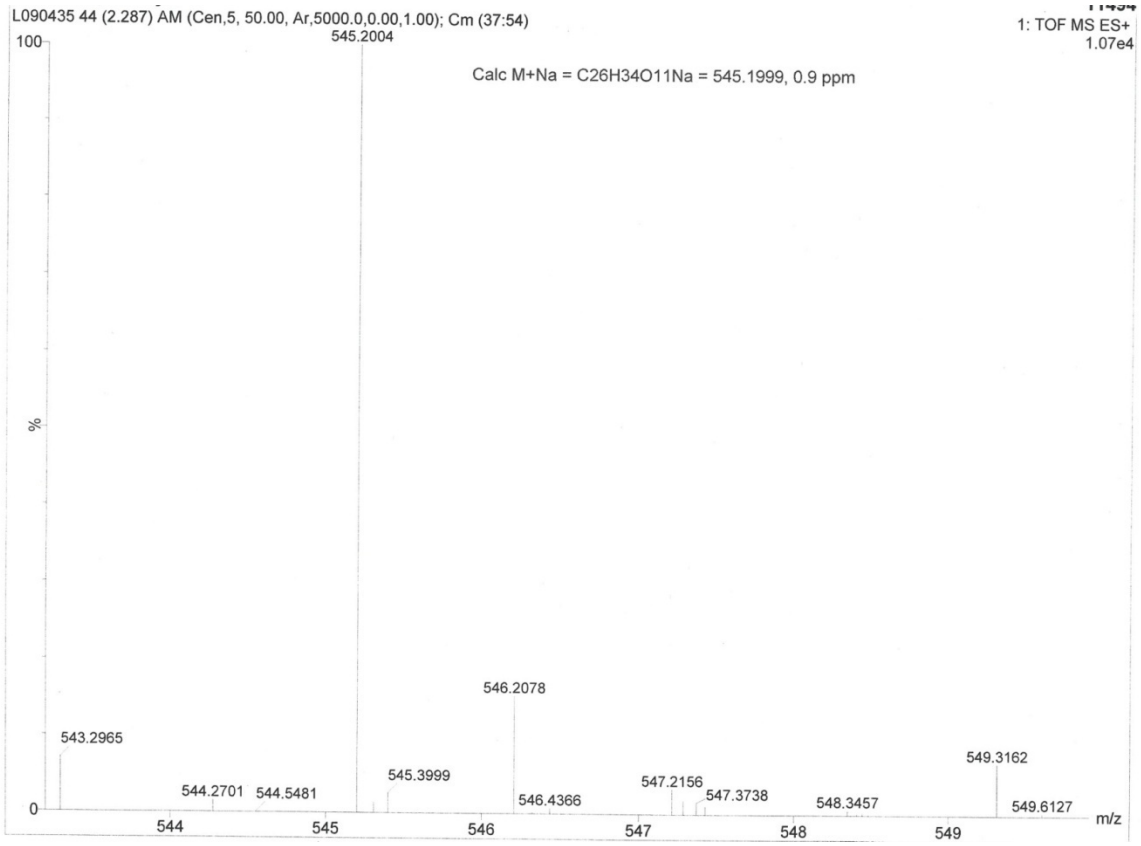

Figure A3 HRESIMS of RAM A (**2**)

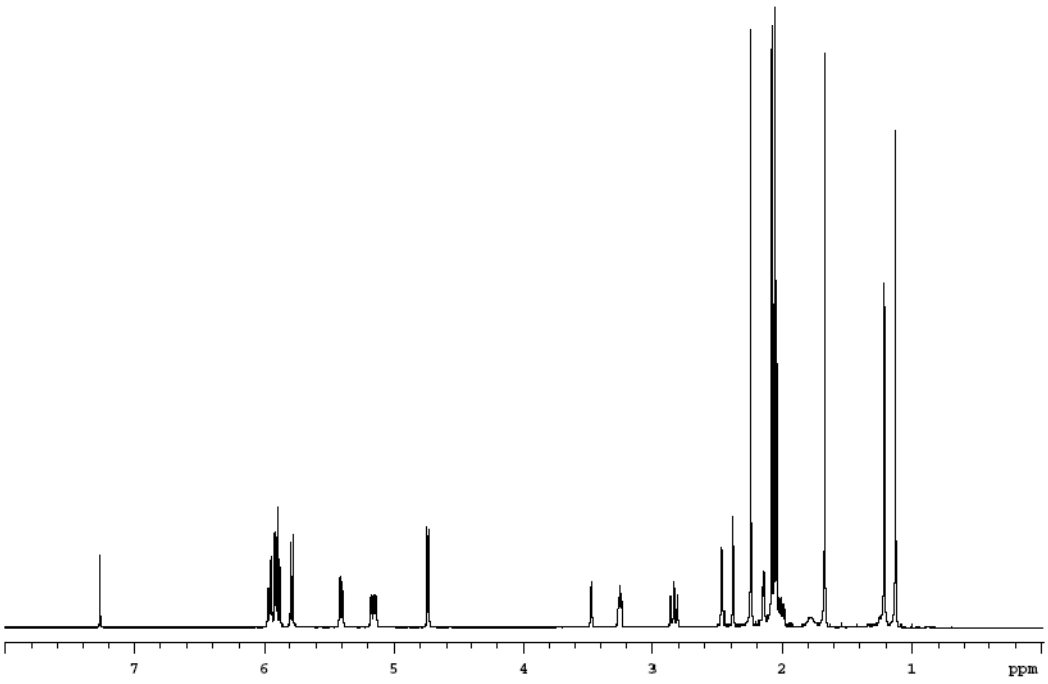

Figure A4 ^{1}H-NMR spectrum (500 MHz, $CDCl_3$) of RAM A (**2**)

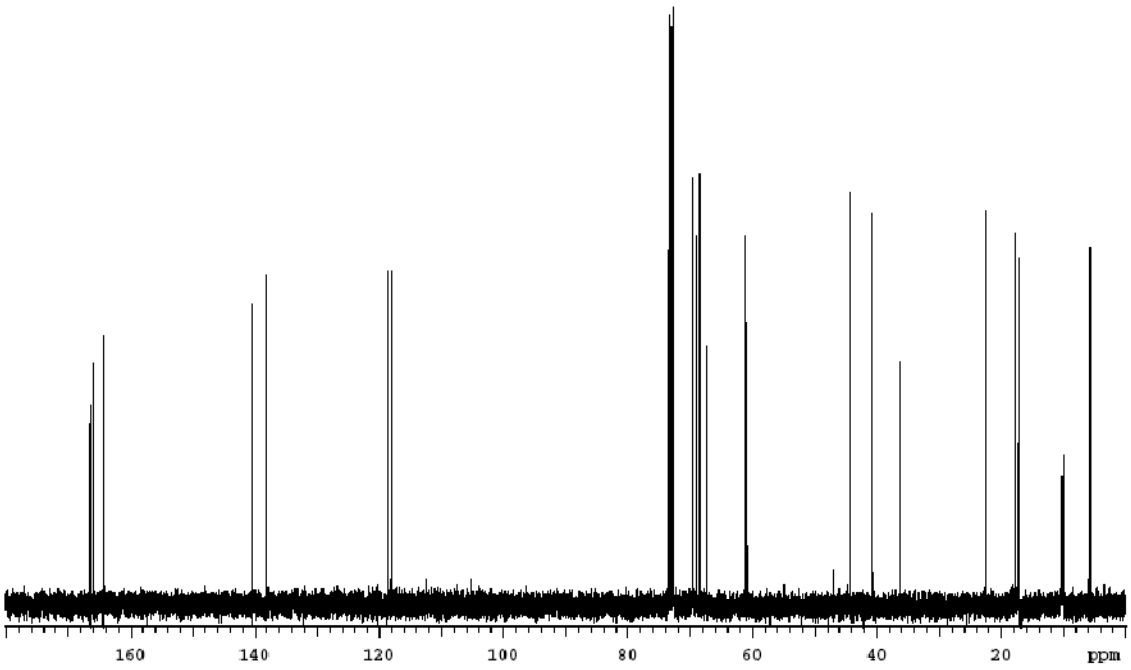

Figure A5 ^{13}C-NMR spectrum (125 MHz, $CDCl_3$) of RAM A (**2**)

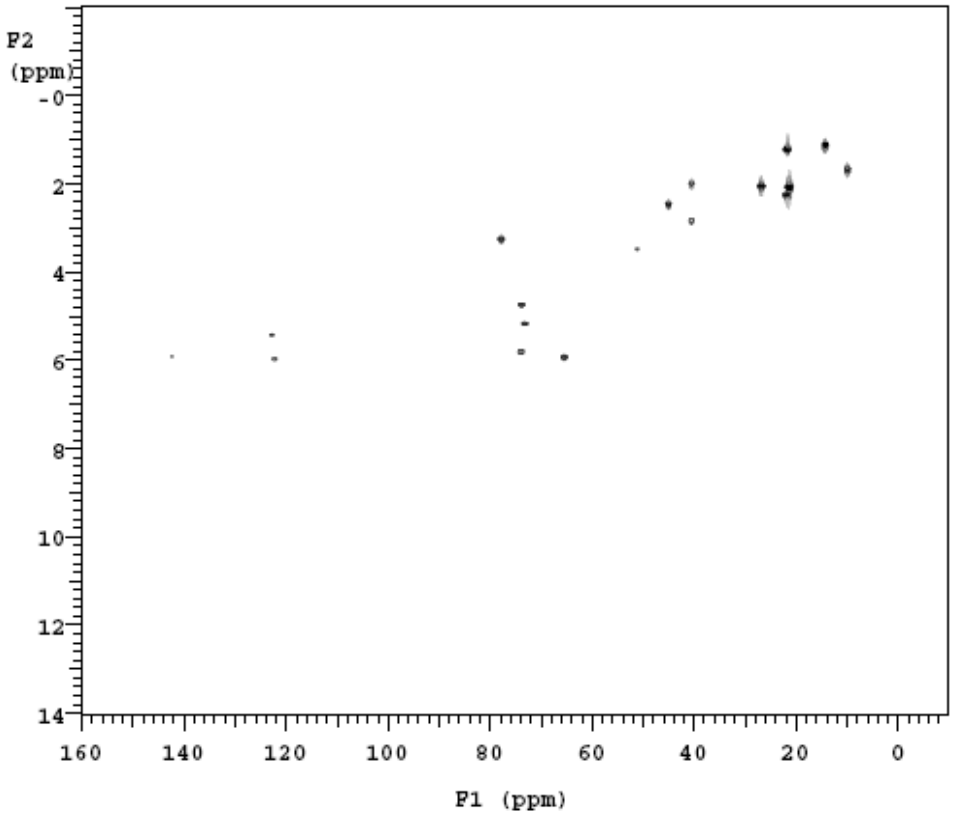

Figure A6 HSQC-NMR spectrum (500 MHz, $CDCl_3$) of RAMA (**2**)

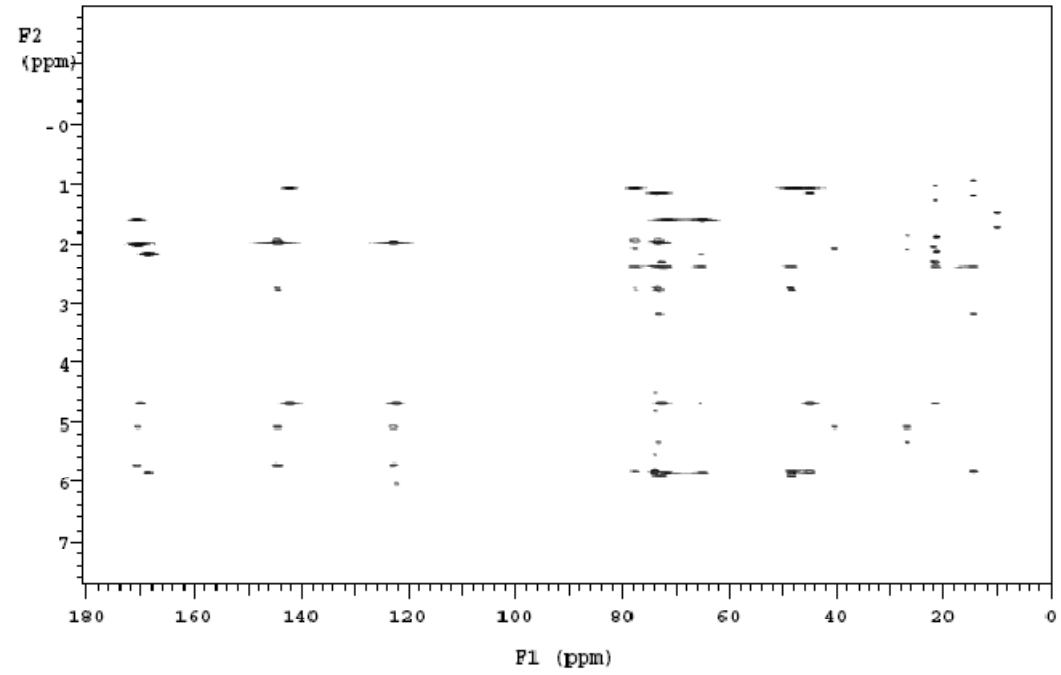

Figure A7 HMBC-NMR spectrum (500 MHz, $CDCl_3$) of RAM A (**2**)

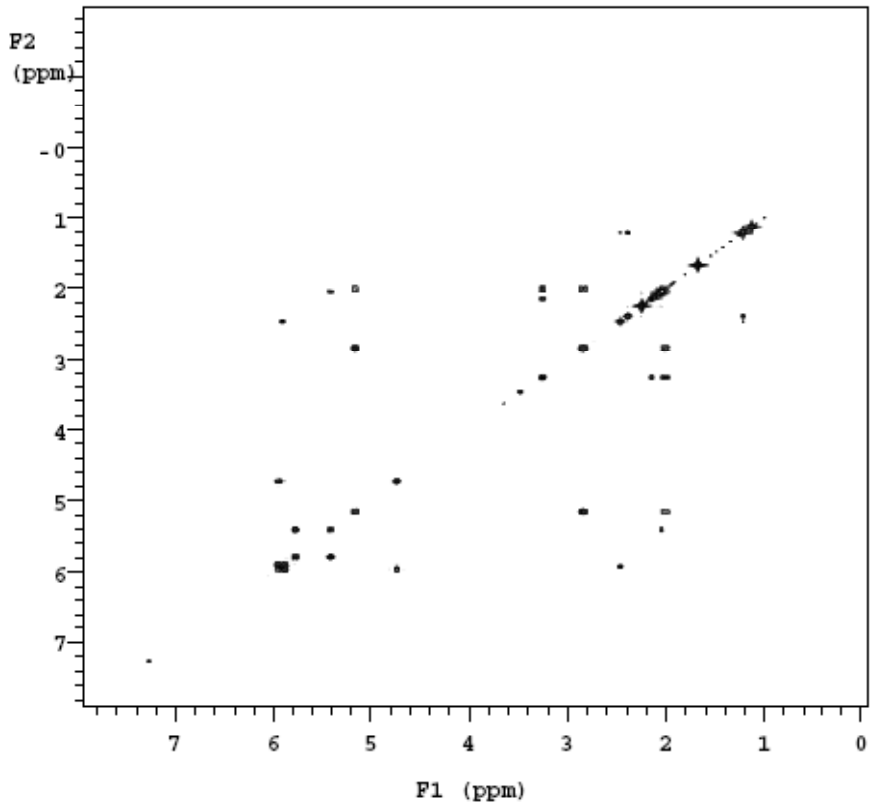

Figure A8 COSY-NMR spectrum (500 MHz, $CDCl_3$) of RAM A (**2**)

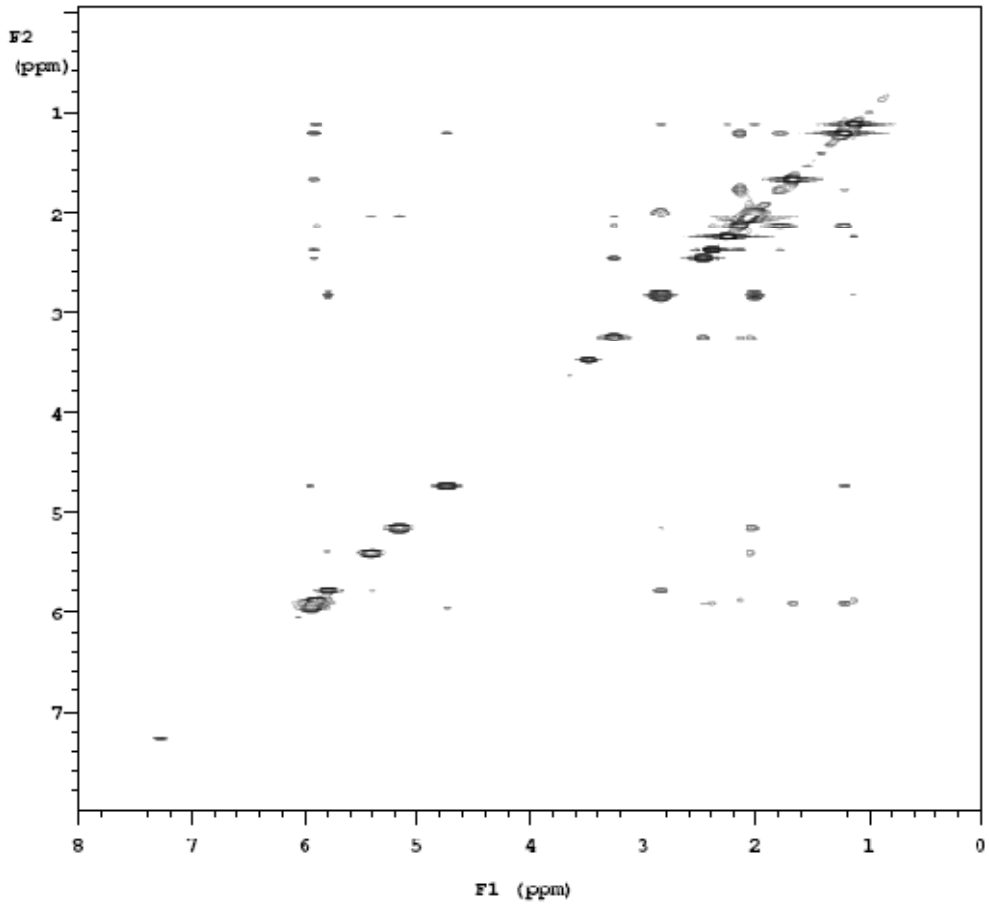

Figure A9 NOESY-NMR spectrum (500 MHz, $CDCl_3$) of RAM A (**2**)

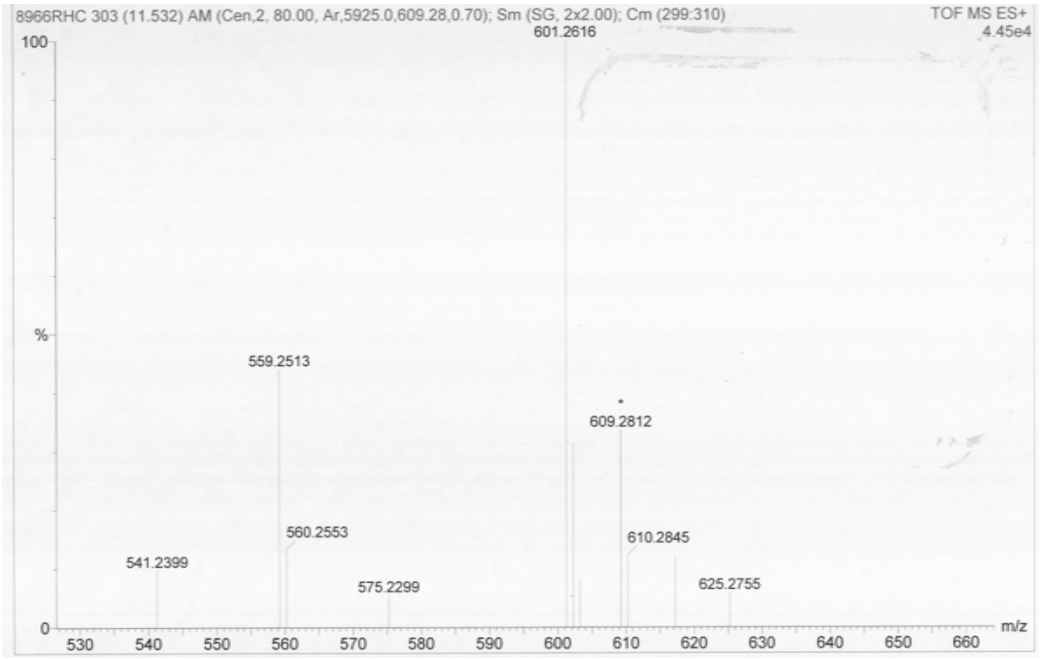

Figure A10 HRESIMS of RAM B (**3**)

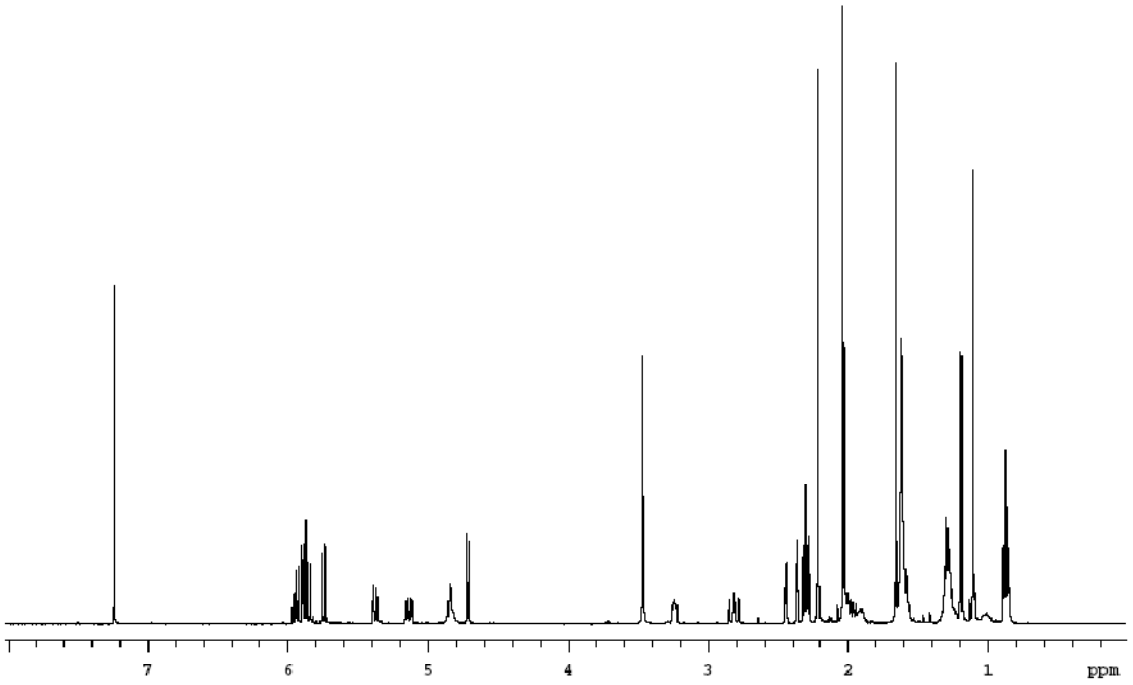

Figure A11 ^{1}H-NMR spectrum (400 MHz, $CDCl_3$) of RAM B (**3**)

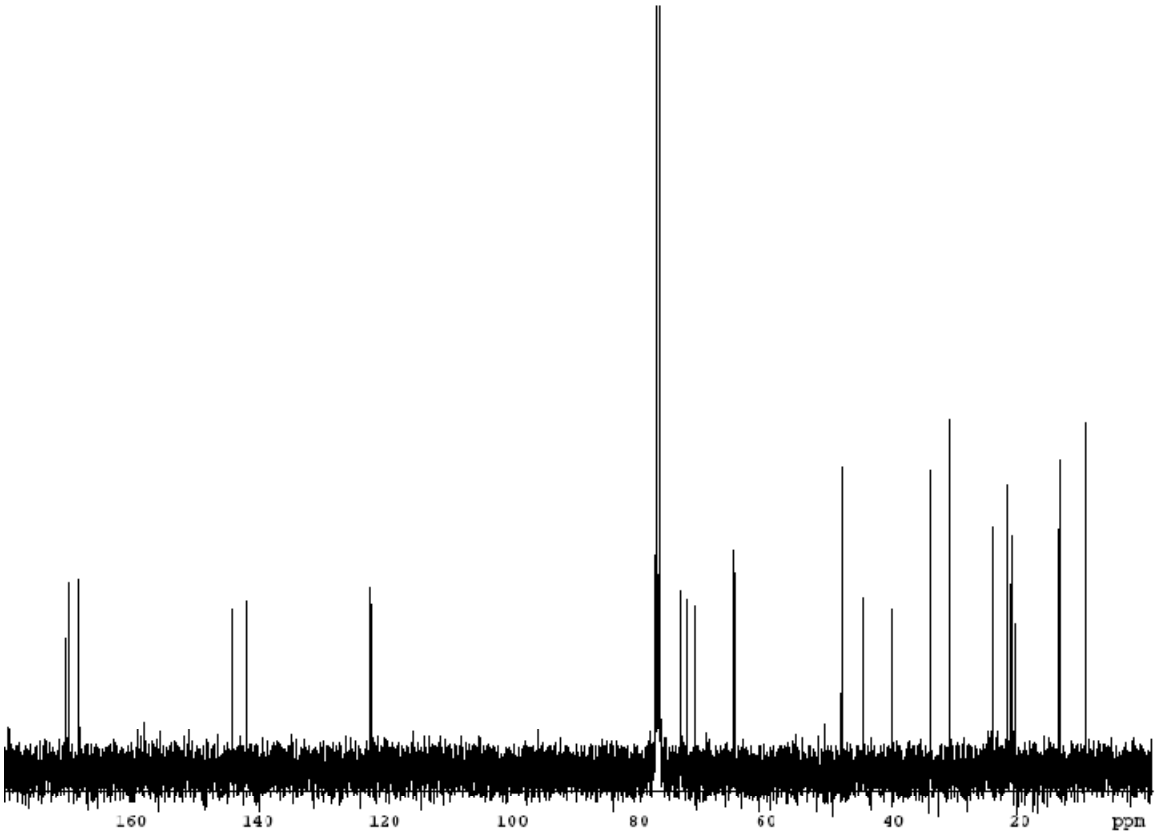

Figure A12 ^{13}C-NMR spectrum (100 MHz, $CDCl_3$) of RAM B (**3**)

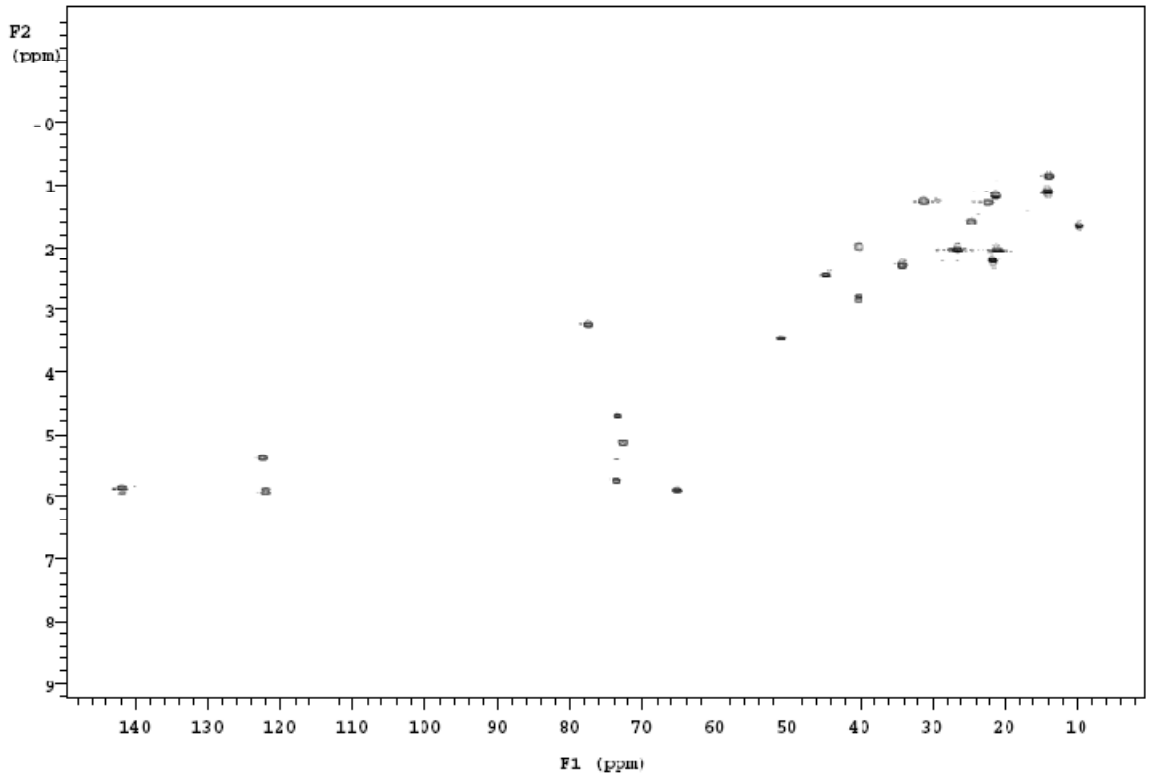

Figure A13 HSQC-NMR spectrum (400 MHz, $CDCl_3$) of RAM B (**3**)

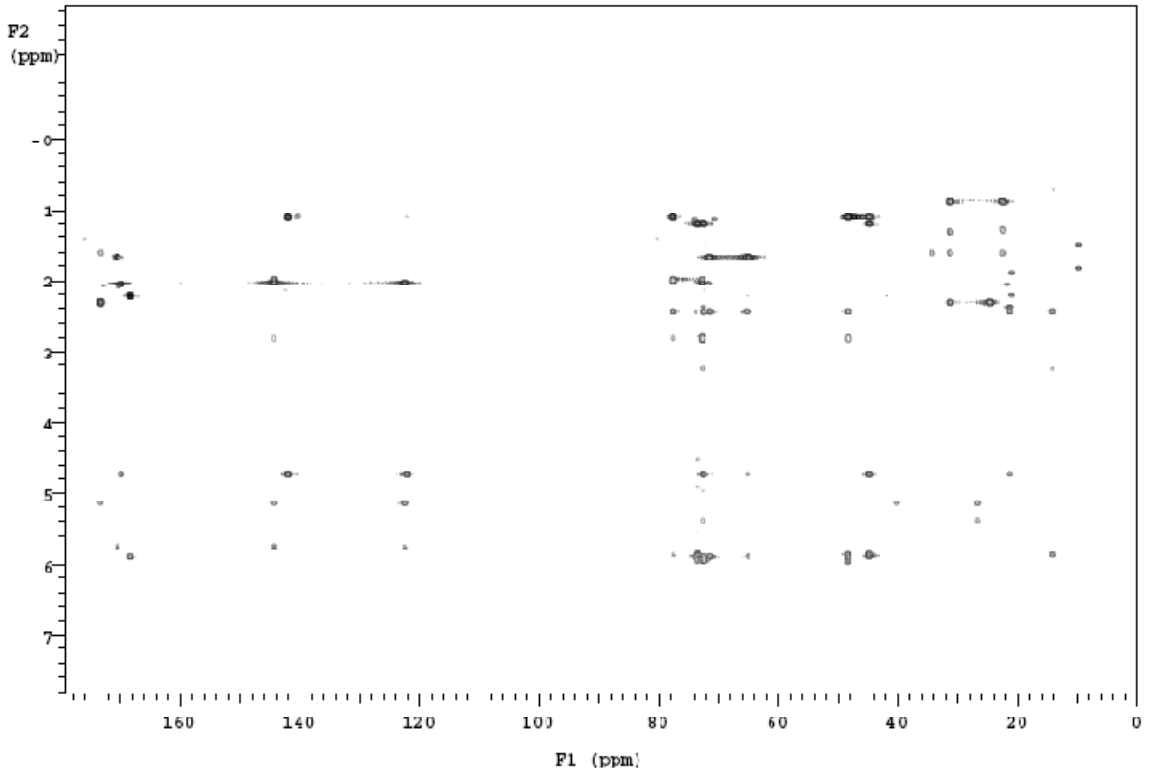

Figure A14 HMBC-NMR spectrum (400 MHz, $CDCl_3$) of RAM B (**3**)

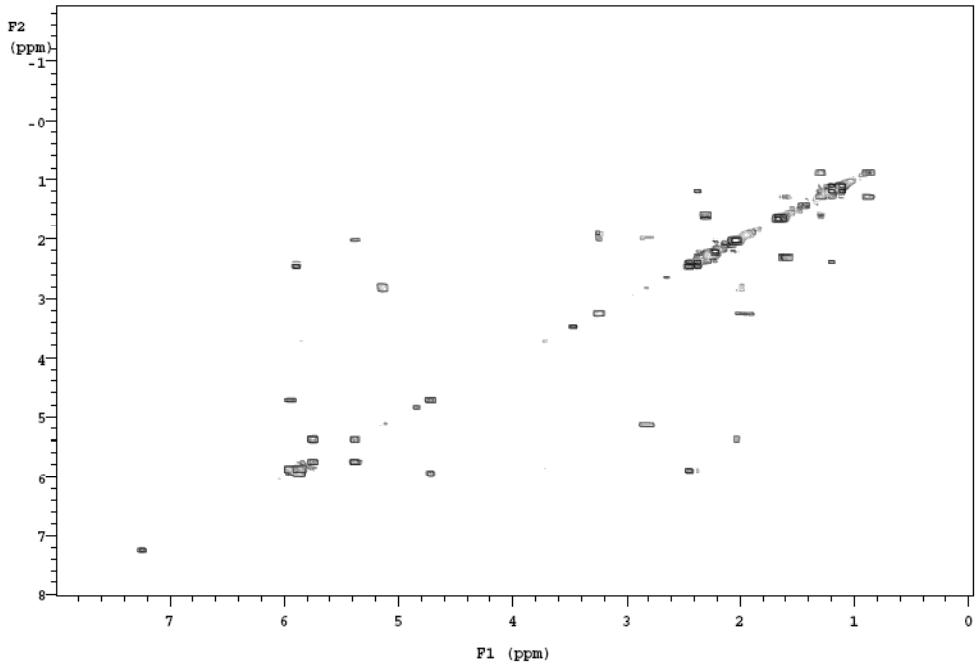

Figure A15 COSY-NMR spectrum (400 MHz, $CDCl_3$) of RAM B (**3**)

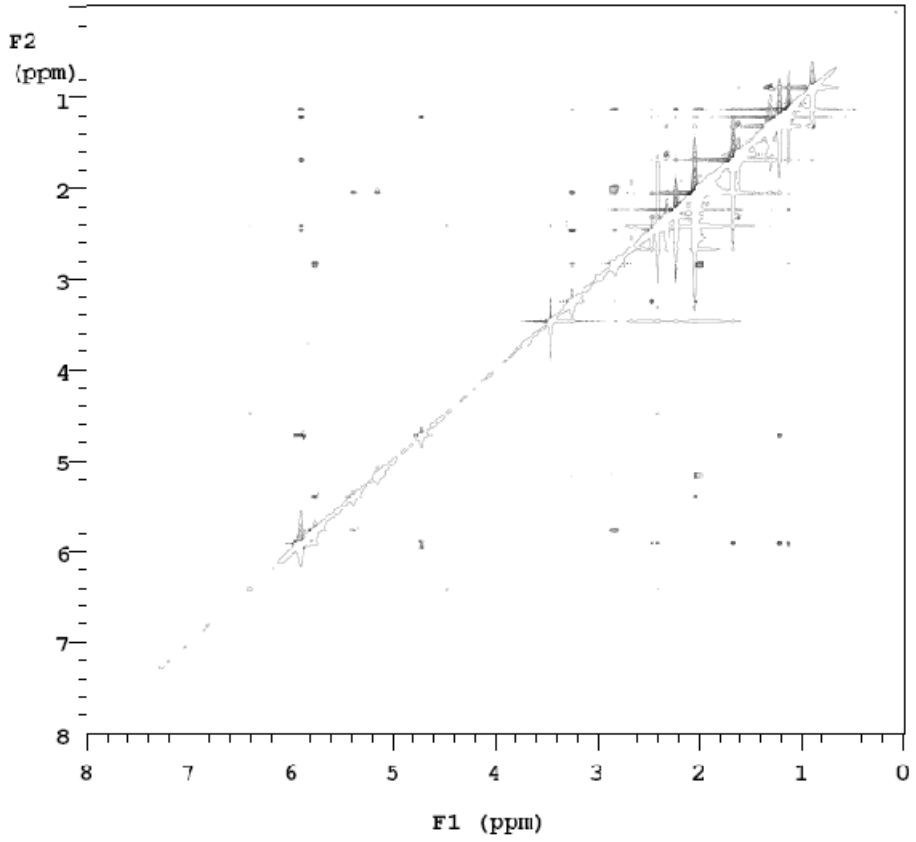

Figure A16 NOESY-NMR spectrum (500 MHz, $CDCl_3$) of RAM B (**3**)

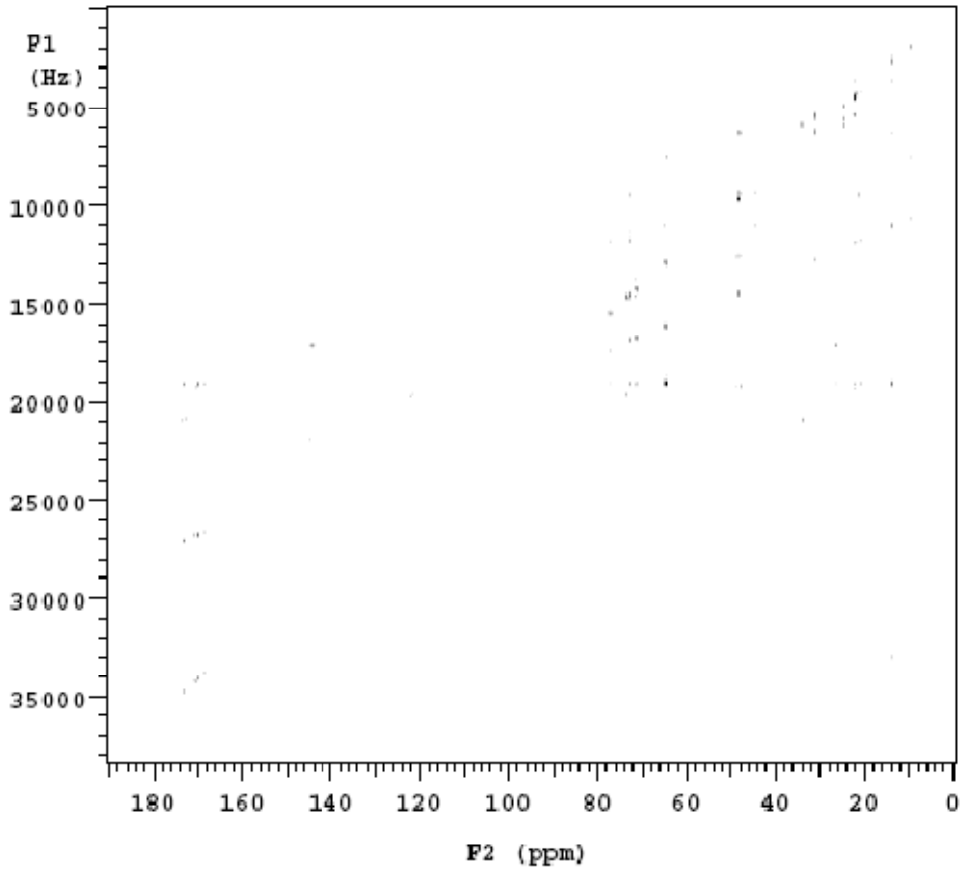

Figure A17 INADEQUATE-NMR spectrum (400 MHz, $CDCl_3$) of RAM B (**3**)

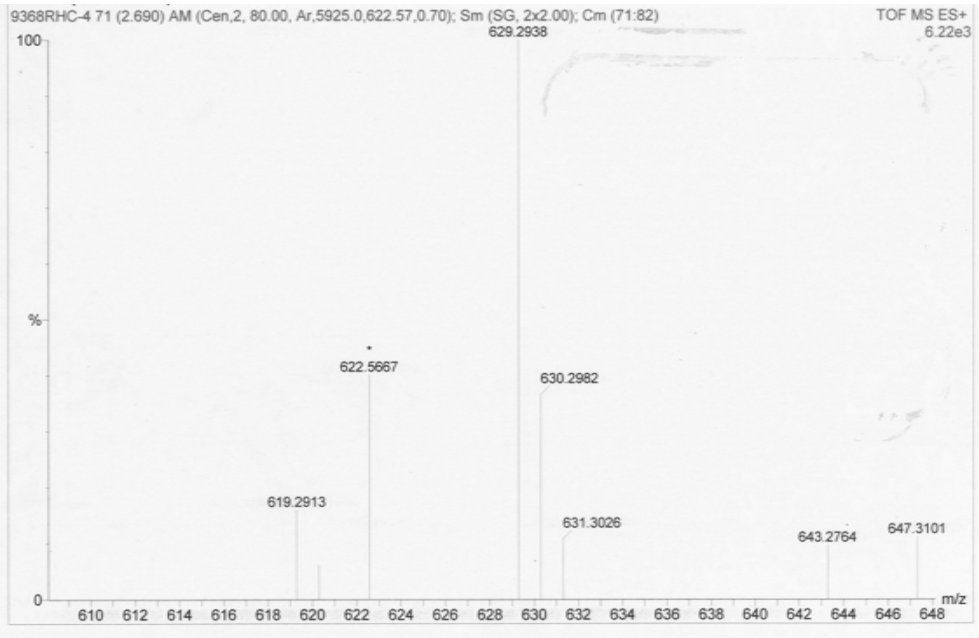

Figure A18 HRESIMS of RAM C (**4**)

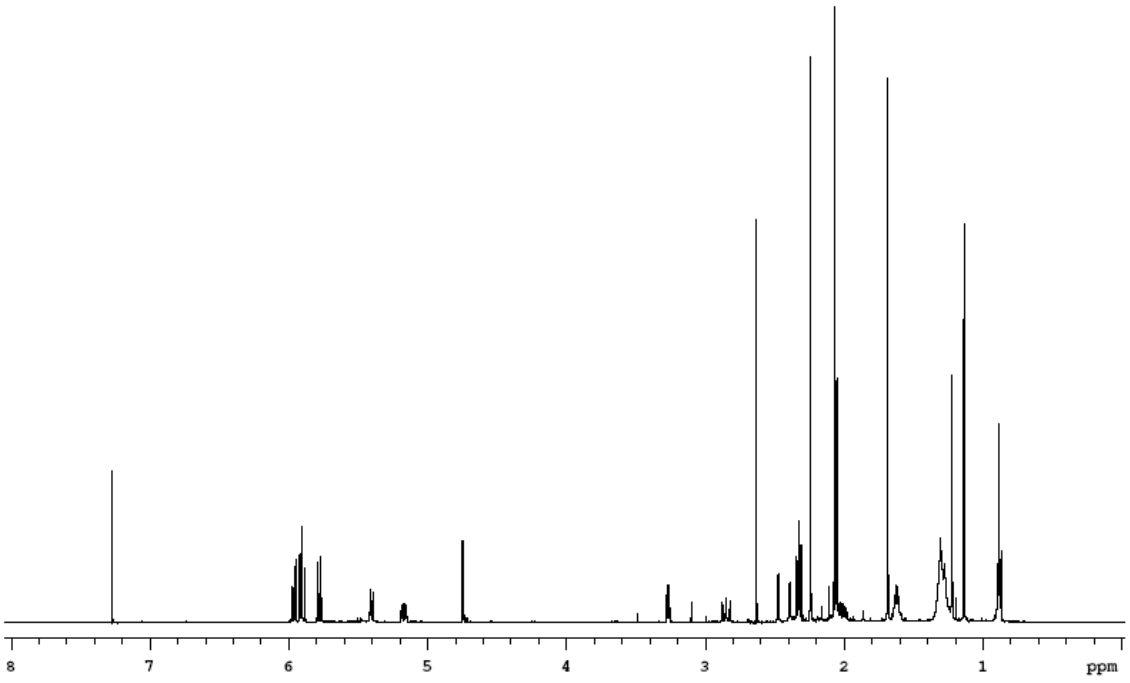

Figure A19 ^{1}H-NMR spectrum (500 MHz, $CDCl_3$) of RAM C (**4**)

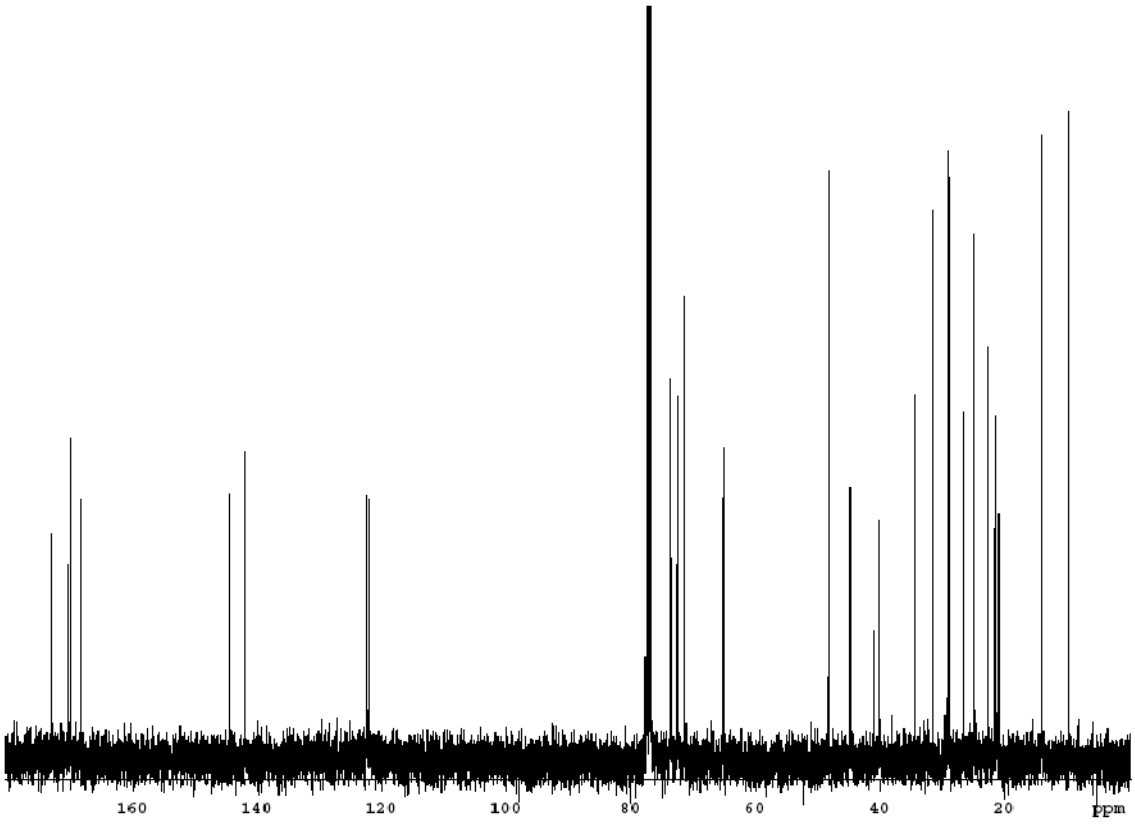

Figure A20 ^{13}C-NMR (100 MHz, $CDCl_3$) of RAM C (**4**)

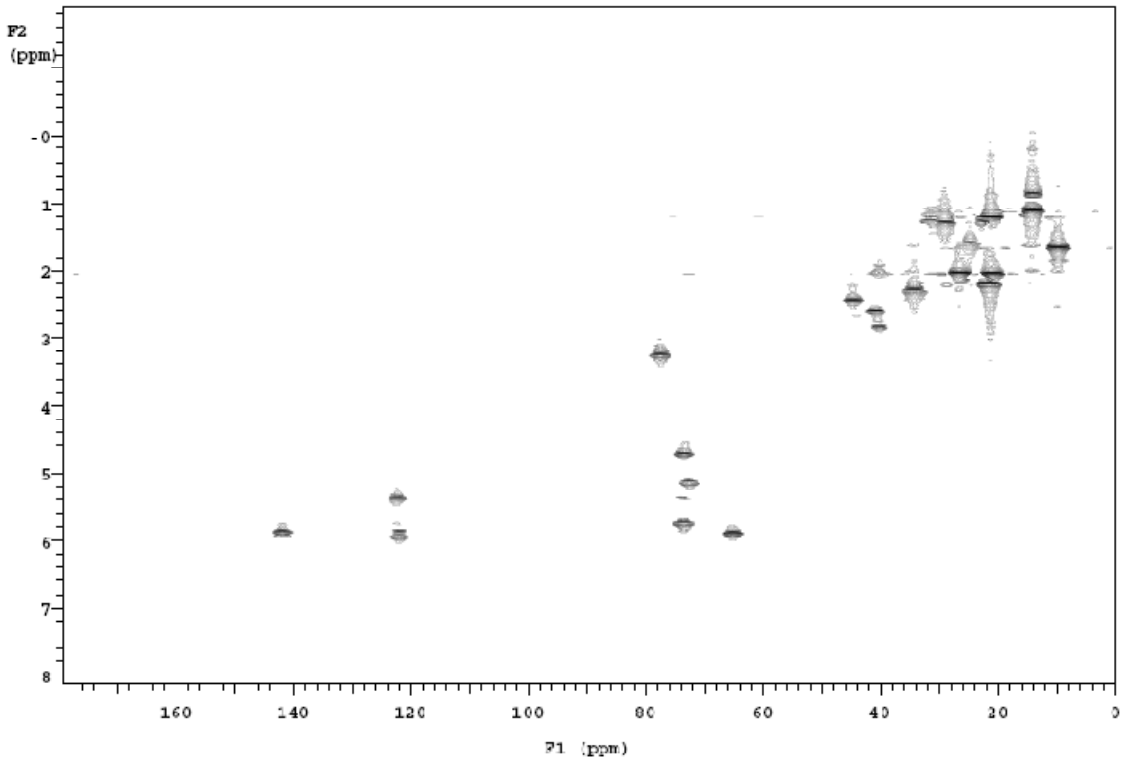

Figure A21 HSQC-NMR spectrum (400 MHz, $CDCl_3$) of RAM C (**4**)

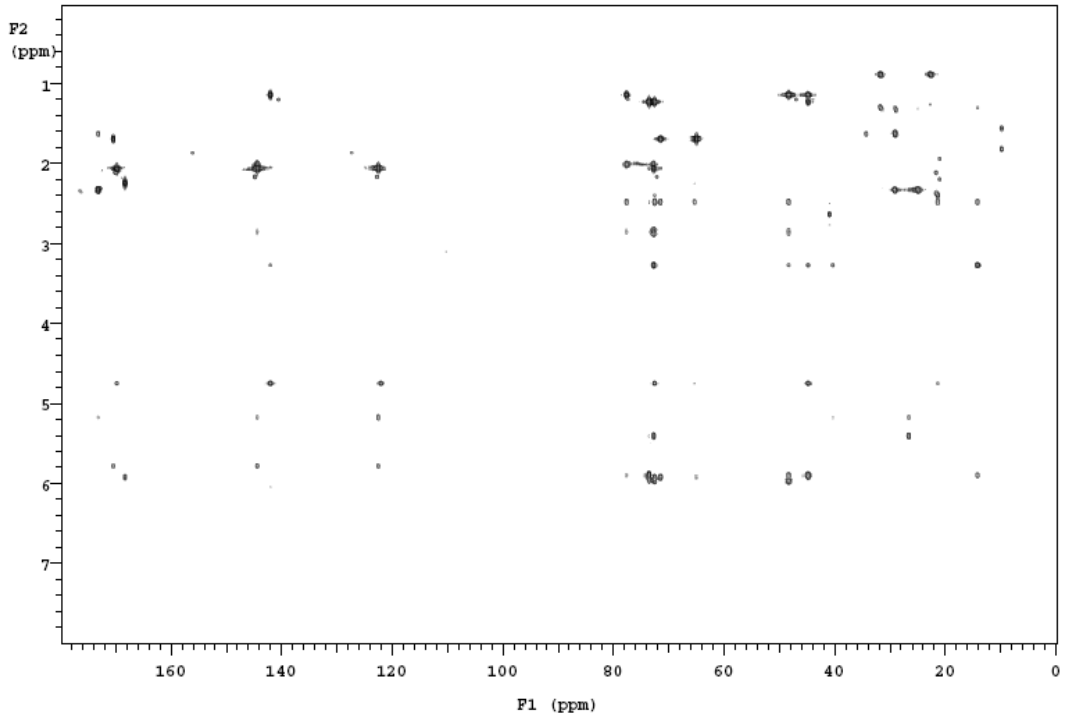

Figure A22 HMBC-NMR spectrum (400 MHz, $CDCl_3$) of RAM C (**4**)

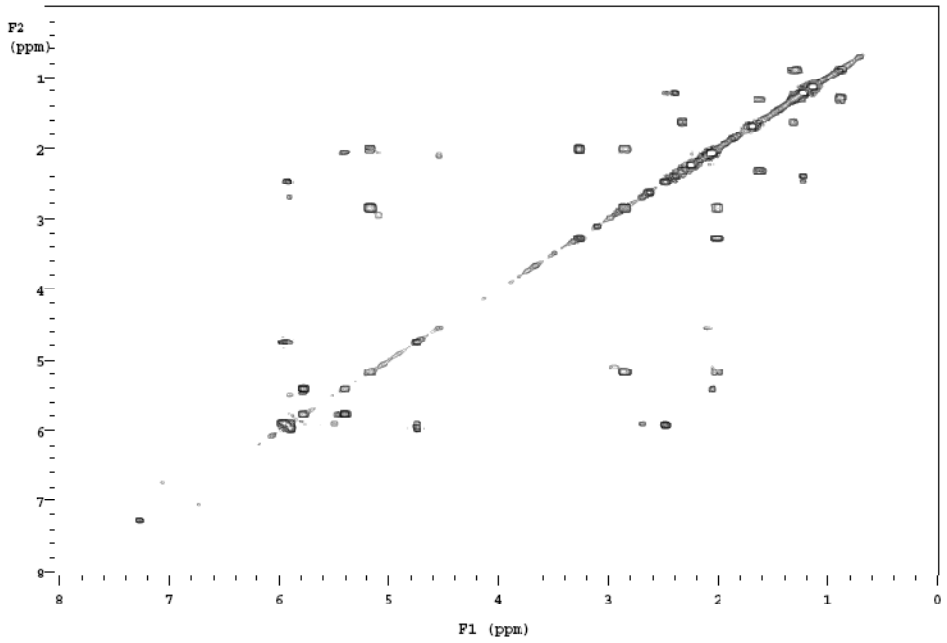

Figure A23 COSY-NMR spectrum (400 MHz, $CDCl_3$) of RAM C (**4**)

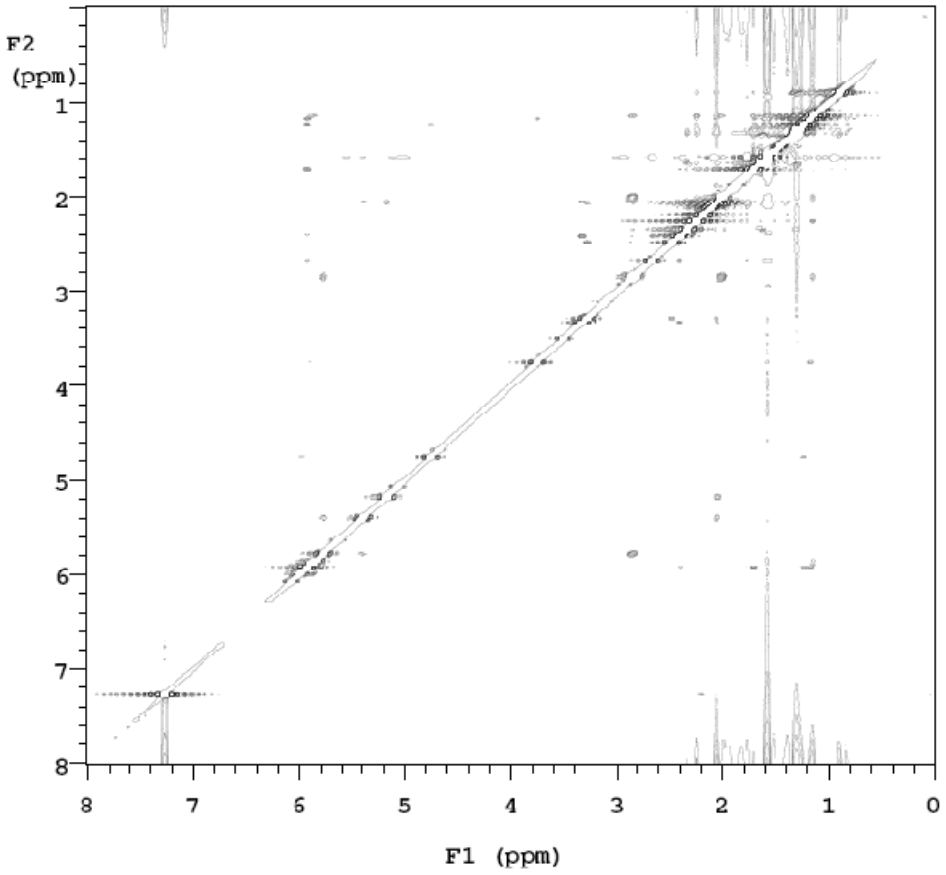

Figure A24 NOESY-NMR spectrum (500 MHz, $CDCl_3$) of RAM C (**4**)

Table A11 Crystallographic data and structure refinement for RAM A-M1 (**2**). Data was collected and interpreted by Dr. Douglas Powell in the Department of Chemistry and Biochemistry at the University of Oklahoma.

Empirical formula	$(C_{24}\ H_{32}\ O_{10}) \cdot (H_2\ O)$ $C_{24}\ H_{34}\ O_{11}$
Formula weight	498.51
Crystal system	Orthorhombic
Space group	$P2_12_12_1$
Unit cell dimensions	a = 8.0444(16) Å α= 90° b = 16.005(3) Å β= 90° c = 18.919(6) Å γ= 90°
Volume	2435.8(10) $Å^3$
Z, Z'	4, 1
Density (calculated)	1.359 Mg/m^3
Wavelength	0.71073 Å
Temperature	100(2) K
F(000)	1064
Absorption coefficient	Semi-empirical from equivalents
Max. and min. transmission	0.995 and 0.955
Theta range for data collection	1.67 to 26.00°
Reflections collected	2721
Independent reflections	2721 [R(int) = 0.0000]
Data / restraints / parameters	2721 / 0 / 316
$wR(F^2$ all data)	$wR2$ = 0.1950
R(F obsd data)	$R1$ = 0.0817
Goodness-of-fit on F^2	1.147
Observed data [I > 2σ(I)]	2270
Absolute structure parameter	0(3)
Largest and mean shift / s.u.	0.000and 0.000
Largest diff. peak and hole	0.379 and -0.324 e/$Å^3$

$wR2 = (\Sigma [w(F_o^2 - F_c^2)^2] / \Sigma [w(F_o^2)^2])^{1/2}$

$R1 = \Sigma ||F_o| - |F_c|| / \Sigma |F_o|$

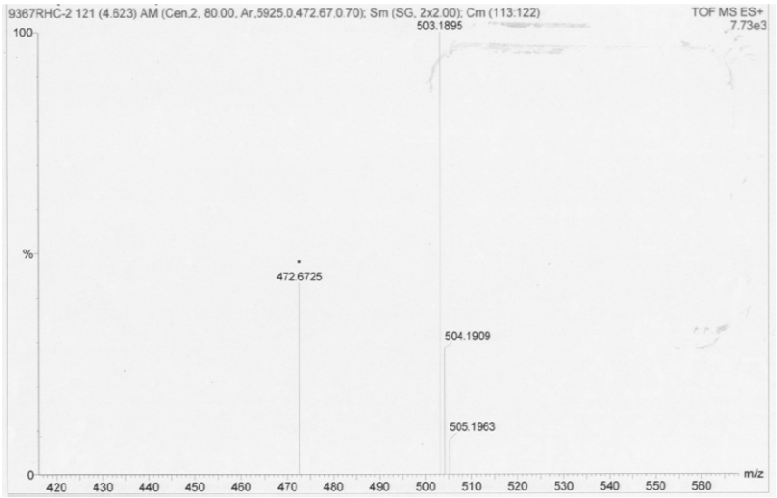

Figure A25 HRESIMS of RAM A-M1 (**5**)

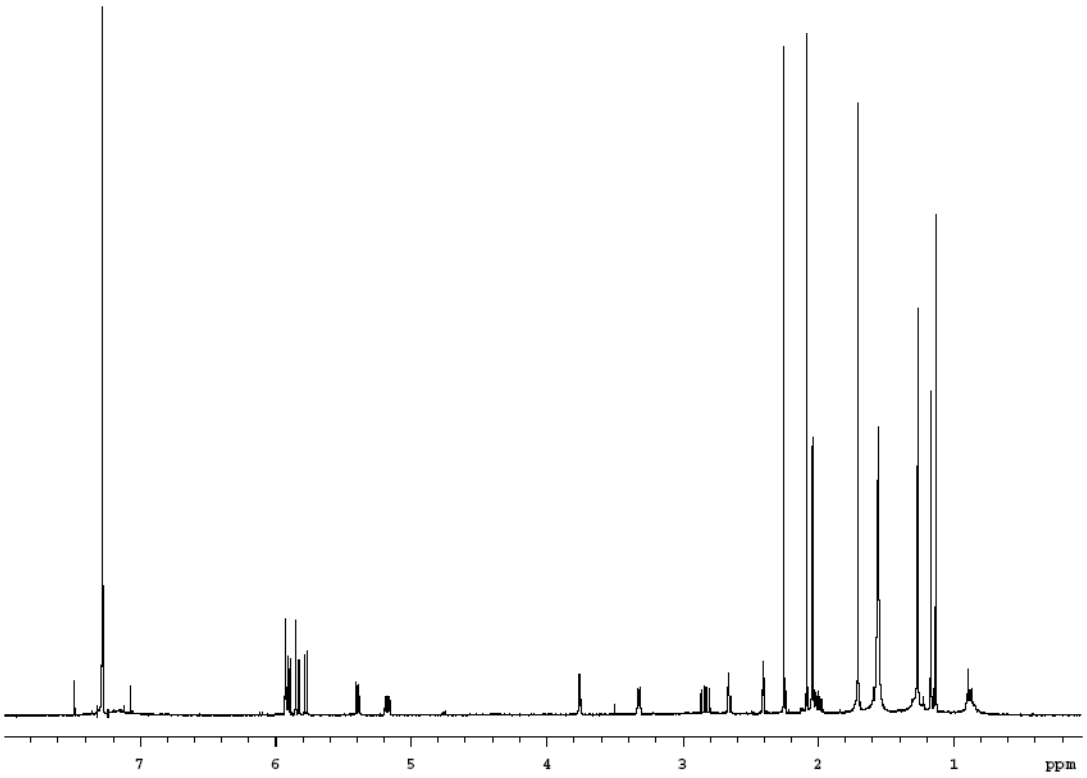

Figure A26 ^{1}H-NMR (500 MHz, $CDCl_3$) of RAM A-M1 (**5**)

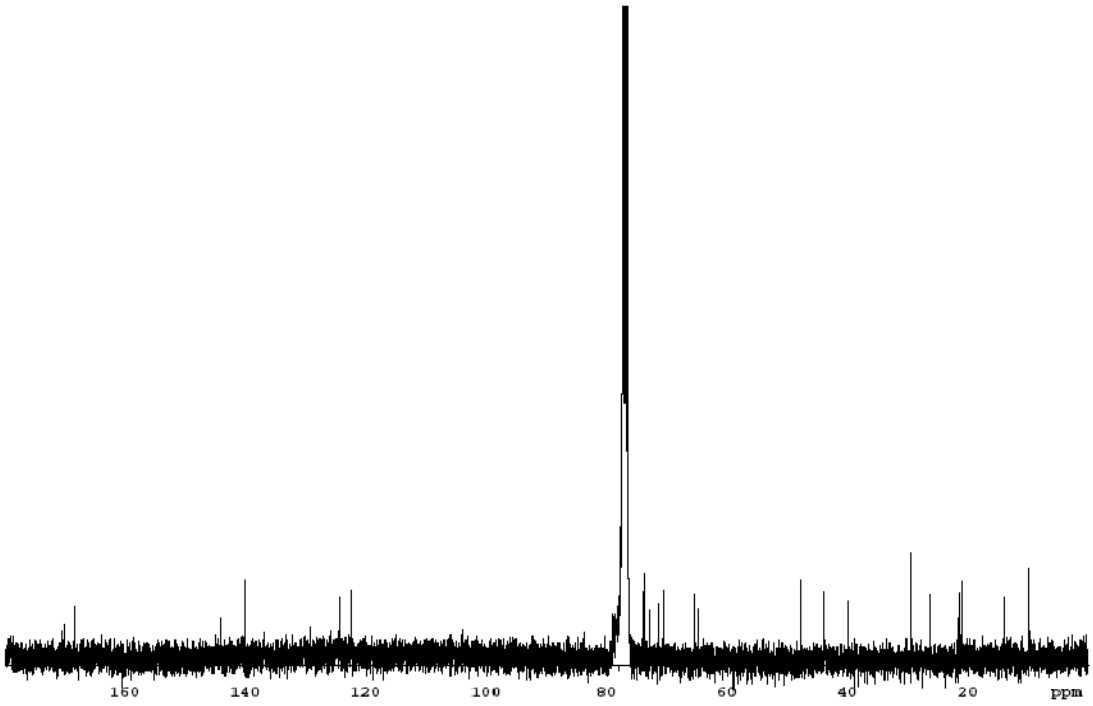

Figure A27 ^{13}C-NMR (100 MHz, $CDCl_3$) of RAM A-M1 (**5**)

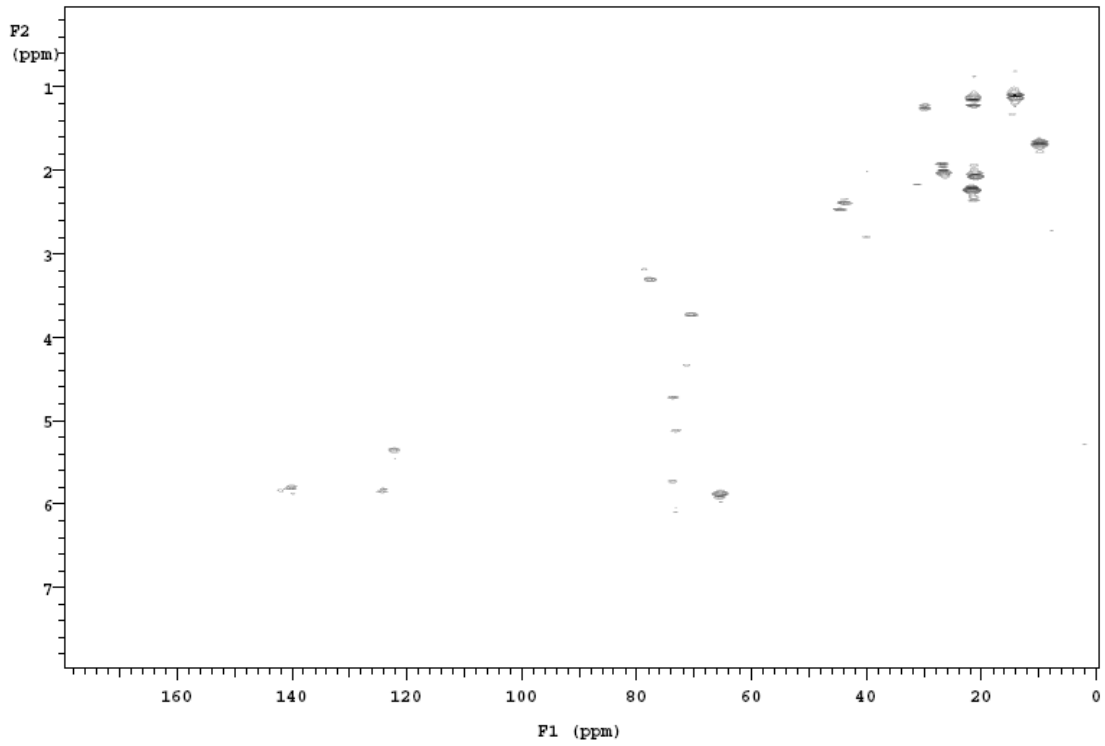

Figure A28 HSQC-NMR (400 MHz, $CDCl_3$) of RAM A-M1 (**5**)

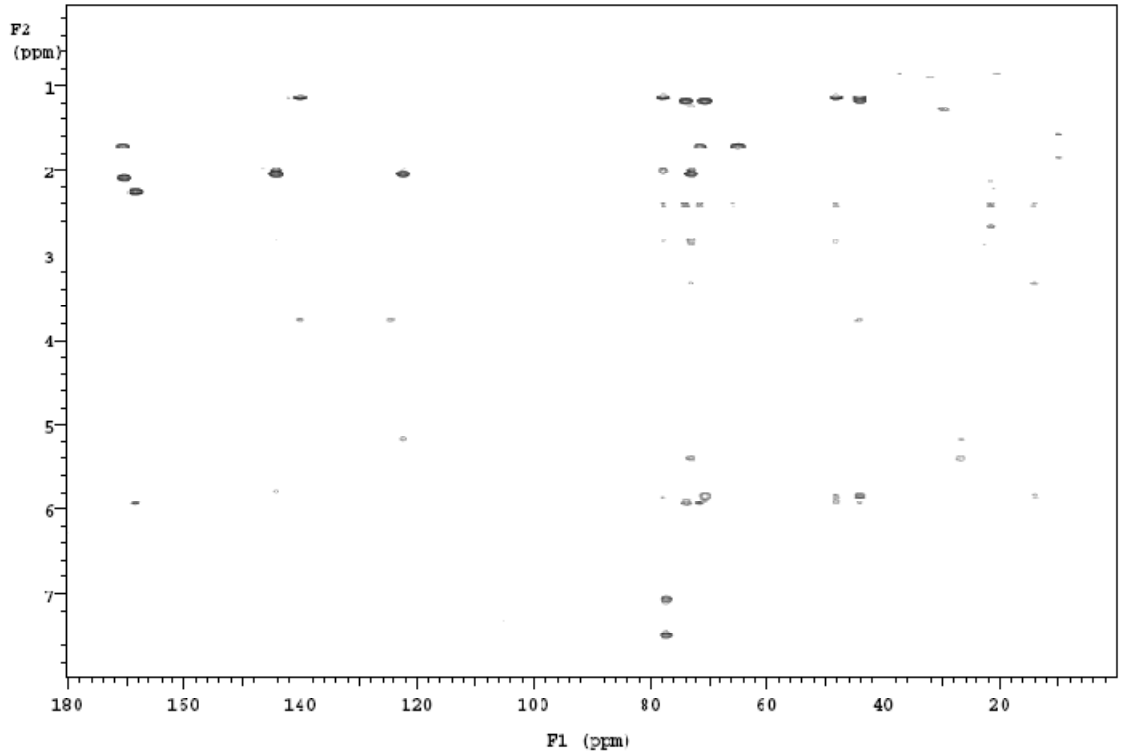

Figure A29 HMBC-NMR (400 MHz, $CDCl_3$) of RAM A-M1 (**5**)

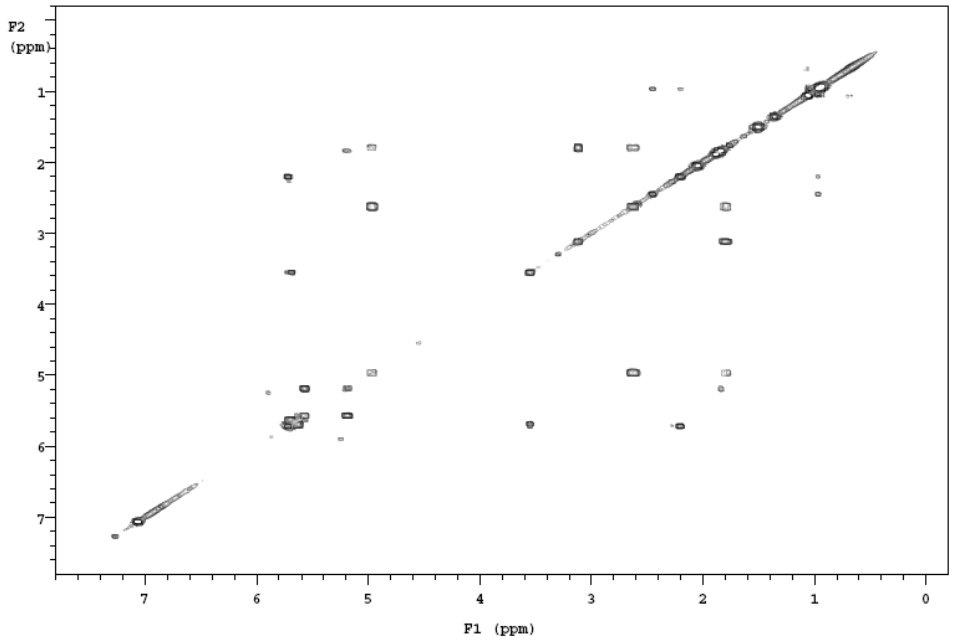

Figure A30 COSY-NMR (400 MHz, $CDCl_3$) of RAM A-M1 (**5**)

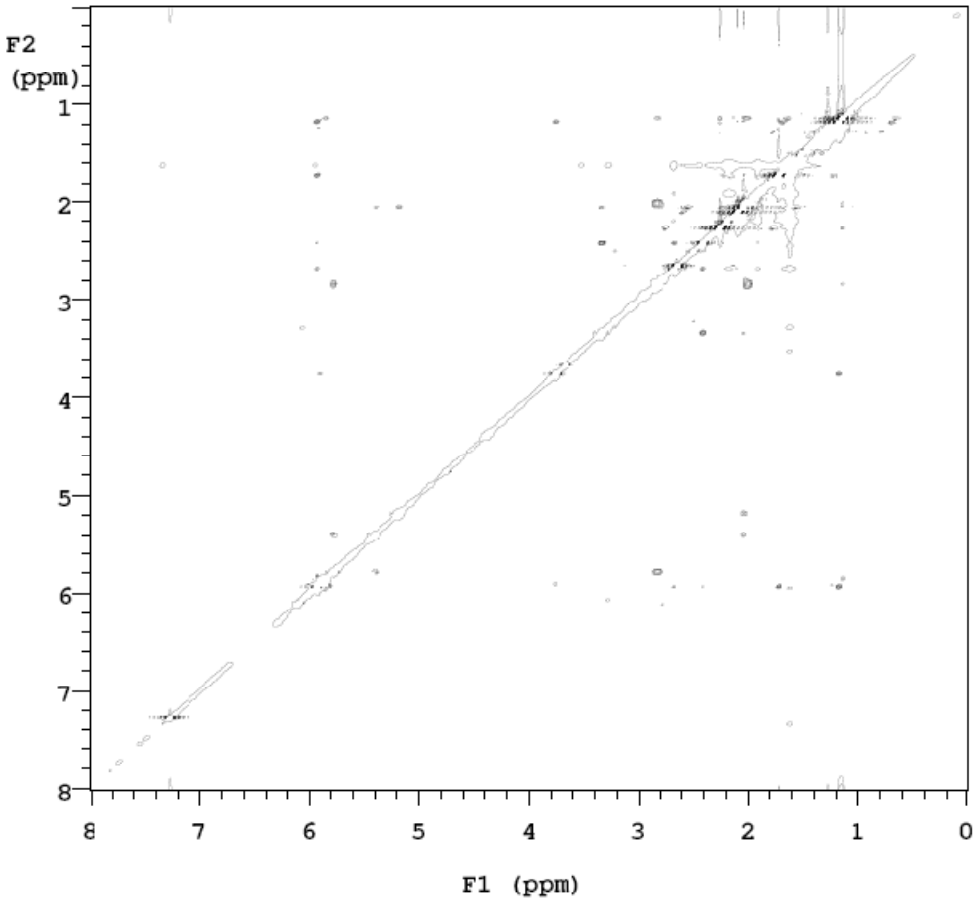

Figure A31 NOESY-NMR (400 MHz, $CDCl_3$) of RAM A-M1 (**5**)

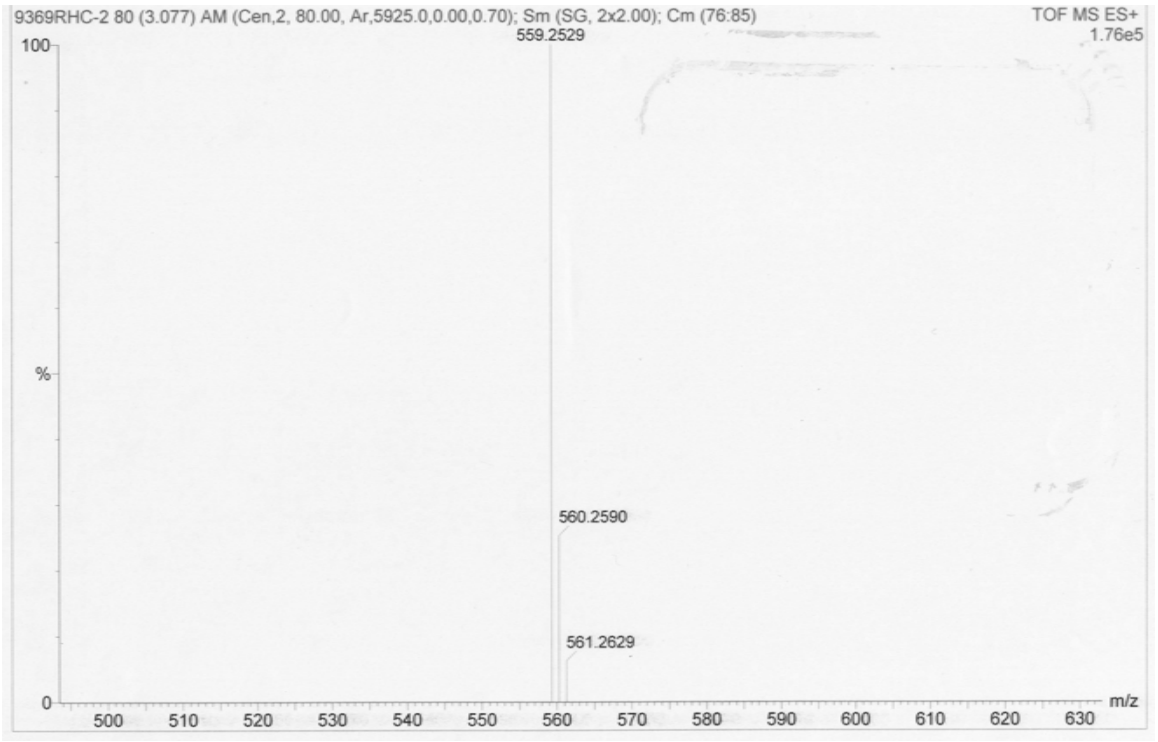

Figure A32 HRESIMS of RAM B-M1 (**6**)

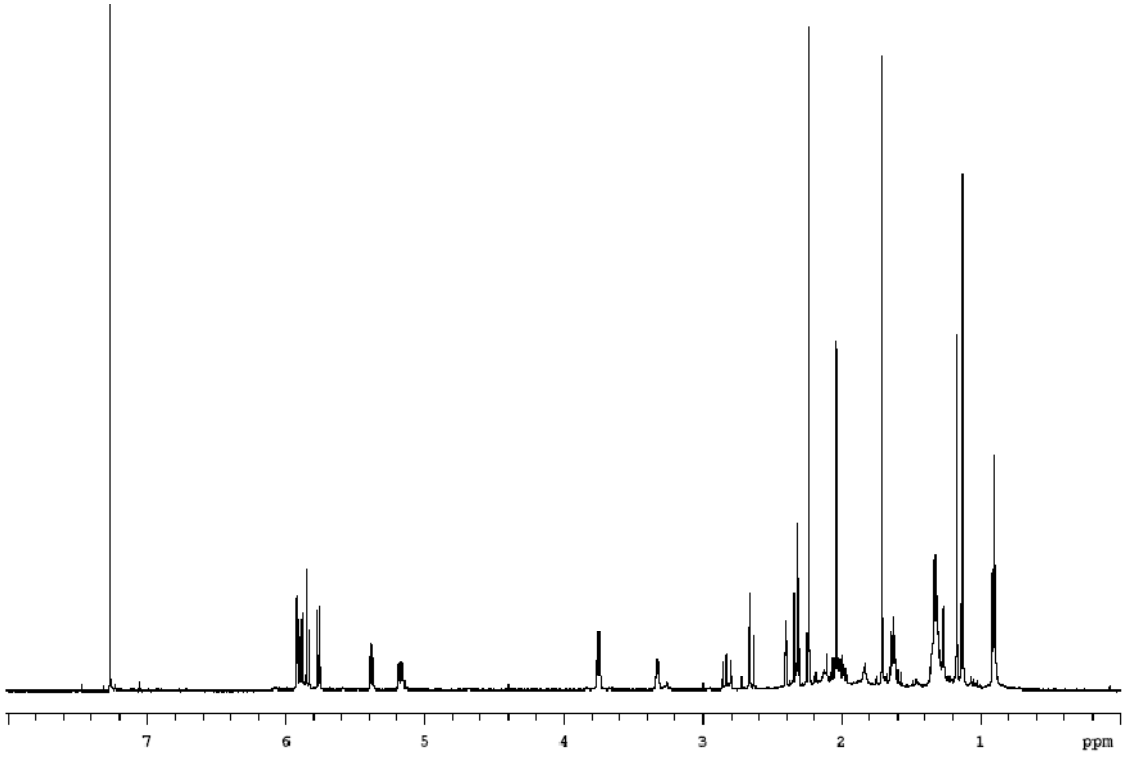

Figure A33 ^{1}H-NMR (500 MHz, $CDCl_3$) of RAM B-M1 (**6**)

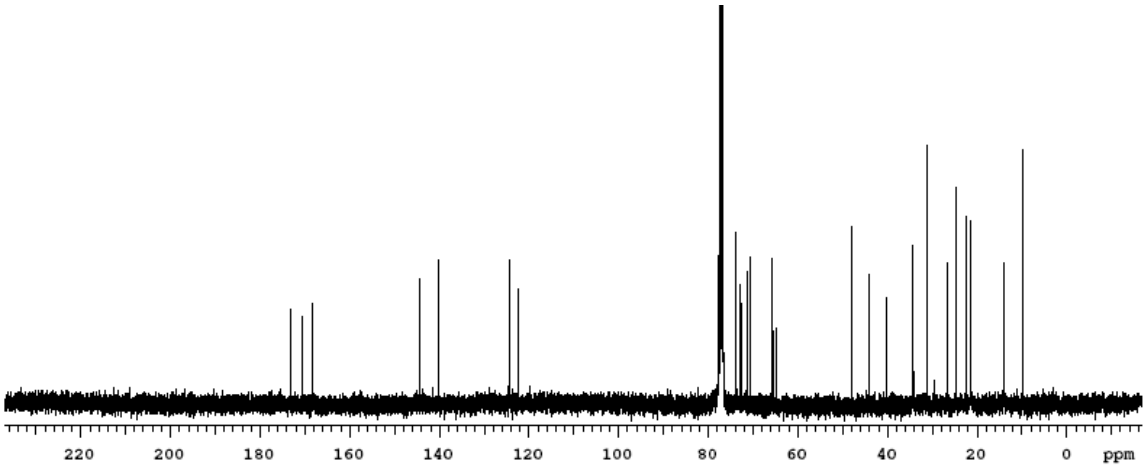

Figure A34 ^{13}C-NMR (100 MHz, $CDCl_3$) of RAM B-M1 (**6**)

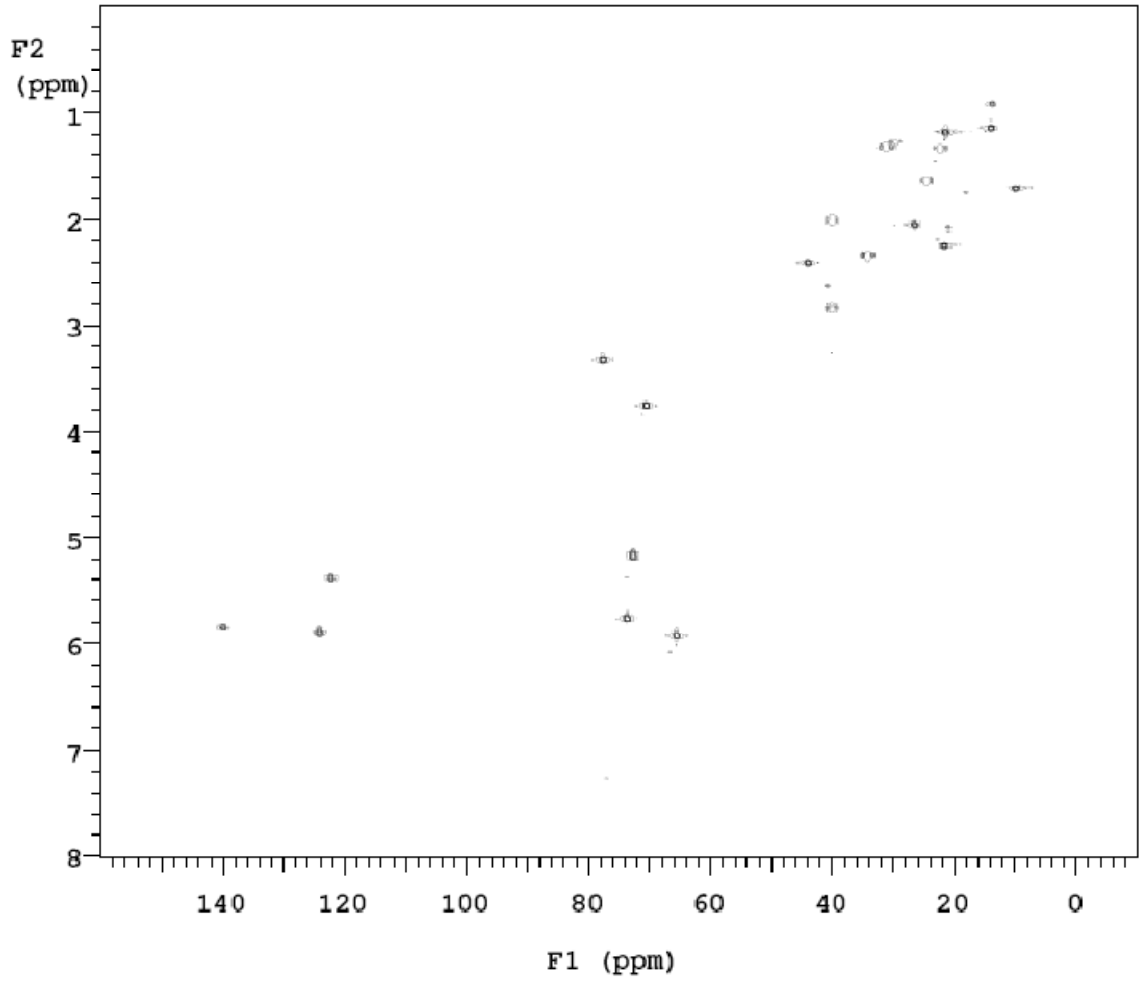

Figure A35 HSQC-NMR (500 MHz, $CDCl_3$) of RAM B-M1 (**6**)

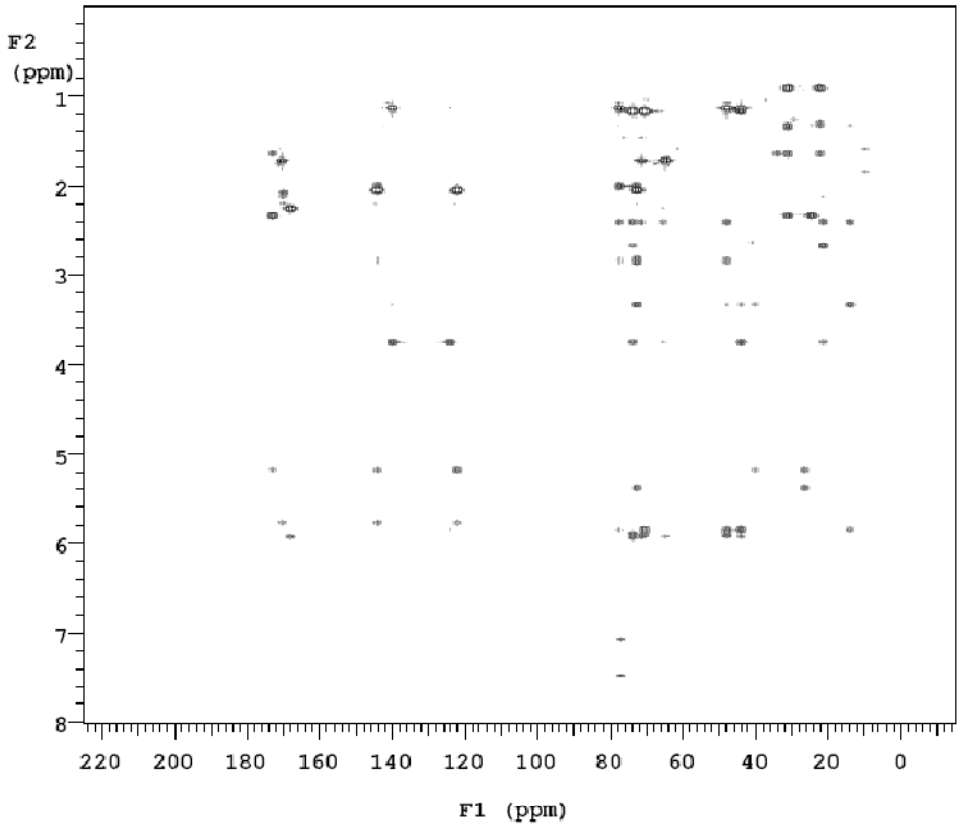

Figure A36 HMBC-NMR (500 MHz, $CDCl_3$) of RAM B-M1 (**6**)

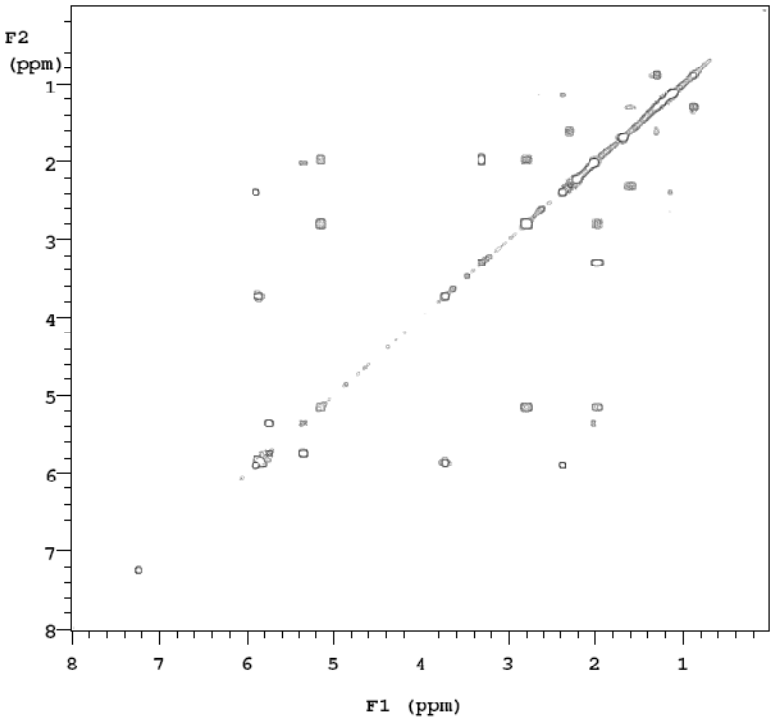

Figure A37 COSY-NMR (400 MHz, $CDCl_3$) of RAM B-M1 (**6**)

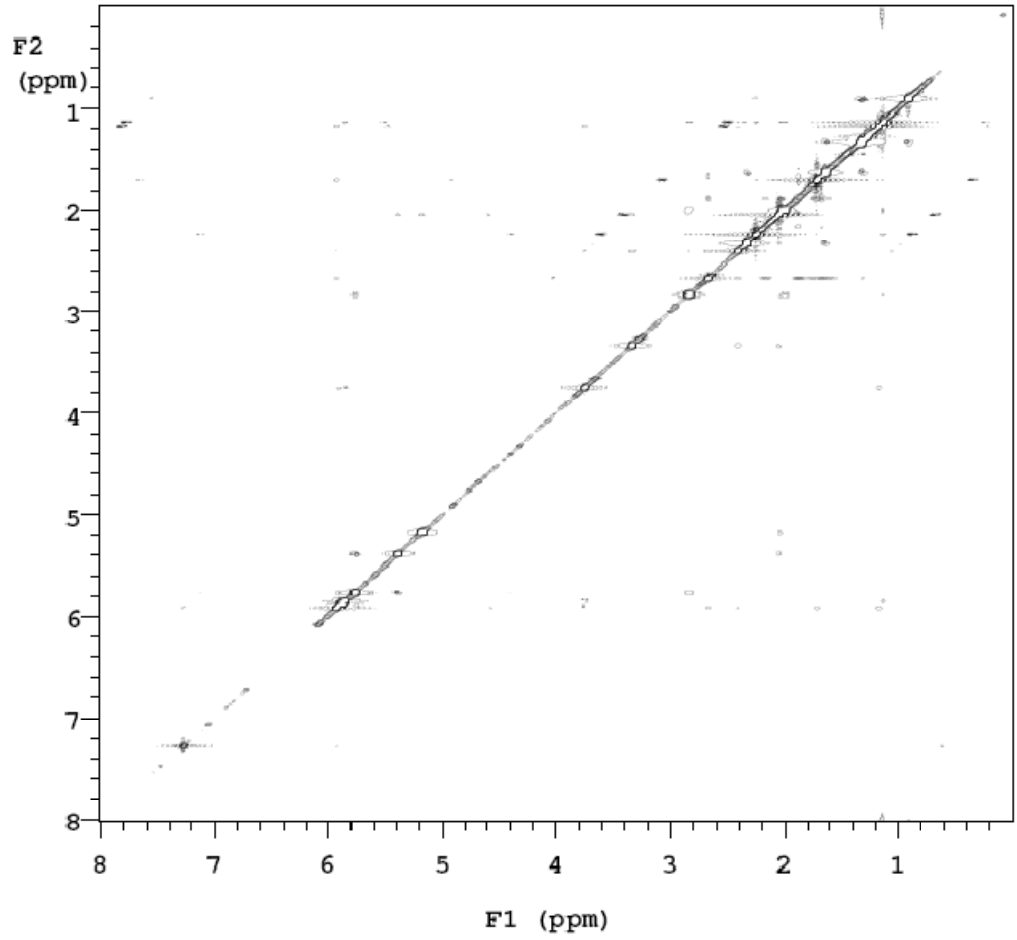

Figure A38 NOESY-NMR (500 MHz, $CDCl_3$) of RAM B-M1 (**6**)

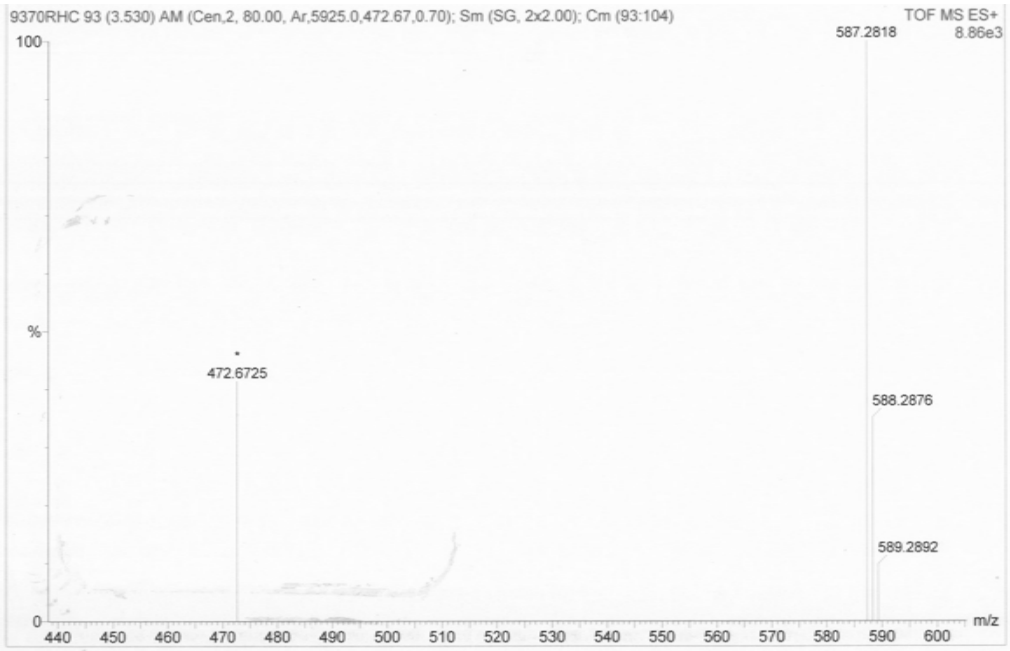

Figure A39 HRESIMS of RAM C-M1 (**7**)

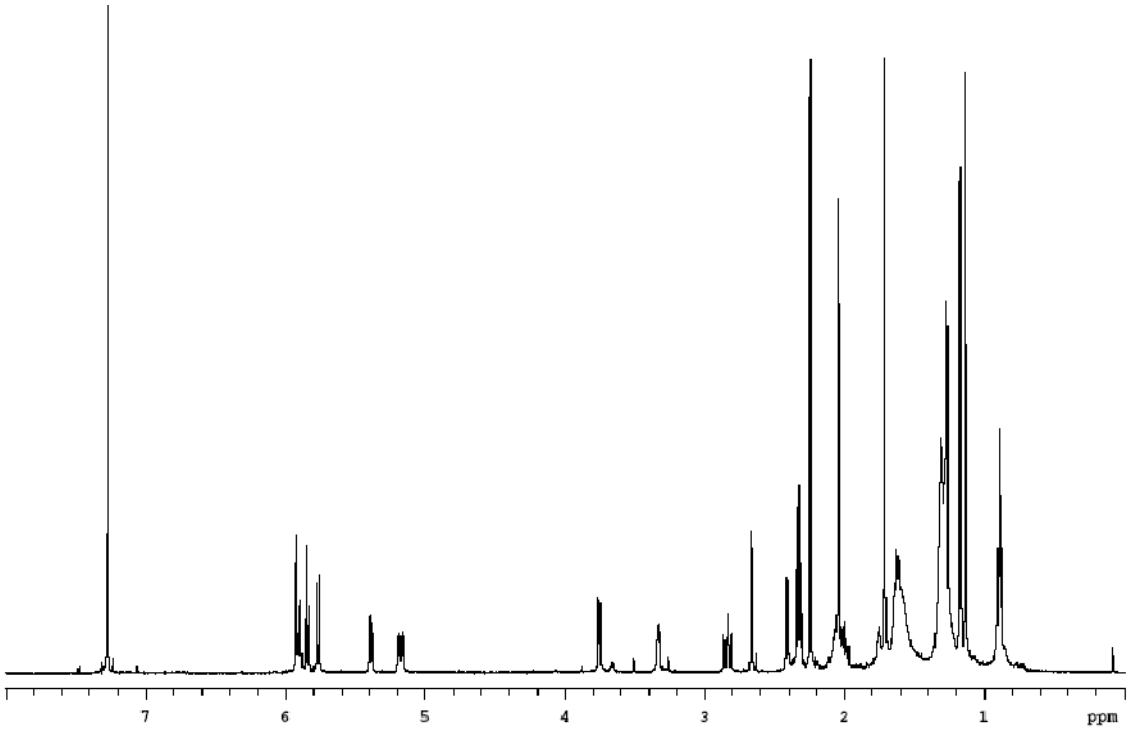

Figure A40 ^{1}H-NMR (500 MHz, $CDCl_3$) of RAM C-M1 (**7**)

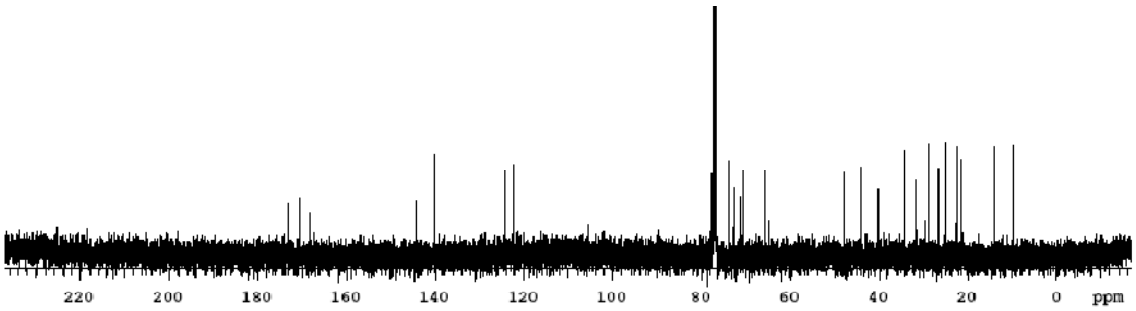

Figure A41 ^{13}C-NMR (100 MHz, $CDCl_3$) of RAM C-M1 (**7**)

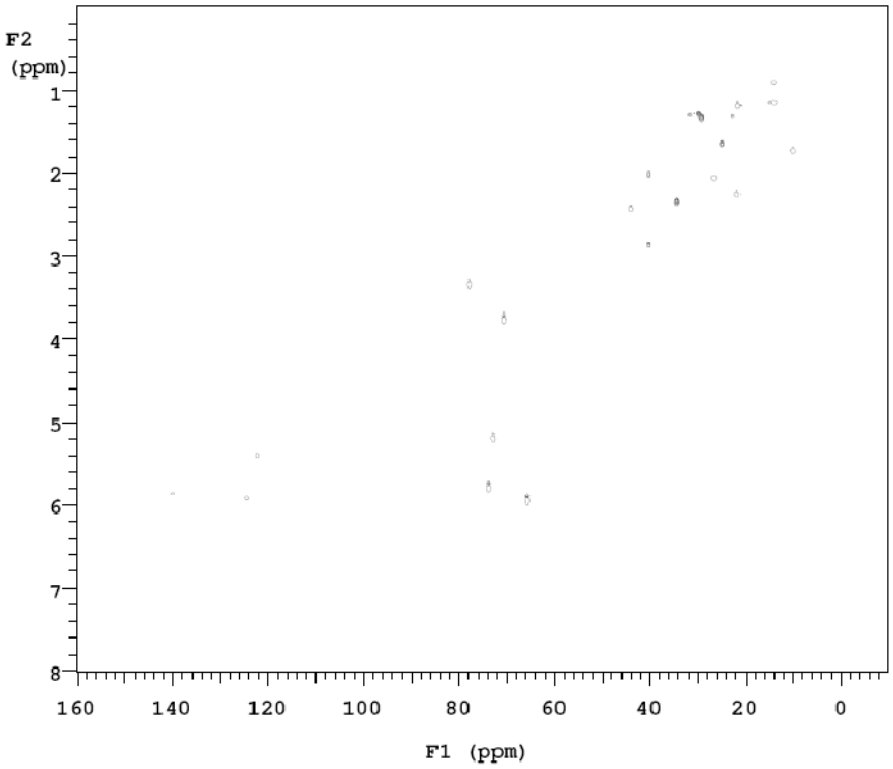

Figure A42 HSQC-NMR (500 MHz, $CDCl_3$) of RAM C-M1 (**7**)

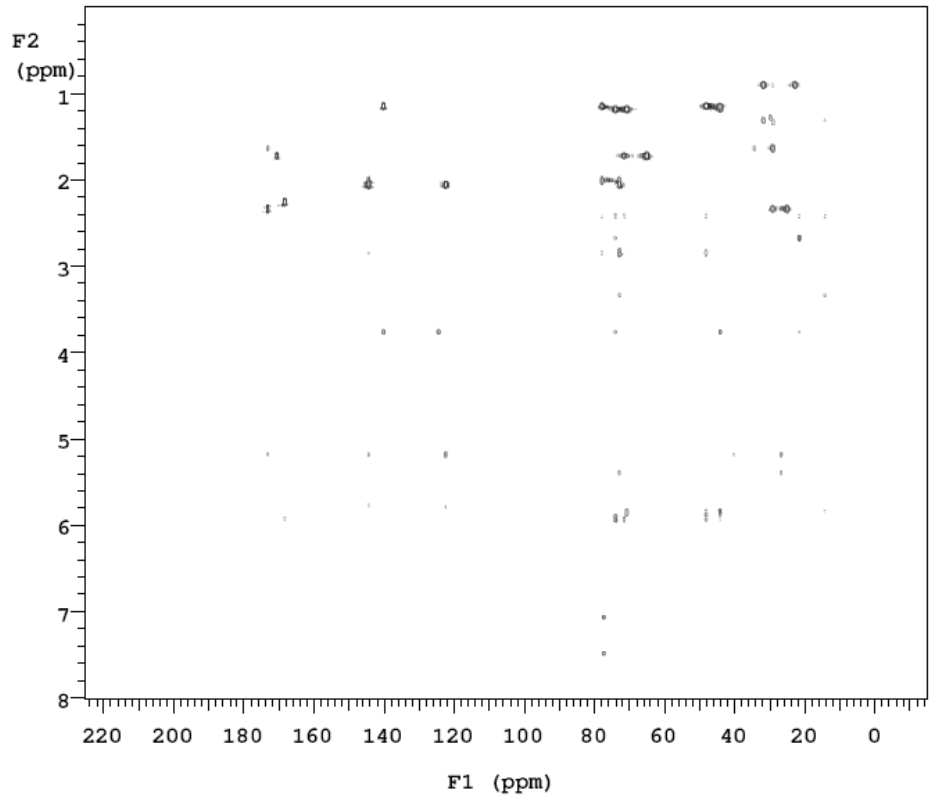

Figure A43 HMBC-NMR (500 MHz, $CDCl_3$) of RAM C-M1 (**7**)

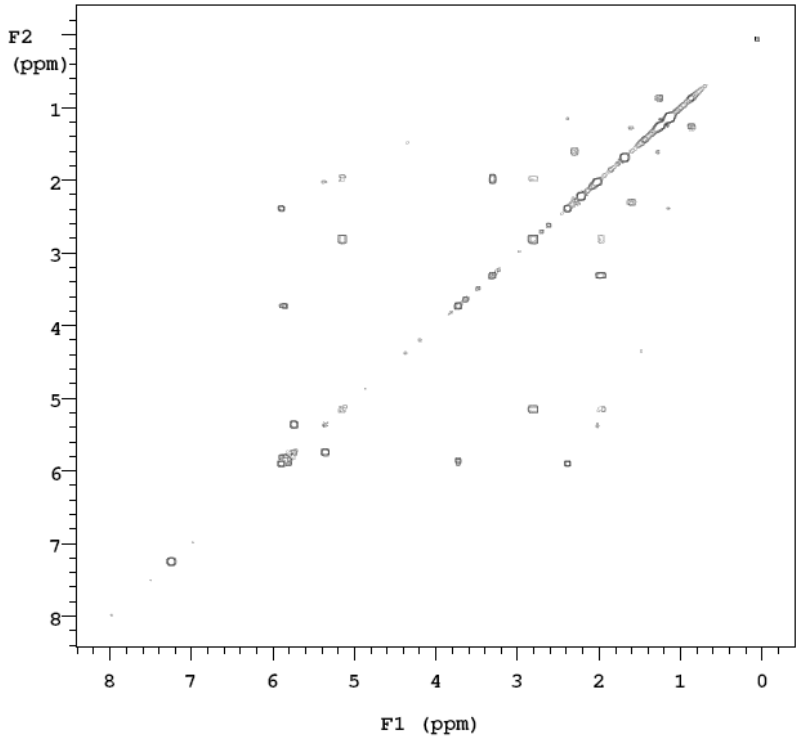

Figure A44 COSY-NMR (400 MHz, $CDCl_3$) of RAM C-M1 (**7**)

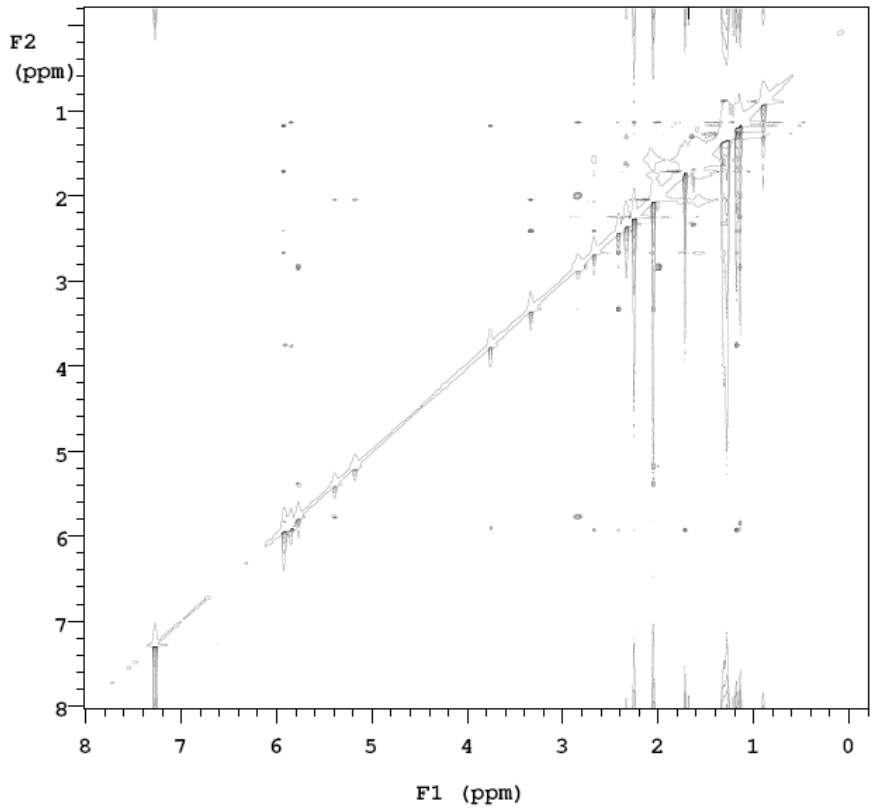

Figure A45 NOESY-NMR (500 MHz, $CDCl_3$) of RAM C-M1 (**7**)